ORNL/Sub-83/43374/1/V3

OAK RIDGE NATIONAL LABORATORY

MARTIN MARIETTA

STUDY TO ASSESS THE EFFECTS OF MAGNETOHYDRODYNAMIC ELECTROMAGNETIC PULSE ON ELECTRIC POWER SYSTEMS

PHASE I

FINAL REPORT

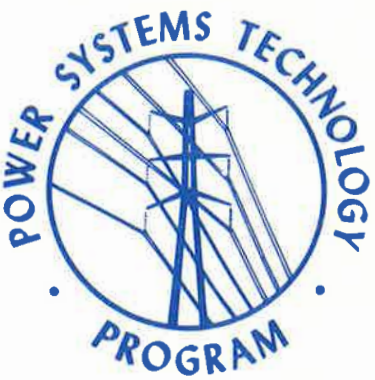

OPERATED BY
MARTIN MARIETTA ENERGY SYSTEMS, INC.
FOR THE UNITED STATES
DEPARTMENT OF ENERGY

Printed in the United States of America. Available from
National Technical Information Service
U.S. Department of Commerce
5285 Port Royal Road, Springfield, Virginia 22161
NTIS price codes—Printed Copy: A07 Microfiche A01

ORNL/Sub-83/43374/1/V3
Dist. Category UC-97a,b,c

Energy Division

STUDY TO ASSESS THE EFFECTS OF MAGNETOHYDRODYNAMIC ELECTROMAGNETIC PULSE ON ELECTRIC POWER SYSTEMS PHASE I FINAL REPORT

J. R. Legro
N. C. Abi-Samra
F. M. Tesche

Manuscript Completed: December 1984
Date Published: May 1985

Report Prepared By

Westinghouse Electric Corporation
Advanced Systems Technology
777 Penn Center Blvd.
Pittsburgh, PA 15235
under
Subcontract 19X-43374C

for

P. R. Barnes, Technical Monitor
Power Systems Technology Program
Energy Division
Oak Ridge National Laboratory
Oak Ridge, Tennessee 37831
operated by
MARTIN MARIETTA ENERGY SYSTEMS, INC.
for the
U.S. DEPARTMENT OF ENERGY
under Contract No. DE-AC05-840R21400

FOREWORD

The Division of Electric Energy Systems (EES) of the United States Department of Energy (DOE) has formulated a program for the research and development of technologies and systems for the assessment, operation, and control of electric power systems when subjected to electromagnetic pulse (EMP). The DOE/EES EMP program plan is documented in a DOE report entitled Program Plan for Research and Development of Technologies and Systems for Electric Power Systems Under the Influence of Nuclear Electromagnetic Pulses, DOE/NBB-003, May 1983. The research documented in this Oak Ridge National Laboratory (ORNL) report was conducted under program plan elements E1, "EMP Surge Characterization and Effects" and E2, "EMP Assessment Methodology Development and Testing."

The research documented in this volume considers electric power system models and methodology applicable to explore the interaction between magnetohydrodynamic-electromagnetic pulse (MHD-EMP) and civilian electric utility systems. The results of this work will be used in subsequent phases of the research program to simulate such interaction, to assess the possible consequences and to explore relevant mitigation techniques.

All data pertaining to MHD-EMP environments have been obtained from public domain documents and unclassified source materials. Such information is presented herein for illustrative purposes only and does not represent actual weapon characteristics or maximum threat environments.

This report is Volume 3 of a 4-volume set that describes an EMP assessment methodology for electric power systems. Volume 1 is an Executive Summary. Volume 2 covers high-altitude EMP (HEMP), Volume 3 (this volume) covers MHD-EMP, and Volume 4 covers source-region EMP (SREMP).

ACKNOWLEDGMENTS

The research for this report was sponsored by the Division of Electrical Energy Systems, United States Department of Energy under Contract No. W-7405-ENG-26 with the Union Carbide Corporation and Contract No. DE-AC05-840R21400 with Martin Marietta Energy Systems, Inc.

The authors wish to acknowledge and thank Mr. Ken Klein of the United States Department of Energy, Mr. P. Randy Barnes, Dr. Thomas Reddoch and Mr. Paul Gnadt of Oak Ridge National Laboratory, Mr. Dennis Grimes of the Westinghouse Defense Center, Mr. Robert Nowlin of the Arizona Public Service Company and Mr. David Cooper of the Southern California Edison Company. The authors also acknowledge the assistance of Dr. Vernon Albertson, University of Minnesota for the understanding of geomagnetic storms and Dr. Conrad Longmire, Mission Research Corporation, for guidance in MHD-EMP environments.

CONTENTS

Page

LIST OF FIGURES

LIST OF TABLES

STUDY TO ASSESS THE EFFECTS OF MAGNETOHYDRODYNAMIC ELECTROMAGNETIC PULSE ON ELECTRIC POWER SYSTEMS

J. R. Legro
N. C. Abi-Samra
F. M. Tesche*

ABSTRACT

The high-altitude burst of a nuclear device over the continental United States can expose electric utility power systems to intense, transient electromagnetic pulses (EMP). In addition to the initial transients designated as fast transient high-altitude EMP (HEMP) and intermediate time EMP, electromagnetic signals are also perceived at times from seconds to hundreds of seconds after the burst. This signal has been defined by the term magnetohydrodynamic-electromagnetic pulse (MHD-EMP). The MHD-EMP phenomena has been both detected in actual weapon tests and predicted from theoretical models.

This volume documents a preliminary research effort to: (1) investigate the nature and coupling of the MHD-EMP environments to electric power systems, (2) define the construction of approximate system response network models and, (3) document the development of a unified methodology to assess equipment and systematic vulnerability.

The MHD-EMP environment is compared to a qualitatively similar natural event, the electromagnetic environment produced by geomagnetic storms.

The research, to date, does not include an attempt to quantify power system performance in an MHD-EMP environment. This effort has been to develop the analytical tools and techniques necessary to perform such assessments at a later time. It is anticipated that the MHD-EMP methodology will be incorporated into a comprehensive EMP assessment process to investigate total system risk.

---

*LuTech Incorporated, LaFayette, CA.

1. INTRODUCTION

In the event of single or multiple high-altitude nuclear bursts over the continental United States, it is expected that a large geographic area of the country will be illuminated by intense transient electromagnetic fields. The first of these events to be perceived on the ground is an extremely fast transient having characteristic rise times related strongly to the gamma radiation output rate from the nuclear device. The total field duration is approximately a microsecond. Known as a high-altitude electromagnetic pulse (HEMP), this transient field has the potential to cause direct and consequential damage to electric power systems as well as system operational upset. Immediately following the initial fast HEMP transient, scattered gamma ray photons and inelastic gammas from weapon neutrons create additional ionization resulting in the second part (intermediate time) of the HEMP signal. This second signal can occur in a time interval from one microsecond to about one second.

Electromagnetic signals are also perceived at much later times (seconds to hundreds of seconds after the burst) due to magnetic bubble formation and hydrodynamic motion of the heated atmosphere and debris remaining from the explosion. This type of electromagnetic transient has been defined by the term magnetohydrodynamic-electromagnetic pulse (MHD-EMP). These MHD-EMP signals have been both detected in actual tests and predicted from theoretical models.

Since the United States electric power network of generation, transmission and distribution may be exposed to EMP environments, it is of critical importance to national security that a quantitative and comprehensive methodology be developed to assess the vulnerability of electric power systems to this new, externally imposed, transient environment. The creation of such an assessment technique would enable all interested parties to quantify the potential risk to existing systems, and explore mitigating system hardware applications and operational strategy. EMP assessments have been performed for other types of electrical systems, such as military aircraft, missiles and

communications facilities. The unique properties of the electric power system, such as its complex electrical interconnection over a vast geographic area strongly indicates that a separate EMP assessment methodology should be developed with specific focus on the electric power system.

Section 2 of this report presents an overview of the physics of MHD-EMP transient generation and environmental definition. Measured results from the Fishbowl test series are presented and the results of numerical simulations of the Starfish nuclear event are summarized. In order to use the calculated data in an efficient manner for power system assessment, an approximate method is suggested for representing the MHD-EMP electric field on the earth's surface.

In Section 3, the coupling of the MHD-EMP transient electric field to the electric power system is discussed. A spectral analysis of the transient is presented in order to demonstrate the validity of modelling the effect of the electric field as "quasi-dc" voltage sources impressed on an equivalent dc power system network. The MHD-EMP environment is compared to a similar power system environment produced by geomagnetic storm phenomena.

Section 4 considers in detail the elements of a power system assessment methodology under MHD-EMP environments. It is shown that significant elements of geomagnetic storm assessment methodology, modified as required, can be evoked to understand the relationship between MHD-EMP and the electric power system.

In Section 5, the topological aspects of the electric power system are discussed. Suitable models for power systems assessment are presented coupled with an analysis of digital computer codes needed to study the impact of MHD-EMP on power systems.

The report concludes with a summary of recommended areas of additional research to better refine both the environmental definition and the assessment methodology.

The research to date, does not include any attempt to quantify power system performance in an MHD-EMP environment. The Phase I effort

has been to define the tools and techniques necessary to perform such assessments in subsequent phases. The development of comprehensive methodology is the prerequisite to consistent and meaningful risk assessment.

2. MHD-EMP ENVIRONMENTAL DESCRIPTION

2.1 Introduction

Any assessment of MHD-EMP impact on electric utility power systems must begin with an understanding of the physical generation of this transient electromagnetic phenomena and an appropriate environmental definition suitable for power system analysis. It is equally important to place in perspective the quantity and quality of measured data and the success of event simulation via digital codes and other analytical techniques.

Much of what is empirically known about a MHD-EMP environment is based upon magnetometer data acquired during actual nuclear events such as the Fishbowl test series conducted in the Pacific Ocean. The data obtained from the Starfish test (1962) has often been chosen as a benchmark case due to the large negative change, over time, in the ambient magnetic flux density as measured at Johnston Island. Figure 1 shows the magnetometer measurements at Johnston Island for Starfish and two other Fishbowl tests.

Thus, the body of measured data, which exists in the open literature, is limited to a very small sample of magnetometer recordings, at a few locations in the Pacific, for tests which occurred over twenty years ago. To the authors' knowledge, no evaluation of the random and systematic uncertainty nor the response characteristics has been offered for the instrumentation. The limited number of tests did not include replication of any single event. The ratification of the above-ground nuclear Test Ban Treaty effectively put an end to event measurement.

In order to estimate an MHD-EMP environment which could exist over the continental United States for a nuclear event comparable to Starfish, Longmire has taken the measured data of Starfish and essentially doubled the magnitude of the change in magnetic flux density [1]. The modification is offered to account for the change in geographic latitude between the Pacific test site and the continental

United States corresponding to the increase in the earth's ambient magnetic flux density as a function of latitude.

Event simulation via digital codes has met with mixed success. In contrast to HEMP, which has been postulated for a longer time as a significant threat to military and civilian systems and whose phenomenology has been investigated by a number of independent research efforts, MHD-EMP threat awareness and significant simulation has been limited to a major research effort sponsored by the Defense Nuclear Agency (DNA).

Given the above perspective on the available research, this section presents an overview of a body of physics to model MHD-EMP generation. Based upon this theory, examples of MHD-EMP simulation will be discussed in terms of the change in the earth's magnetic flux density as measured at the surface. Of more direct interest to electric power system analysis is the translation of this magnetic environment to a corresponding set of surface tangential electric fields. The section concludes with a suggested approximate format for MHD-EMP electric field definition to facilitate the numerical evaluation in a power system assessment mechanism.

2.2 The Physics of MHD-EMP Generation

In response to the Starfish measurements, several analytical efforts have attempted to develop a theory for predicting the mechanisms for generating the MHD-EMP environment in general and Starfish in particular. As discussed in the Defense Nuclear Agency (DNA) EMP Course [2], at least two distinct physical mechanisms are thought to be responsible for generating the MHD-EMP environment. The first results in the early portion of the MHD-EMP signal (less than ten seconds after the burst) while the second produces the response later than ten seconds.

As illustrated in Figure 2, a nuclear burst at high altitudes gives rise to a rapidly expanding ionized fireball, consisting of bomb debris and hot gas. This plasma tends to be diamagnetic, in the sense that it excludes the earth's magnetic field from the interior of the fireball.

As the fire ball expands and rises, it will deform the earth's geomagnetic field lines, creating a magnetic field disturbance of wide spread propagation. Directly under the burst point, a temporary layer of ionized air is created by atmospheric absorption of x-rays produced by the weapon. This region tends to shield the area under the burst for the "early" portion of the MHD-EMP signal.

As time progresses, the hot ionized air under the burst begins to rise and moves across the earth's geomagnetic field lines causing large atmospheric currents to flow. This motion may account for the second phase of the MHD-EMP signal. As shown in Figure 3, these atmospheric currents are imaged in the earth. An observer on the ground would measure a change in the earth's ambient magnetic flux density.

Under contract to the Defense Nuclear Agency (DNA) several theoretical efforts have been undertaken by Mission Research Corporation (MRC) in an attempt to model MHD-EMP production and obtain a numerical simulation of the Starfish magnetic flux variations. The initial research [3] focused on the large negative change associated with Starfish since it was postulated that this signal would have the more significant impact. For this purpose, the MHDEMP code written by MRC computes the transient magnetic flux density at the surface of the earth as a function of time. This calculation is based upon input data supplied by the MICE code [4] which computes the behavior of the disturbed atmosphere in the vicinity of the burst.

The MRC simulation, given this version of the MHDEMP code, extends for a period of time from 20 seconds to 110 seconds after the burst in an attempt to replicate the measured change in magnetic flux density as obtained for Starfish at Johnston Island. This research is significant in the sense that, for the first time, the response predicted by the simulation, based on first principles, tends to correspond to measurements at Johnston Island. The actual accuracy of the data fit must be evaluated given:

- The uncertainty factors contained in the MICE input data.
- The elimination of any Beta patch effects.

- The distortion introduced by the finite spatial boundaries of the simulation grid.
- The required shift in spatial location for Johnston Island from an actual distance of approximately 23 km north of the burst to a "best fit" distance of 179 km north in the simulation.
- The weaker correlation at elapsed times less than forty seconds.

Given all of the above qualifications, it remains that this simulation, for the first time, tended to agree with measured data at a given spatial location.

Continuing research by MRC modified the MHDEMP code to include the effects of initial magnetic bubble expansion, plasma pressure gradients and ion inertia in an attempt to simulate the first forty seconds of the Starfish event. The research project also investigated the sensitivity of the simulation to the atmospheric conductivity which exists between the burst point and ground.

An equally important output of the MRC research is that the numerical simulations indicate spatial variations of the MHD-EMP magnetic flux over a wide surface area. The MRC research [3,5] presents a series of such contour plots illustrating the magnitude of the change in magnetic flux density $\Delta|\bar{B}|$ on the earth's surface at discrete points in time. This phenomena is illustrated in Figure 4 for Starfish at an elapsed time after the burst. In this plot, the origin (0,0) is directly under the burst point while Johnston Island is at the approximate coordinate (23.4,0) in kilometers from the origin.

Since the change in magnetic flux density is a vector quantity it is necessary to understand direction as well as magnitude. The corresponding direction of the magnetic phenomena illustrated in Figure 4 is displayed as Figure 5 of this report.

2.3 Determination of The MHD-EMP Electric Field

The environments of more direct interest to electric power system assessment are the time and spatially varying electric fields associated

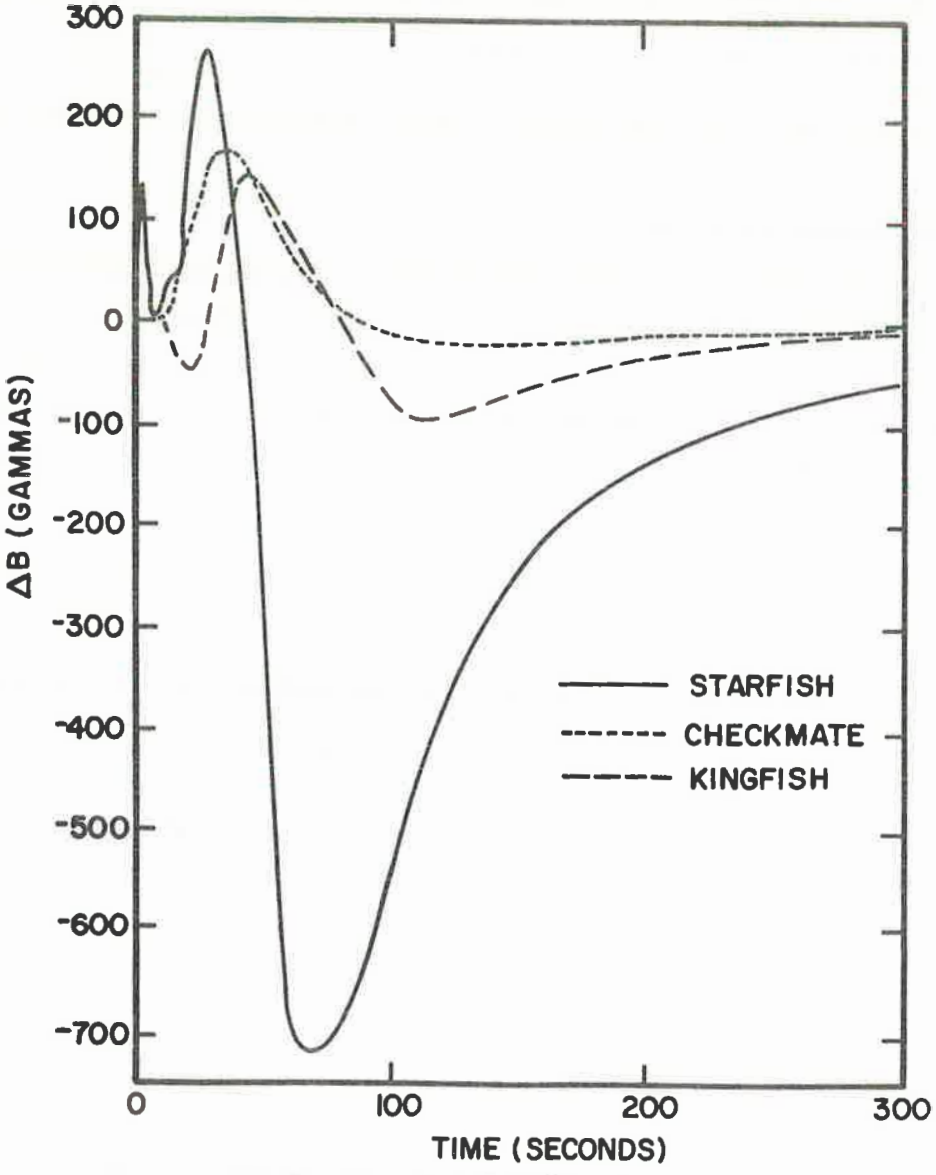

Fig. 1. Measured magnetometer data at Johnston Island for select Fishbowl tests [3].

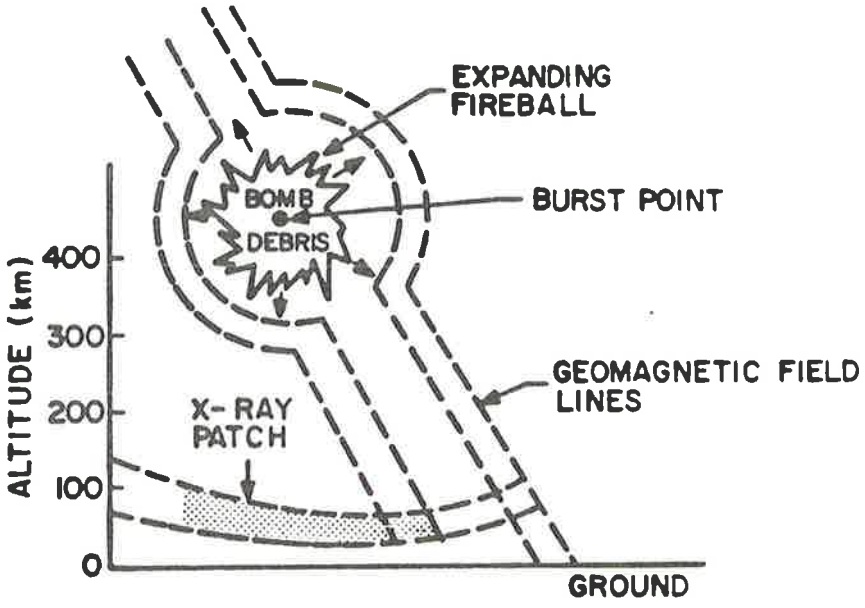

Fig. 2. Generation of initial MHD-EMP signal. (0.1 to 10 seconds)

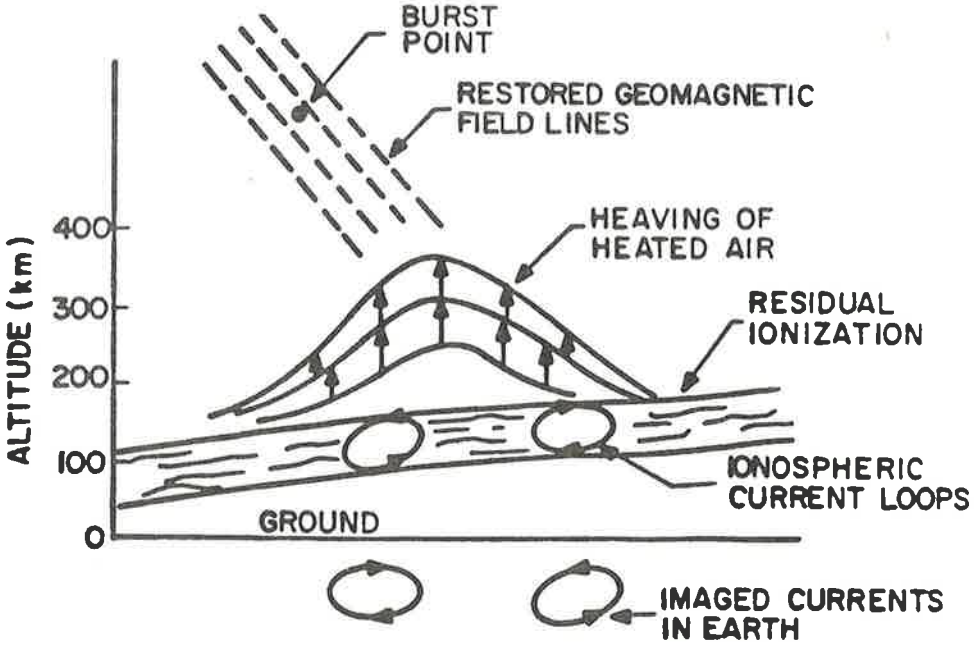

Fig. 3. Generation of late-time MHD-EMP. (Greater than 10 seconds)

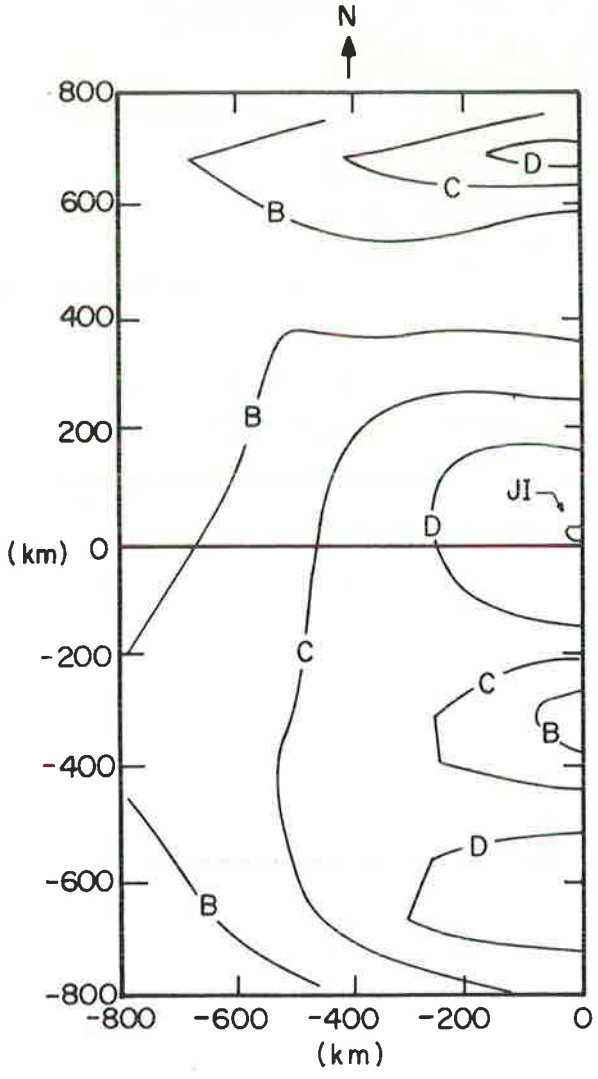

Contour	Gauss
B	0.002
C	0.004
D	0.006

Fig. 4. MRC Starfish simulation surface magnetic field contours.

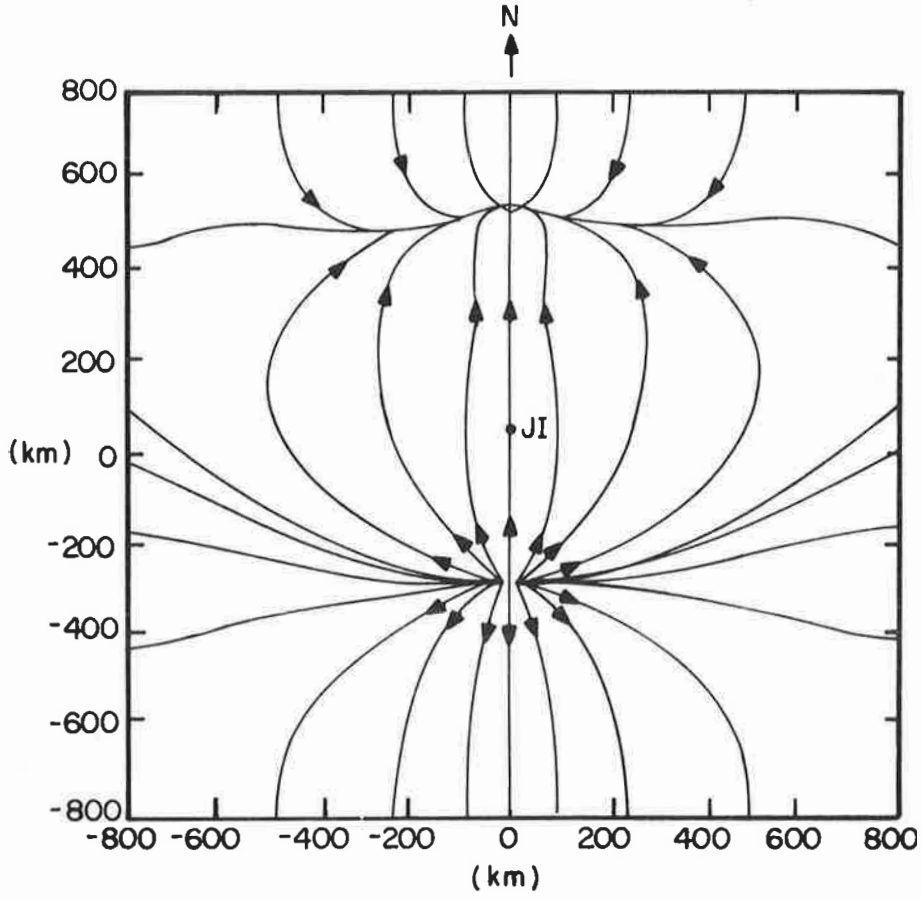

Fig. 5. MRC Starfish simulation surface magnetic field direction.

with the change in magnetic flux environment caused by the MHD-EMP event. It is the existence of this electric field environment which serves as the direct stimulus to the electric utility network. This electric field arises from the interaction of the MHD-EMP magnetic field and the finite conducting earth. The electric field of interest is tangential to and located at the surface of the earth.

The relationship is based upon the impressed magnetic field density computed from the MICE/MHDEMP codes at the earth's surface. For a magnetic field density denoted as B_x, orientated in the x direction, the corresponding electric field which is locally orientated in the y direction and assumed to be independent of the x and y coordinates can be expressed as:

$$E_y(\omega) = \frac{1}{\sqrt{\sigma\mu j\omega}} j\omega B_x(\omega) \qquad (1)$$

where the earth is assumed to have an electrical conductivity of σ mhos/meter and a permeability μ equal to that of free space. Since equation (1) is of the form:

$$F(\omega) = G(\omega)\, H(\omega) \qquad (2)$$

It is possible to express equation (1) through the convolution operator as:

$$f(t) = g(t)*h(t) = \int_0^t g(t-\tau)h(\tau)\, d\tau \qquad (3)$$

Employing the appropriate transform pairs for equation (1) yields the following expression for the time dependent electric field in terms of the magnetic fields:

$$E_y(t) = \frac{1}{\sqrt{\sigma\mu\pi}} \int_0^t \frac{1}{\sqrt{t-t'}} \frac{\partial B_x}{\partial t'}(t)\, dt' \qquad (4)$$

The details of the above derivation are contained in Appendix A of this report. Equation (4) may be evaluated by direct integration or equation (1) may be evaluated in the frequency domain and the inverse transform taken numerically to obtain the time dependent, transient electric field.

In equation (4), the magnitude of the time dependent electric field is inversely proportional to the square root of the earth conductivity (σ). For the purpose of this report, a value of $\sigma=10^{-3}$ mhos/meter has been selected. A method to accommodate local earth conductivities different from the assumed value is discussed in Subsection 3.3.5.

For the MRC simulation of the Starfish event, the values of the electric field contours have been calculated as shown in Figure 6. The electric field direction is generally normal to the magnetic flux direction as shown in Figure 7.

2.4 MHD-EMP Electric Field Approximation

As indicated in the previous discussion of MHD-EMP fields, the behavior of the electric field is rather complicated. Not only does the electric field differ from the magnetic flux in its dependence on time, but the spatial dependence is geographically complex. A rigorous electric field environmental definition would require a numerical solution resulting in a set of spatial electric field contour plots and the corresponding directional plots at many discrete times after the burst. In lieu of this definition it is desirable to formulate more approximate models of electric field environment to simplify the power system assessment.

A first approximation could be constructed where the environment is defined as an electric field which is spatially uniform for the system or facility under investigation. This uniform field has a given time dependence. Field polarization is taken into account by the assumption that the field is always parallel to a conductor, thereby providing a "worst case" response.

In a sense, this approach is similar to what is done for the HEMP environment. For a system or facility whose physical dimensions are small compared to the distances over which the incident field changes, such an approximation may be acceptable.

In the case of a large, interconnected power system, the usual geographic size is much greater than the distance over which the field changes. This necessitates a more accurate, and complex, environmental definition.

One possible way to achieve this objective is to approximate the time dependent electric field as a product of three independent terms:

$$\bar{E}_t\ (x,y;t) = \varepsilon(x,y)\ \bar{e}(x,y)f(t) \qquad (5)$$

In this approximation we separate the time and spatial behavior of the electric field environment. The term $\varepsilon(x,y)$ represents the spatially dependent, time invariant magnitude of the field. The term $\bar{e}(x,y)$ is a unit vector describing the spatially dependent, time invariant direction of the field. The function $f(t)$ describes the time dependent, spatially independent behavior of the field. Using such an approximation, both small geographic and large geographic systems can be considered.

In order to more accurately conform to the origins of the MHD-EMP magnetic signal, it may be preferable to separate the definition of the electric field environment into a "sum of products" expression of the form:

$$\bar{E}_t(x,y;t) = \varepsilon_1(x,y)\bar{e}_1(x,y)f_1(t) + \varepsilon_2(x,y)\bar{e}_2(x,y)f_2(t) \qquad (6)$$

The first product term corresponds to the early MHD-EMP signal, while the second accounts for the later time environment. As a logical extension of the above, multiple MHD-EMP events could be formatted into a finite series of "sums of products" in an effort to describe the complete environment as one expression.

A conceptual example of an electric field format given by equation (5) is shown in Figures 8, 9, and 10. The data is derived from the MRC simulation of Starfish [5]. Figure 8 graphically illustrates a possible f(t) which is spatially invariant. Figure 9 depicts a time independent contour plot of electric field magnitude $\varepsilon(x,y)$ while Figure 10 is the corresponding unit vector function $\bar{e}(x,y)$. As of the date of this report, the authors have not examined the error introduced by representing the transient electric field in the above format.

2.5 Summary

In this section, the origin and characteristics of the MHD-EMP phenomena have been discussed. The environment of direct interest for power system assessment has been defined as the transient electric field tangent to and located at the surface of the earth. This electric field can be obtained from measured or simulated values of the change in magnetic flux density evaluated at the same location. There exists only a limited amount of test data obtained during actual nuclear bursts. The nature of the experiment precludes direct replication or additional opportunity. Environmental simulations, based on existing techniques, have achieved only limited success for the quantative emulation of the measured event.

In equation (5) an approximate representation for the electric field environment has been introduced which considers the spatial dependence to be independent of the time dependence. It is recommended that Oak Ridge National Laboratory (ORNL) evaluate the suggested format in conjunction with Defense Nuclear Agency (DNA) and other MHD-EMP researchers so that future investigations of the environments also include studies of how to reasonably represent the electric field in a directly usable form for power system assessment.

This recommendation is made in support of the ORNL intent to develop a set of environmental scenarios serving as the inputs to power system risk assessment studies. Employing the scenarios in the preliminary risk assessments to be performed during Phase II of the

research may result in a smaller subset of environments which can then be considered as "reasonable worst case" inputs.

Adoption of the suggested format may also allow for the following:

- Environmental definition which can accommodate multiple MHD-EMP generation in an efficient manner by the addition of "sum of product" terms as required.
- Development of a public domain definition of the environment available to power systems researchers interested in assessing the system vulnerability under the MHD-EMP environment.

Given the inherent uncertainty contained within the measured data and the simulation techniques, use of an approximate format of the suggested type may be a practical and cost efficient vehicle to facilitate system assessment.

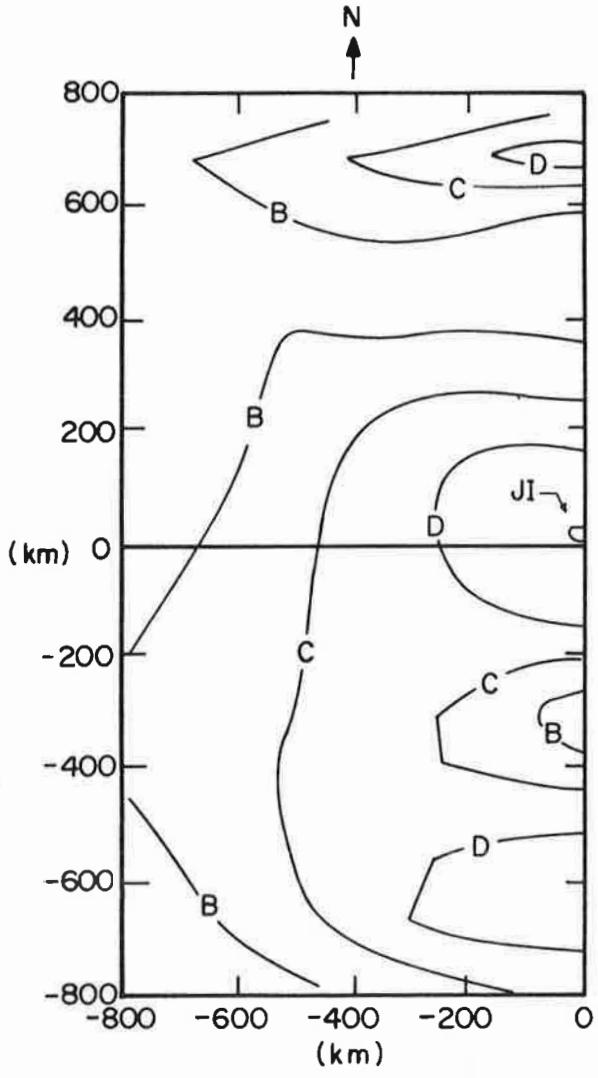

Contour	Volts/km
B	0.81
C	1.63
D	2.44

Fig. 6. MRC Starfish simulation surface electric field contours.

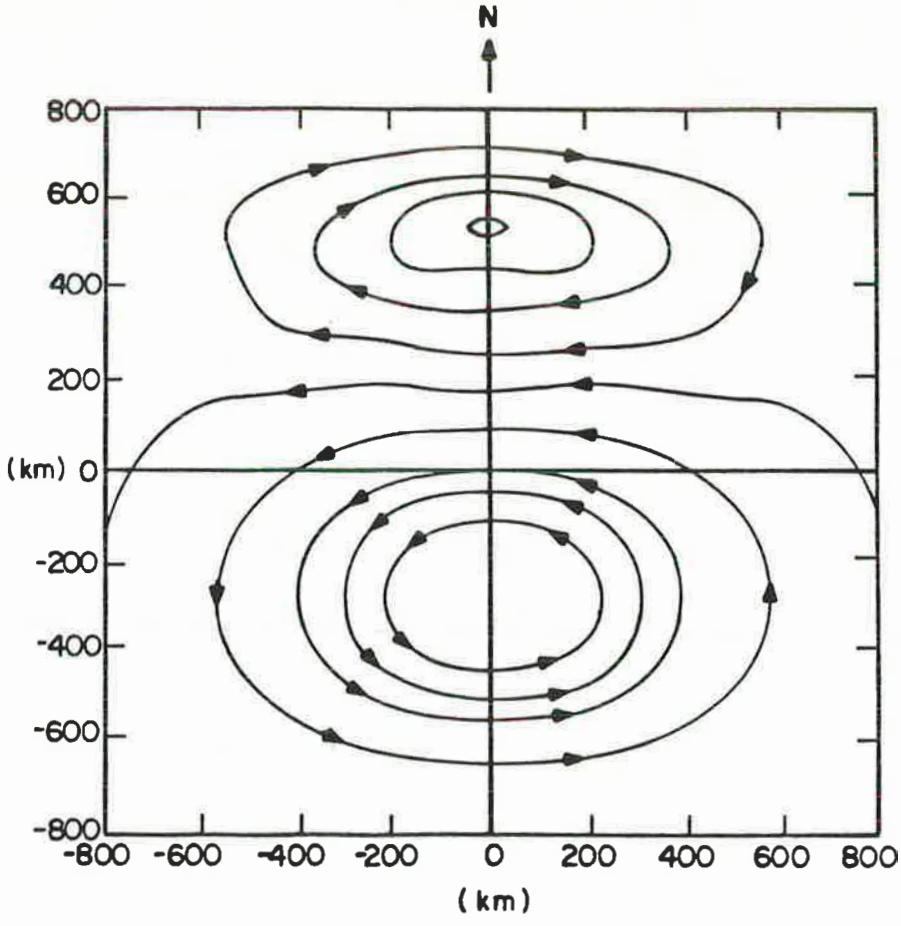

Fig. 7. MRC Starfish simulation surface electric field direction.

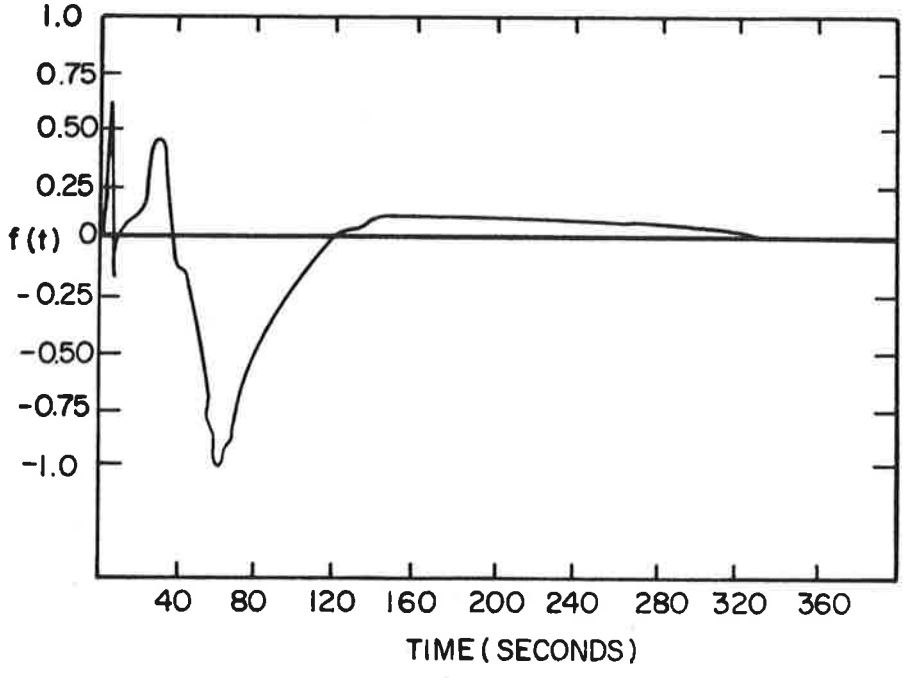

Fig. 8. Spatial invariant f (t) function for MHD-EMP.

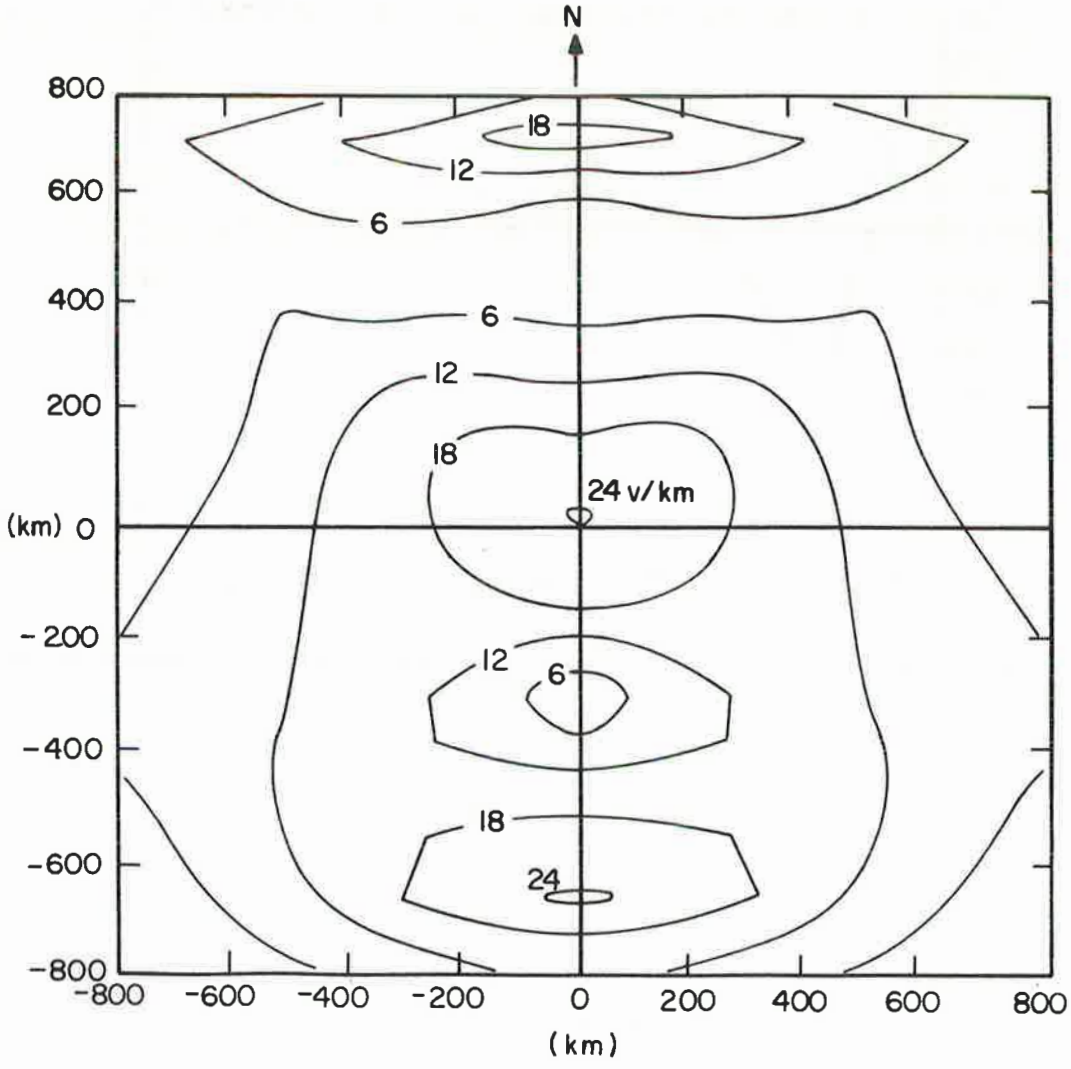

Fig. 9. Magnitude function $\varepsilon(x,y)$ for MHD-EMP.

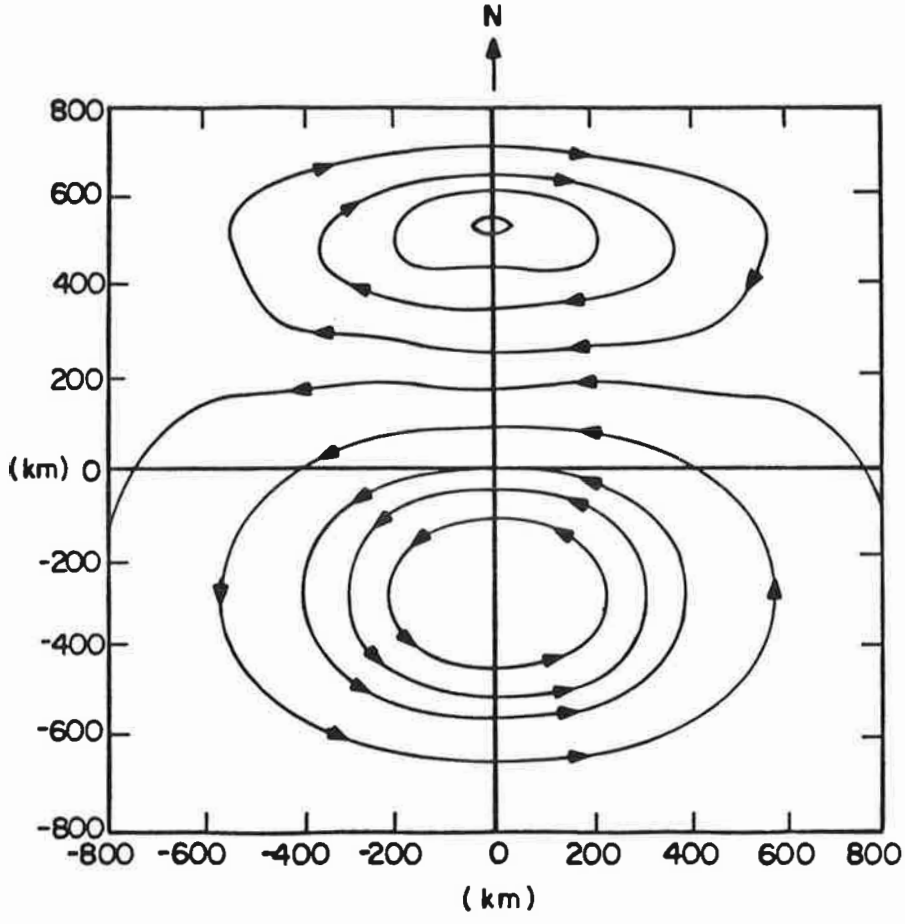

Fig. 10. Unit vector function $\bar{e}(x,y)$ for MHD-EMP.

3. MHD-EMP COUPLING TO POWER SYSTEMS

3.1 Introduction

The MHD-EMP environment, detected and simulated as a transient change in the ambient magnetic flux density at the earth's surface, can be considered in terms of the corresponding transient electric field. It has been shown that this electric field, tangent to and located at the surface of the earth, exhibits complex spatial and time characteristics.

In order to understand the coupling of the electric field to power system lines and components, this section begins with a discussion of the frequency distribution of the magnetic and electric transients. Such analysis is necessary to determine if the power system excitation models must employ ac concepts or, if the spectral content is such, that the electric field can be reasonably approximated as a quasi-static (dc) excitation.

Since MHD-EMP environments can only be created by the detonation of a nuclear device at high altitudes over the earth's surface, it would facilitate the understanding of the environment if one could identify a phenomena, naturally occurring, whose transient electric and magnetic environment has similar characteristics to the MHD-EMP event. This section discusses geomagnetic storm phenomena as such a candidate environment. The investigation continues with a discussion of the electric field coupling mechanism to single and multi-conductor lines. The approach taken by geomagnetic storm researchers is shown to be consistent with and essentially equivalent to a more general development based on conductor excitation via electromagnetic field scattering theory.

The section concludes with a simple numeric example illustrating the coupling of the MHD-EMP electric field environment to a three-phase 161-kV transmission line. The response of interest is expressed as the very low frequency circulating current similar to geomagnetic induced current.

3.2 Spectral Analysis of MHD-EMP Fields

In order to understand and model the coupling of the MHD-EMP electric field environment to the power system network, it is necessary to examine the spectral content of such excitation. MHD-EMP is different from HEMP and SREMP in that the electric fields produced are characterized by low field magnitudes (volts/km rather than kilovolts/m), limited spectral content and longer time duration (hundreds of seconds rather than microseconds). These differences suggest that a separate coupling mechanism and power system network models should be developed specifically for MHD-EMP assessment.

Based upon the time domain plots constructed by Longmire [1] for the magnetic flux density and corresponding electric field, a frequency domain plot for each was constructed. The results are shown as Figure 11 and Figure 12. It is significant that even though the time domain MHD-EMP behavior has several rapidly rising spikes at elapsed times less than 40 seconds, the corresponding spectrum is seen to contain only low frequency components less than 1 Hz. In the case of magnetic flux, above 0.05 Hz, the spectral components are two orders of magnitude below the primary spectral components at lower frequencies.

To assess the coupling mechanism of such excitation to the power system, one can consider an appropriate system response function. Such a function might be the respective current flowing in a conductor for a unit excitation in the frequency domain. If the transient behavior of this response function has a characteristic time which is less than typical signal times, it is reasonable to construct a coupling model of the system using dc concepts only. In the frequency domain, this implies that the network will have natural resonances at frequencies higher than those contained in the driving waveform and that a constant is all that is needed to represent the system coupling response. A reasonable break point frequency for power system networks is on the order of 0.1 Hz. The MHD-EMP spectral distributions strongly suggests that a reasonable coupling model may be constructed where the electric field takes the form of dc excitation and the network topology for coupling is a multiple-source, dc resistive network.

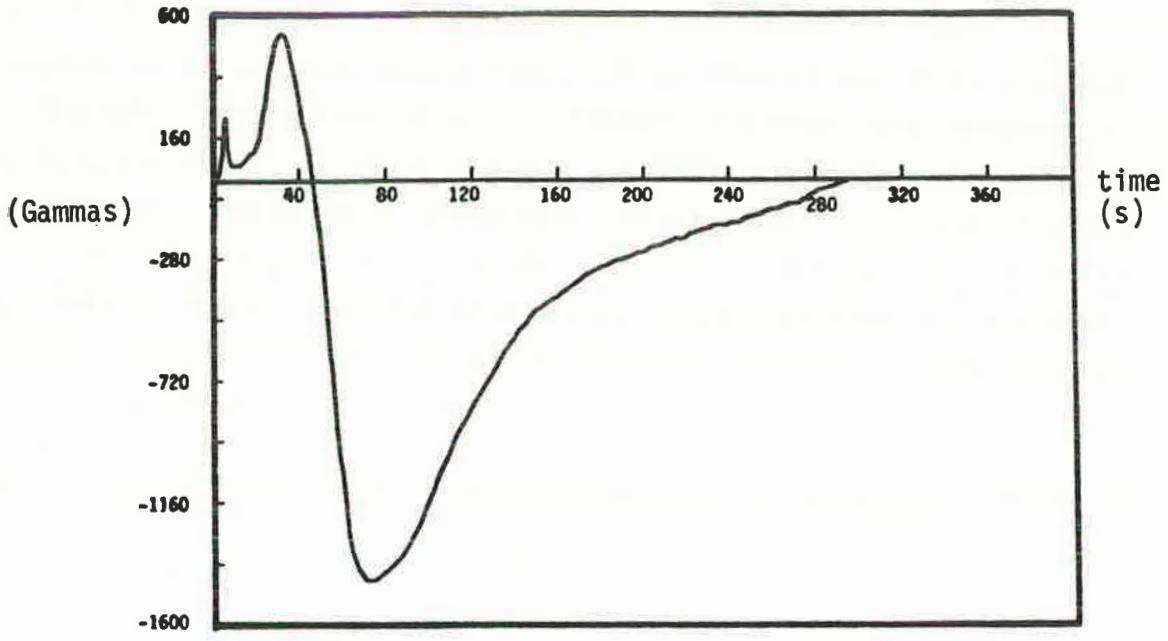

Fig. 11(a). Time domain magnetic flux density.

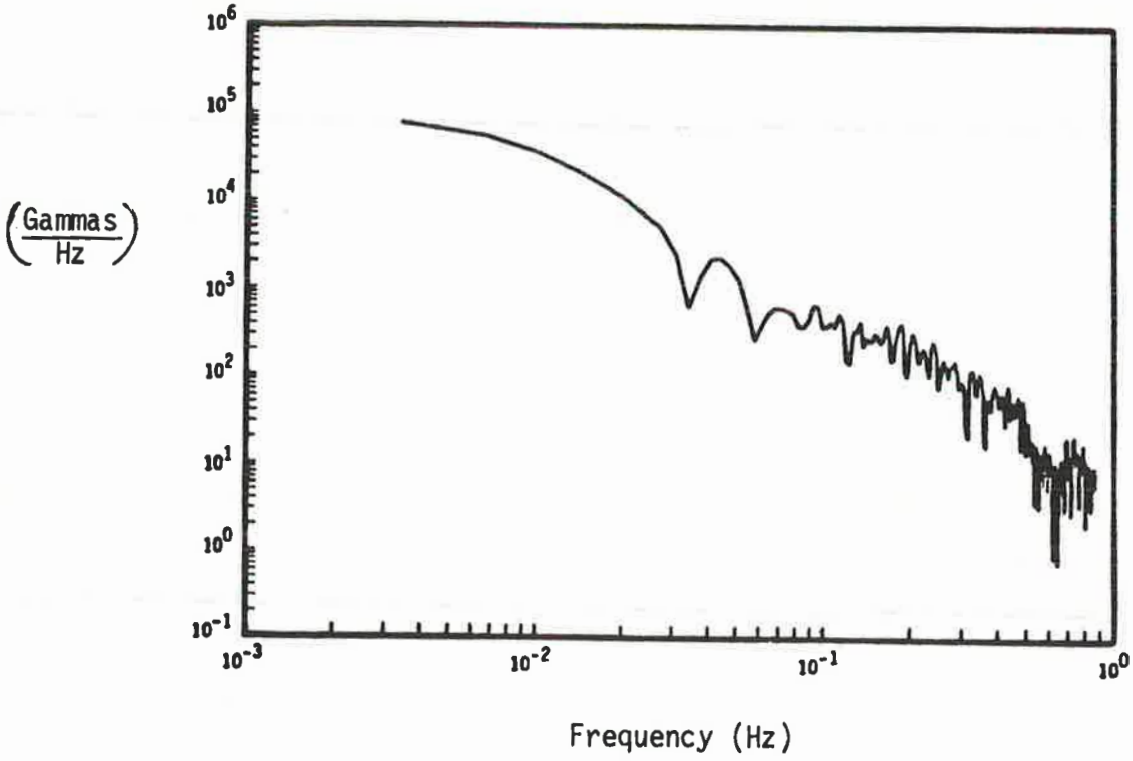

Fig. 11(b). Frequency domain magnetic flux density.

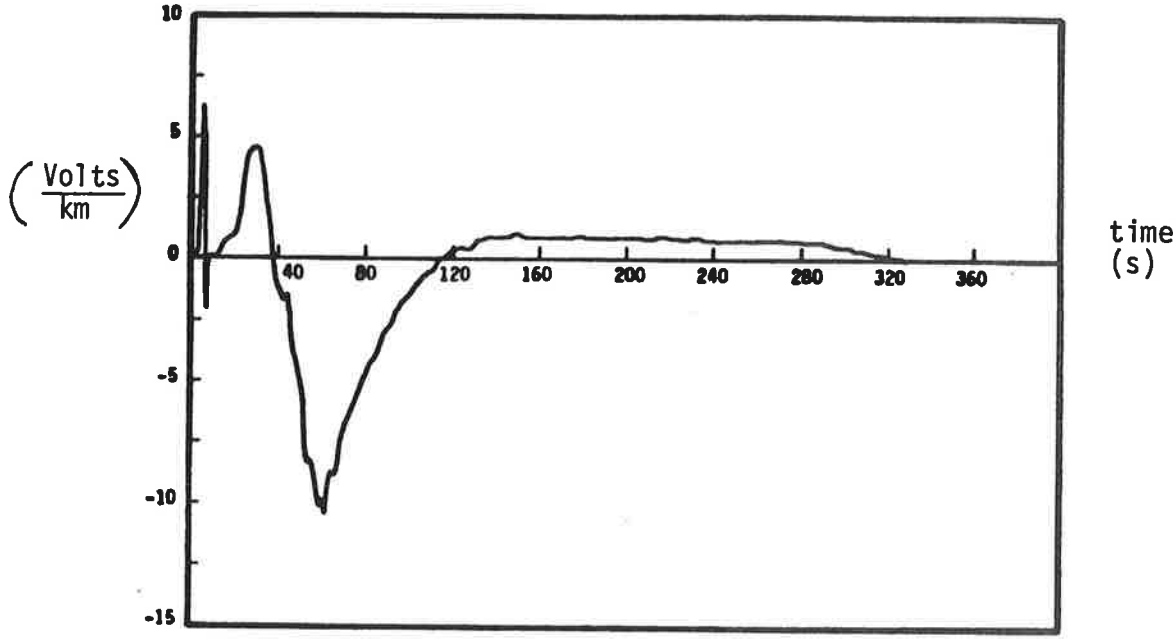

Fig. 12(a). Time domain electric field.

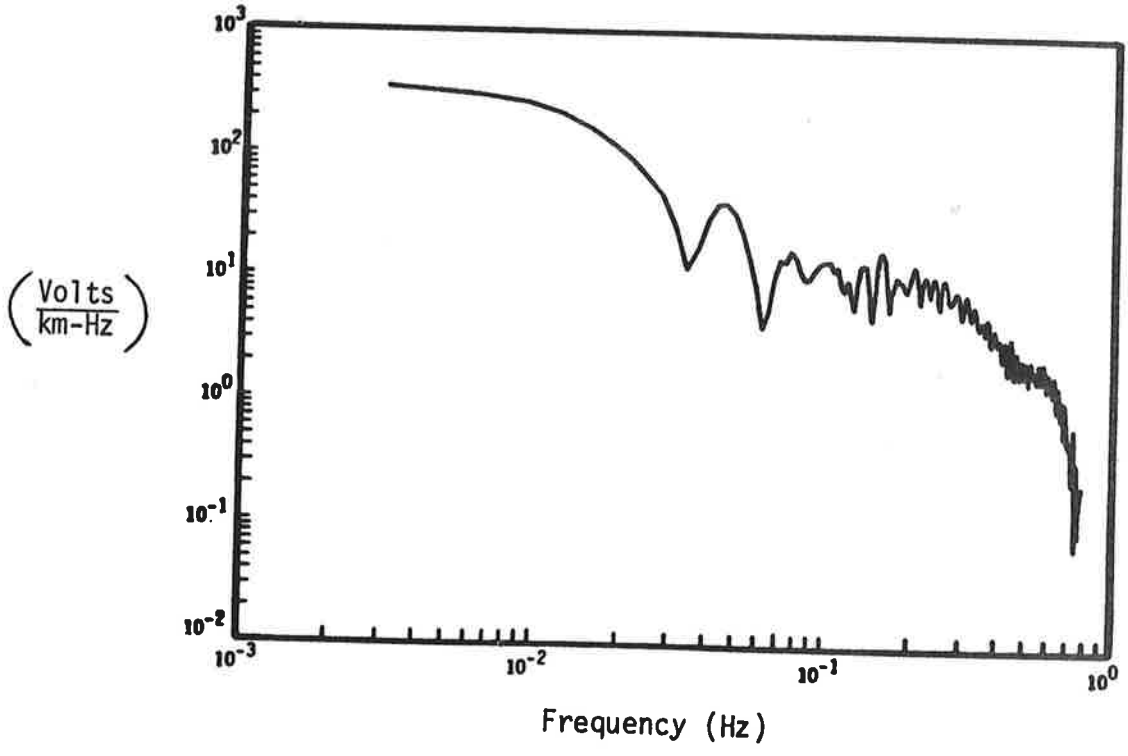

Fig. 12(b). Frequency domain electric field.

3.3 Comparison of MHD-EMP to Geomagnetic Storm Environments

Solar flare activity can result in the transient emission of particles which then are captured by and interact with the earth's ionosphere and magnetic field. The corresponding transient variations in the ambient magnetic flux density can be measured at the surface of the earth. For power systems analysis, this phenomena has been defined by the term geomagnetic storms. A typical magnetometer record for such phenomena is shown as Figure 13. The particle interaction is thought to cause extensive changes in the topside ionosphere and has been modelled as a trans-global ring current. For the northern hemisphere, this circulating current is postulated to exist at altitudes above 100 km and located approximately 60^{o} north latitude.

It has been known for over thirty years that geomagnetic storms have the potential to damage or operationally impact electric power systems. From an engineering perspective, the interaction of the impressed magnetic signal on the earth can give rise to earth-surface potentials (ESP). For power system lines which are grounded at both ends, at remote locations, the ESP stimulus results in a corresponding circulating current in the line with a ground return path. This very low frequency "quasi-dc" has been defined as geomagnetic induced current (GIC). Analysis of the geomagnetic storm environment and its impact on electric power systems have been extensively investigated by Albertson et. al. in a series of technical papers and reports [6,7,8,9]. The initial parameter which invites comparison between these two independent events is the measured magnetometer data. The large negative transient contained in Starfish, as shown in Figure 11(a) has the same shape as the negative transient, located between 60 and 120 minutes, in the storm signal (Figure 13). Although the Starfish data exhibits a faster rise time plus a larger $|\Delta \bar{B}|$ magnitude, from a qualitative perspective, the measured events have many similar features. A more detailed comparison is presented below.

3.3.1 Duration

The duration of geomagnetic storm effects on electric power systems in a specific geographic region will be on the order of tens of minutes to hours with degree of intensity varying unpredictably from low to severe during the storm period. As indicated in Figure 13, this environment is characterized by brief periods of relatively rapid signal change contained within much longer periods of constant signal magnitude. When the relationship between the change in magnetic flux density ($\Delta\bar{B}$) as a function of time and the corresponding electric field as computed by equation (4) is examined, it can be shown that, for a constant earth conductivity, a magnetic signal variation of 200 gammas or less occurring in a time period of 60 minutes will result in a very small electric field. The electric fields of significance are produced by the rapid $\Delta\bar{B}/\Delta t$ events. Due to the long duration of the environment, it is not practical for geomagnetic storm researchers to evaluate the entire event [6]. A reasonable "worst case" approach has been adopted to consider only major signal variations and compute the "worst case" electric field that can exist for a time period of minutes.

The magnetic environment created by a single MHD-EMP event is expected to effectively last no more than 400 seconds. Thus, although a finite sequential series of MHD-EMP events will not continuously illuminate the power system for any length of time comparable to geomagnetic storms, the MHD-EMP transient excitation is similar to the reasonable "worst case" geomagnetic storm excitation in terms of duration.

3.3.2 Magnetic Flux Density

A key element in the characterization of both environments is the magnitude and time rate of change of the surface magnetic flux density. For geomagnetic storm signals, the range of the time rates of change (Δt) extends from 30 seconds to 3600 seconds. A typical "severe" environment at the northern border of the continental United States could be considered as a $|\Delta\bar{B}|$ = 800 gammas with a corresponding Δt = 180

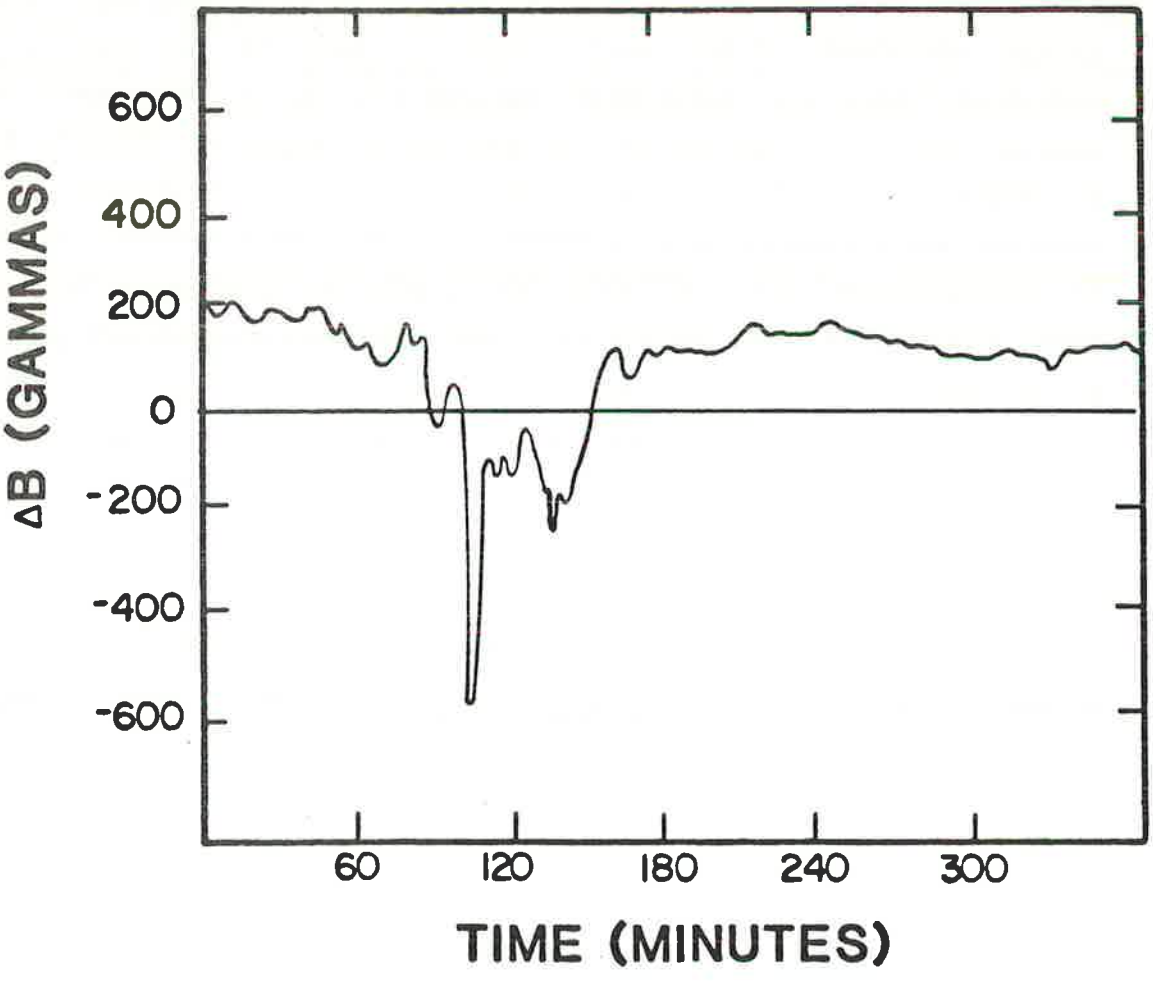

Fig. 13. Typical measured magnetometer data in the Northern United States for a geomagnetic storm.

seconds. On a normalized base this environment can be expressed as 4.44 gammas/second.

In contrast, MHD-EMP magnetic transients have time rates of change for measured events (Starfish) from four seconds to forty seconds (late negative heave). Expressed on the same normalized base, this approximately equals 30.0 gammas/second to 18 gammas/second. Longmire's estimate for Starfish over mid-America would essentially double the above values.

3.3.3 Electric Field Magnitude

Previous research in geomagnetic storm environments [7] have numerically evaluated a "severe" electric field at 6.2 volts/km (10.0 volts/mile) for electric power systems located near the Canadian border and an assumed earth conductivity of 10^{-3} mhos/meter. On the same assumption, the MHD-EMP electric field as shown in Figure 9 can achieve an approximate value of 24 volts/km (38.4 volts/mile) at select locations.

A frequency comparison can be undertaken if a period is developed for these aperiodic transient electric fields. For a period constructed from the time rate of change of the form:

$$T = 2\Delta t \qquad (7)$$

The geomagnetic storm contains an equivalent frequency of 0.003 hertz or less. The MHD-EMP stimulus can range from 0.07 hertz to less than 0.01 hertz (Starfish late negative signal). This quantification supports the contention that both types of field environments can be considered as "quasi-static" (dc) excitation in power system analysis.

3.3.4 Electric Field Spatial Characterization

The fixed location, in the Northern hemisphere, of the auroral current zone created by the geomagnetic storm results in a storm invariant spatial distribution for the electric field. Maximum field exposure is experienced at or under the current zone. The tangential

surface electric field is polarized in a near east-west direction. For areas of constant earth conductivity, the local field magnitude decreases proportional to latitude.

As is clearly evident by Figures 9 and 10, the spatial characterization of the MHD-EMP electric field is a direct function of blast location. For constant earth conductivity, a longitudinal shift in the blast location will result in an equivalent shift for the field pattern. Analysis requiring a latitudinal shift in blast location is more complex. This movement will impact both the pattern and the magnitude of the electric field due to burst position as a function of the angle of the earth's magnetic field. It may be necessary to compute a new MICE/MHDEMP simulation for any scenario which requires a latitudinal shift.

3.3.5 Earth Conductivity

For both environments, the local magnitude of earth conductivity at or near the surface will determine the local magnitude of the electric field. An approach to this concern can be developed from the relationship between the magnetic flux density and the electric field shown as equation (4). The conductivity (σ) is constant with respect to the integration. The electric field can be computed assuming a uniform value for conductivity. To accommodate a local conductivity different from the assumed value, the electric field magnitude can be corrected by a constant K as follows:

$$K = \frac{1}{\sqrt{\sigma/\sigma_0}} \qquad (8)$$

where σ = actual conductivity

σ_0 = assumed conductivity

For example, assume an electric field of 10 volts/km computed for a σ_0 of 10^{-3} mhos/meter must be adjusted for a σ of 10^{-4} mhos/meter.

Using equation (8) the required correction factor is computed as K=3.16 and adjusted value of the electric field is 31.6 volts/km.

In summary, despite the quantitative differences between the two phenomena, there exists sufficient similarity to invoke many of the methodologies and models developed for geomagnetic storm assessment as directly applicable for MHD-EMP investigation.

3.4 MHD-EMP Excitation of A Single Conductor

In Section 3.2, it has been shown that the MHD-EMP electric field environment can reasonably be approximated as a very low frequency (quasi-static) excitation for grounded systems. Previous research [6] in the coupling of like fields, due to geomagnetic storms, has used the auroral current/magnetic flux density to compute the tangential electric field at the surface of the earth. An earth surface potential model (ESP) is then evoked to calculate the geomagnetic induced current (GIC). An alternate, yet consistent approach is to use the description of the surface electric field to determine the total incident field on a conductor and thus the excitation source. This method employs electromagnetic field scattering theory, modified as required to account for lossy ground and finite conductor parameters.

A general development of this approach is discussed as Appendix B of this report. As indicated in this Appendix, the very low frequency of the MHD-EMP electric field allows the following simplifications:

- The long wavelength of the exciting field allows for a reasonable approximation of the electric field at the height of the conductor to be equal to the field at the surface of the earth.
- Since any vertical field component at the earth's surface is neglected, the incident field at the conductor is only the tangential field along the conductor.
- For any conductor section the very low frequency (quasi-static) incident field eliminates any need to incorporate capacitive and inductive conductor parameters. The conductor is characterized solely by resistive elements.

The conductor excitation is in the form of a distributed, per-unit length voltage source whose value is identical to the incident plus ground-reflected electric field tangential to the conductor at every point expressed as:

$$V_s(y) = E_t^{inc}(y) + E_t^{ref}(y) \qquad (9)$$

The excitation is polarized only in the horizontal plane. The total voltage source (V_o) for the length of conductor is computed by:

$$V_o = \int V_s(y)dy = \int [E_t^{inc}(y) + E_t^{ref}(y)]dy \qquad (10)$$

Knowledge of the total series circuit resistance allows the response, the corresponding quasi-static current, to be computed by Ohms Law.

3.5 MHD-EMP Excitation of A Multi-Conductor Line

As discussed in Appendix B, general field coupling to a multi-conductor line will result in each conductor having a different voltage source, depending on the variations of the phase of the incident field as it passes over the line. In practice, however, for the quasi-static MHD-EMP fields, these phase variations are negligible. Each conductor excitation source can be modeled as equal and identical to the field tangential to the surface of the earth. Given this approximation, it can be shown, by general network theory, that the identical voltage sources located in the equivalent conductors can be shifted to and equivalenced by a single voltage source in a reference conductor (earth) with no change in the net response of the circuit. Thus, the source of line excitation can be considered as a voltage source in or at the surface of the ground. The line response can be determined from an earth-surface potential approach.

It should be noted that this approach is correct only as long as the voltage sources in each conductor are identical in phase as can be approximated in the case of MHD-EMP excitation. In the case of higher frequency excitation, such as that encountered in high altitude EMP

(HEMP), the phase differences of the incident field from conductor to conductor are important and a surface ESP approach cannot be employed.

3.6 Transmission Line Sample Calculation

The concept of MHD-EMP power system excitation, and the computation of the response current is illustrated in the following example. Consider a hypothetical 161-kV single circuit (three-phase) line connecting substations A and B. The spatial orientation of the line and the MHD-EMP electric field environment is shown as Figure 14. The location of the burst is at origin coordinate (0,0).

The MHD-EMP electric field environmental parameters are as follows:

- Magnitude function $\varepsilon(x,y)$ as shown in Figure 14. For this example, the magnitude is set equal to 20 volts/kilometer for the entire line. The voltage source will be modeled as an earth-surface potential (ESP).
- Unit vector function $\bar{e}(x,y)$ as shown in Figure 14. The unit vector general direction is from east to west with the polarization as shown.
- Time function $f(t)$ as shown in Figure 8.

The above characterization is consistent with the MHD-EMP electric field approximation discussed in Section 2 of this report. The 161-kV line parameters are as follows:

- Total length (L) of the line is 170 kilometers.
- Per-unit resistance of each conductor is 0.06 ohms/kilometer. Total conductor resistance (R_L) is calculated by the product of the per unit resistance and the length of the conductor. In this example R_L is equal to 10.2 ohms.

The substation parameters are as follows:

- At each substation the line is terminated by a two-winding transformer as shown in Figure 15. The wye-delta winding configuration serves to isolate the 161-kV line from the remaining grid for a dc analysis.

Each transformer wye winding resistance (R_y) is equal to 0.18 ohms per phase.

- At each substation there exists an additional termination ground resistance equal to 1.0 ohms from the wye winding neutral to a remote ground point.

The three-line dc model circuit is shown in Figure 16 of this report. The effect of any shield wires has been removed from this example calculation.

To facilitate calculation of the MHD-EMP field coupling to the 161-kV line, the line has been partitioned into three segments as shown in Figure 17. For each section, the line and the exciting field have been translated to their equivalent north-south and east-west components. The excitation is computed for each section as shown in Table 1.

Table 1

EXCITATION OF 161-KV LINE BY SECTION

Section	Length(Km)	E-Field(V/Km)	Excitation(Volts)
1	28.0 $\angle 90^0$	20.0 $\angle 270^0$	(560)
	48.5 $\angle 180^0$	0.0 $\angle 180^0$	0.0
2	38.1 $\angle 270^0$	20.0 $\angle 270^0$	762
	22.0 $\angle 180^0$	2.0 $\angle 180^0$	0.0
3	50.0 $\angle 270^0$	18.8 $\angle 270^0$	940
	50.0 $\angle 180^0$	6.8 $\angle 180^0$	340

For each section, the local excitation is the product of the line length and the tangential electric field at this spatial location. Due to the specific orientation of this line and the electric field direction, the local excitation for Section 1 is assumed to be opposite in sign with respect to the remainder of the line. The net total excitation (V(t)) is the sum of the individual section excitations. In this example V(t) is equal to 1482 f(t).

For this example, the initial line response of interest is the magnitude and direction of the neutral current $I_N(t)$ caused to flow by voltage source V(t). To facilitate this calculation the equivalent single-line dc model is constructed as shown in Figure 18. The resistance of each parallel line conductor can be set to an equivalent equal to $R_y/3$. The same logic is employed for each transformer to achieve an equivalent parallel winding resistance equal to $R_y/3$. The voltage source is set at 1482 f(t).

The corresponding neutral current $I_N(t)$ is computed using Ohms Law. In this example $I_N(t)$ is equal to 268.5 amperes f(t). A graphic illustration of this response current is shown as Figure 19. An approximate value for each phase dc magnitude can be determined as one-third of the neutral current magnitude.

3.7 Summary

Spectral analysis of the MHD-EMP magnetic flux density and surface to tangential electric field indicates only very low frequency content. For power system analysis, the electric field can be considered as a quasi-static type of excitation. This type of excitation is qualitatively similar to that experienced by the power system during a geomagnetic storm. This similarity allows the adoption of existing geomagnetic storm analyses techniques and models for MHD-EMP investigation.

The interaction between power lines and the quasi-static electric field can be obtained from an earth-surface potential (ESP) or an incident field scattering theory development. For MHD-EMP environments, either approach yields comparable results. For digital code computational and modeling efficiency, the ESP excitation model requires fewer voltage sources for the same grid under analysis. As shown in the 161-kV line example, the response of interest (the circulating quasi-dc current) is a strong function of the spatial orientation of the line analysis, the corresponding electric field and the dc resistance values for line, transformer and ground termination model elements.

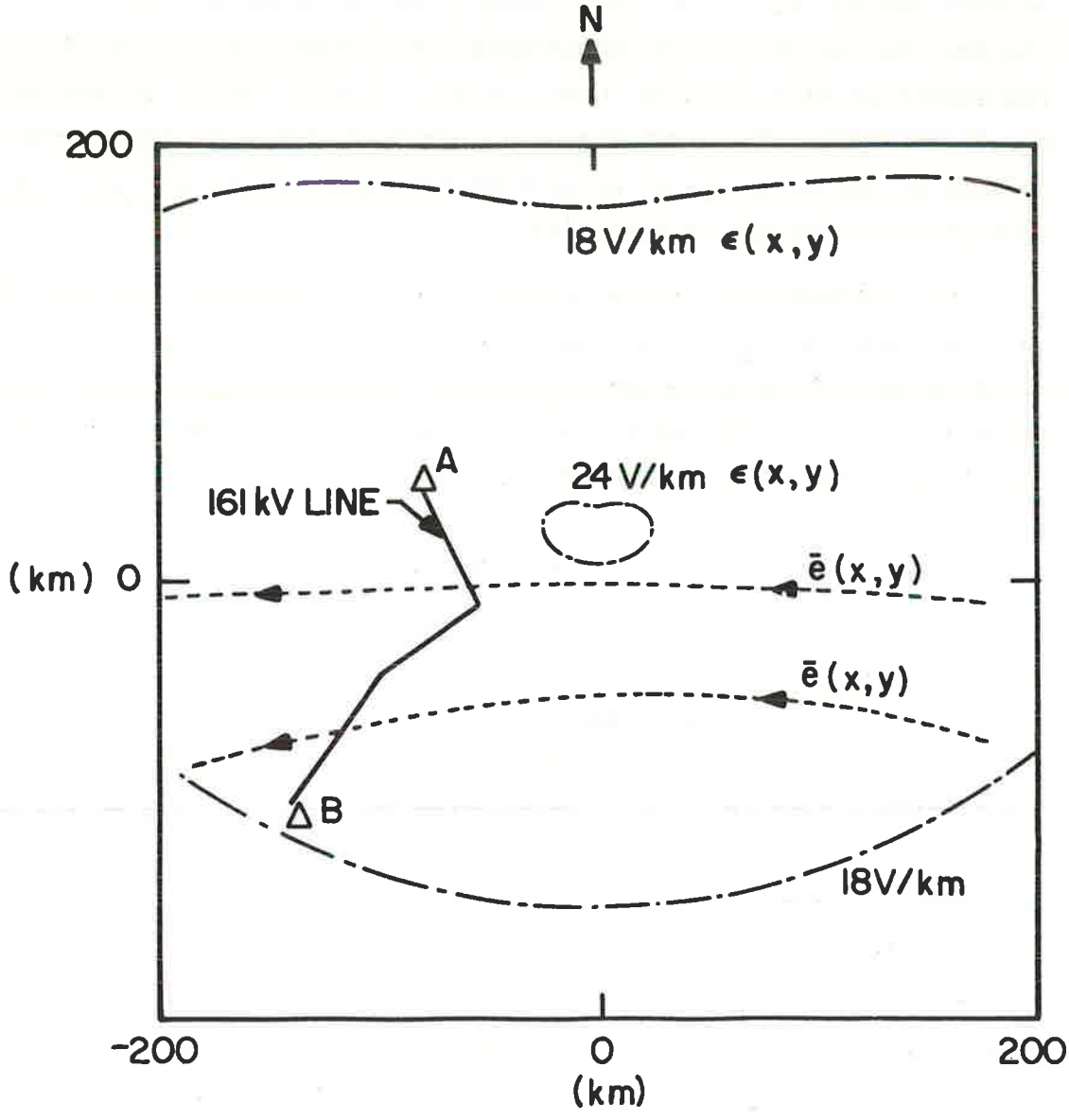

Fig. 14. Spatial orientation of 161-kV line and MHD-EMP electric field.

Fig. 15. 161-kV Circuit AC single line diagram.

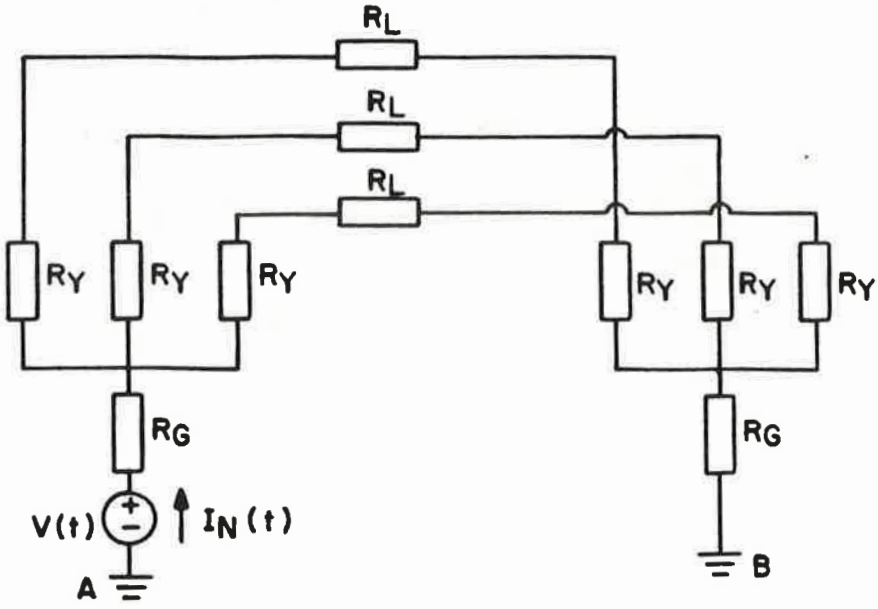

Fig. 16. DC model 3-line diagram for 161-kV circuit.

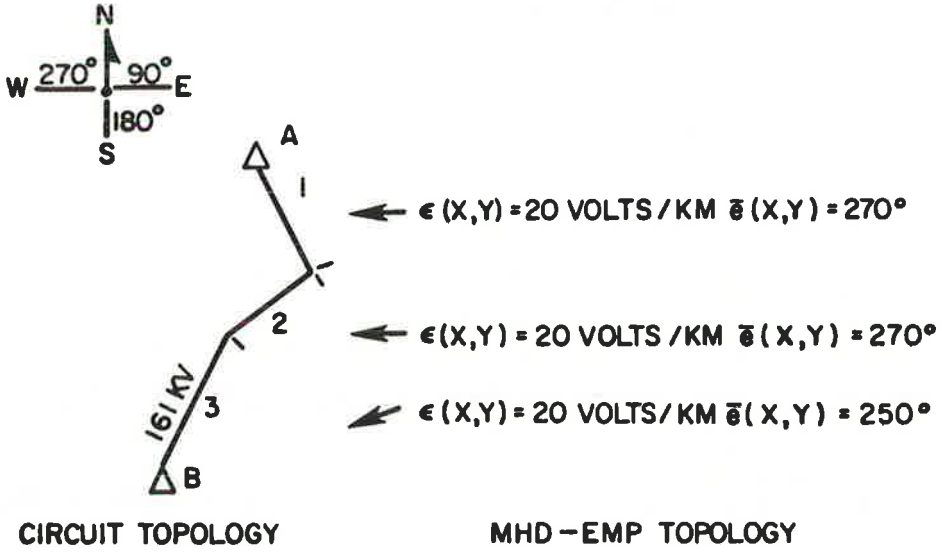

Fig. 17. Segmentation of 161-kV circuit to facilitate excitation calculations.

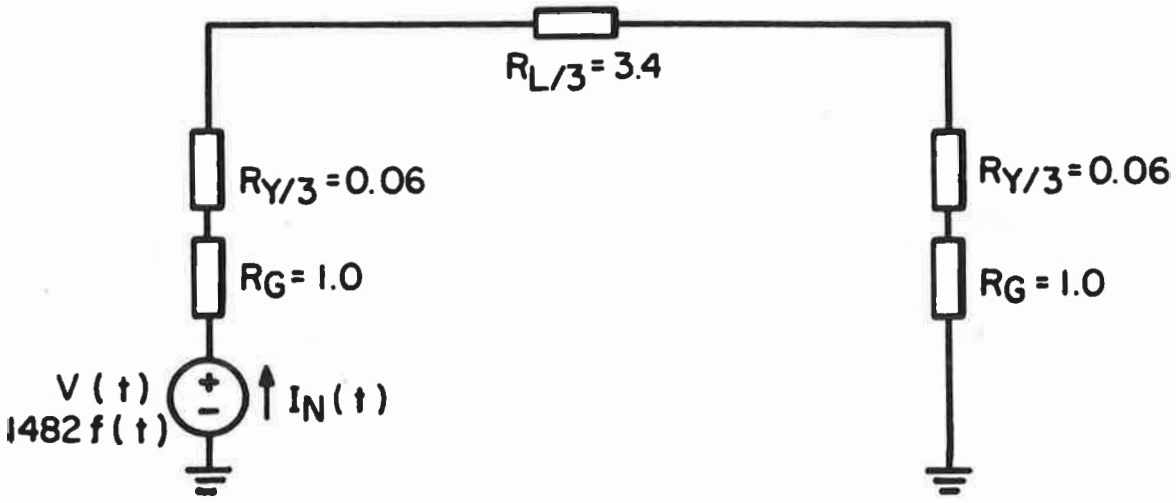

$$I_N(t) = \frac{1482\,f(t)}{2(R_G + R_{Y/3}) + R_{L/3}} = \frac{1482\,f(t)}{5.52}$$

$$I_N(t) \simeq 268.5\,f(t) \text{ DC AMPERES}$$

Fig. 18. 161-kV circuit modeled to calculate the MHD-EMP neutral current $I_N(t)$.

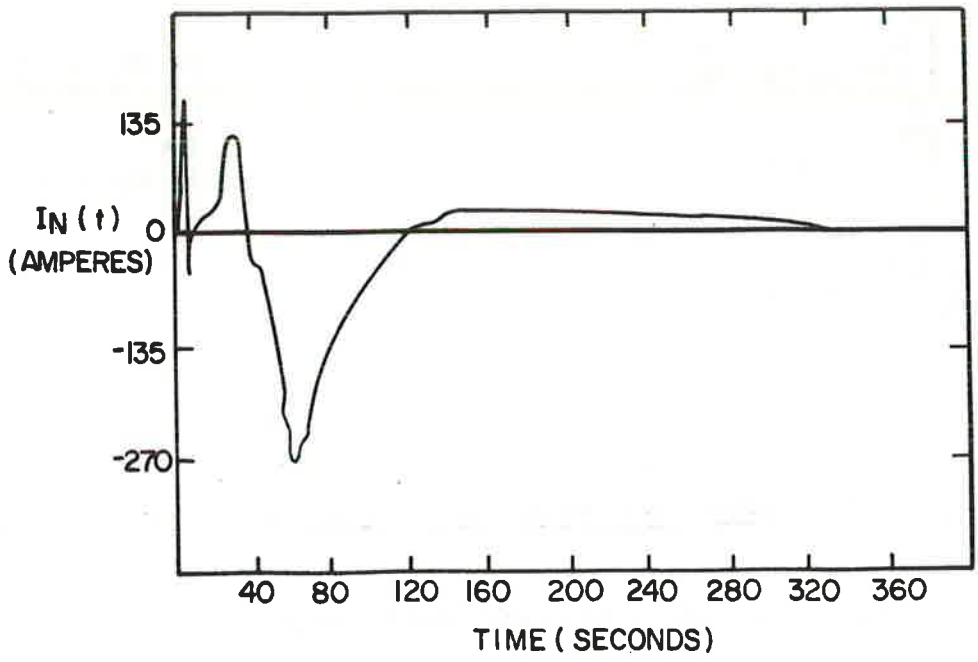

Fig. 19. Sample problem neutral current as a function of time for MHD-EMP excitation.

4. MHD-EMP ASSESSMENT METHODOLOGY

4.1 Introduction

This section discusses the overall development of a process to assess the effects of an MHD-EMP environment on electric power systems. The methodology must be considered in context with the entire event. For a single high-altitude nuclear burst, the MHD-EMP environment will always be preceded by an HEMP environment. As shown in Figure 20, the two distinct environments, as perceived by the power system, are separated in time. The system under investigation will sense and react to the existence of HEMP for seconds until the formation of the MHD-EMP environment. In power systems analysis, where devices operate in the order of 60 Hz cycle times and short-term stability is a concern, an elapsed time of second(s) between the two environments is a significant separation. The power system will change "state" due to the existence of HEMP, but many of the transient operations occurring within this change of "state" will essentially be completed within an elapsed time of seconds. The power system can be considered to be in a new "state" which serves as one set of initial conditions for MHD-EMP assessment.

This separation by "state" within the framework of an overall assessment technique, may also be required due to the vast differences in the natures of the environments and the corresponding power system modeling techniques. Initial investigation indicates that it may be practically impossible to employ a single set of models within a unified assessment code to simulate both HEMP and MHD-EMP effects. The environmental format suggested in this report may be applicable for single or multiple MHD-EMP environments only. The assessment of scenarios which require the simultaneous existence of both HEMP and MHD-EMP environments must be addressed in future research.

Investigation into the nature of the MHD-EMP phenomena indicates that a reasonable expression for the coupling of the environment to the power system can be expressed as a set of quasi-dc branch currents caused to flow in system lines and cables. This coupling response is

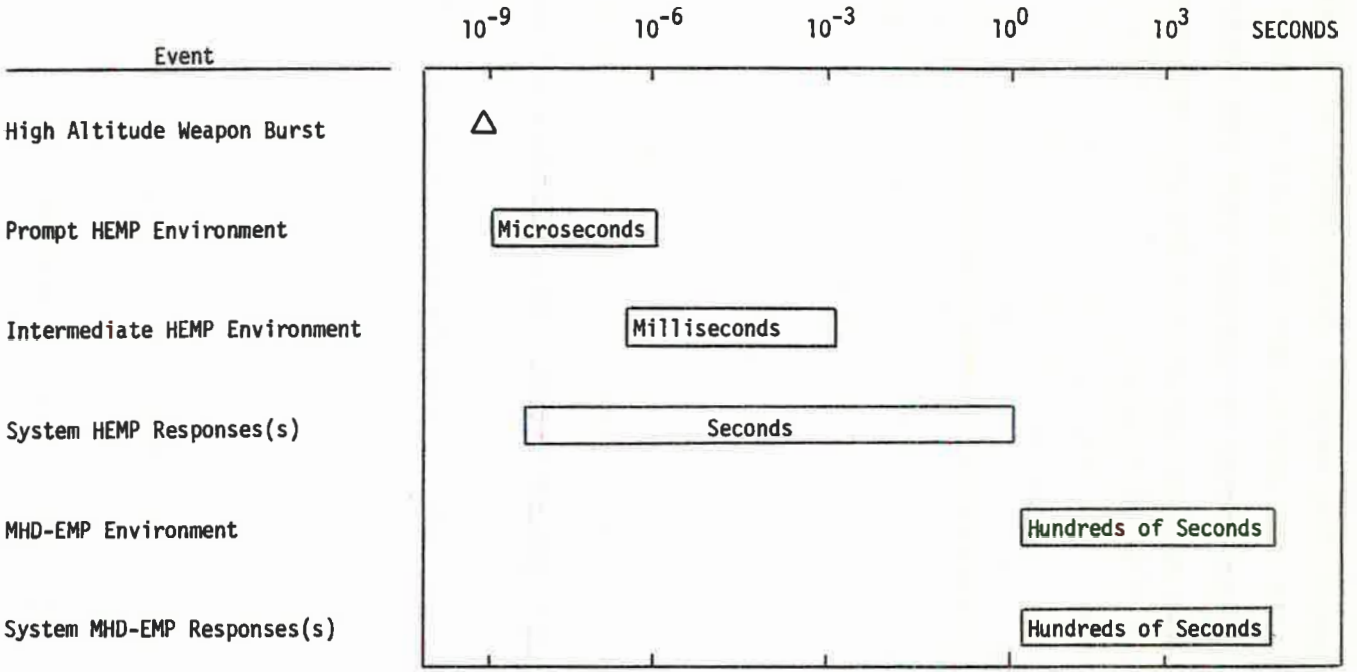

Fig. 20. Sequence of events for single, high altitude weapon burst.

qualitatively similar to the concept of geomagnetic induced currents (GIC) formed in response to the solar storm environment. Therefore, with an appropriate change in environmental definition, the MHD-EMP assessment methodology can build upon the existing body of research and analysis techniques developed to assess the impact of GIC. The assessment "wheel" needs not to be "re-invented" but rather adapted and expanded to suit the event. In a complementary manner, detailed assessment concerning the impact of MHD-EMP on the power system can lead to a greater understanding of the cause and effects of GIC on the same system.

4.2 Methodology Structure

By definition, methodology is a system of principles, practices and procedures applied to a set of knowledge to achieve a specified objective. The process is structured; it can be considered as a series of interrelated tasks. Each task may take the form of: (1) information gathering, the establishment of required data bases, (2) information transformation, the modeling and simulation of systems by analytical techniques, and (3) assessment, the comparison of two or more data bases in an attempt to quantify cause and effect relationships. The MHD-EMP assessment methodology has been developed within the context of this definition.

For the purpose of this report, the complete set of tasks which constitute the methodology process has been partitioned into several subsets which address specific aspects of the assessment. These subsets are defined as:

- MHD-EMP Coupling and System Response
- Power Transformer Analysis
- System State Analysis
- DC Transmission Analysis
- Generator Analysis
- Instrument Transformer Analysis

- Instrumentation Control and Protective Relay System Analysis
- Power Fuse Analysis
- Utility Communications System Analysis

The corresponding flowchart for each of these subsets is illustrated as Figure 21(a) through 21(i). The specific assessment formed from one subset may modify, or cause additional iterations of another subset. For example, the mis-operation of a protective relay scheme due to the presence of power frequency harmonic generation by power transformer increased excitation may result in breaker operation. The circuit switching creates a new set of conditions the impact of which can be assessed in terms of change in system load flow and transient stability. The complete process should include multiple, recursive assessments to understand the sensitivity of the range of individual component responses on total system performance.

4.3 MHD-EMP Coupling and System Response

The methodology process begins with the translation of the MHD-EMP environment, as seen by a power system grid, into the corresponding initial system response. This objective is achieved by the sequential accomplishment of four tasks.

4.3.1 Data Base: MHD-EMP Environment (A1)

In task A1, a data base is established to quantify the MHD-EMP environment defined as the tangential electric field $\bar{E}(x,y;t)$. A possible format can be similar to that proposed in Section 2.4. It is envisioned that a group of such data bases will be given to the research team by Oak Ridge National Laboratory corresponding to simulations of interest. The expression of the event in terms of the electric field only may serve to decouple the cause from the environment sufficient to consider the formatted data bases as "canonical" and therefore available in the public domain.

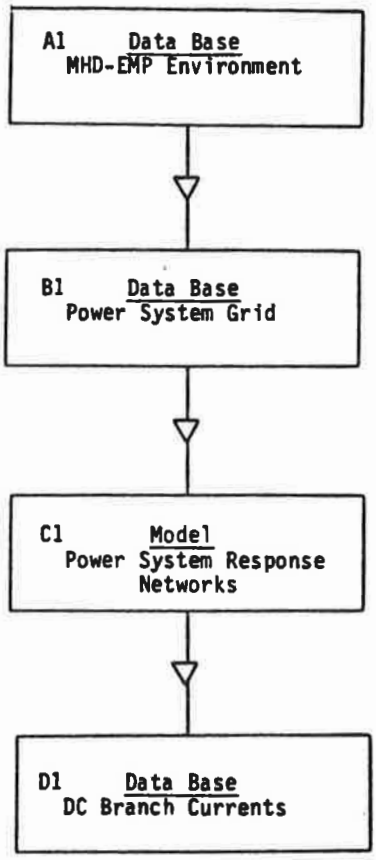

Fig. 21(a). Flowchart for MHD-EMP coupling and system response.

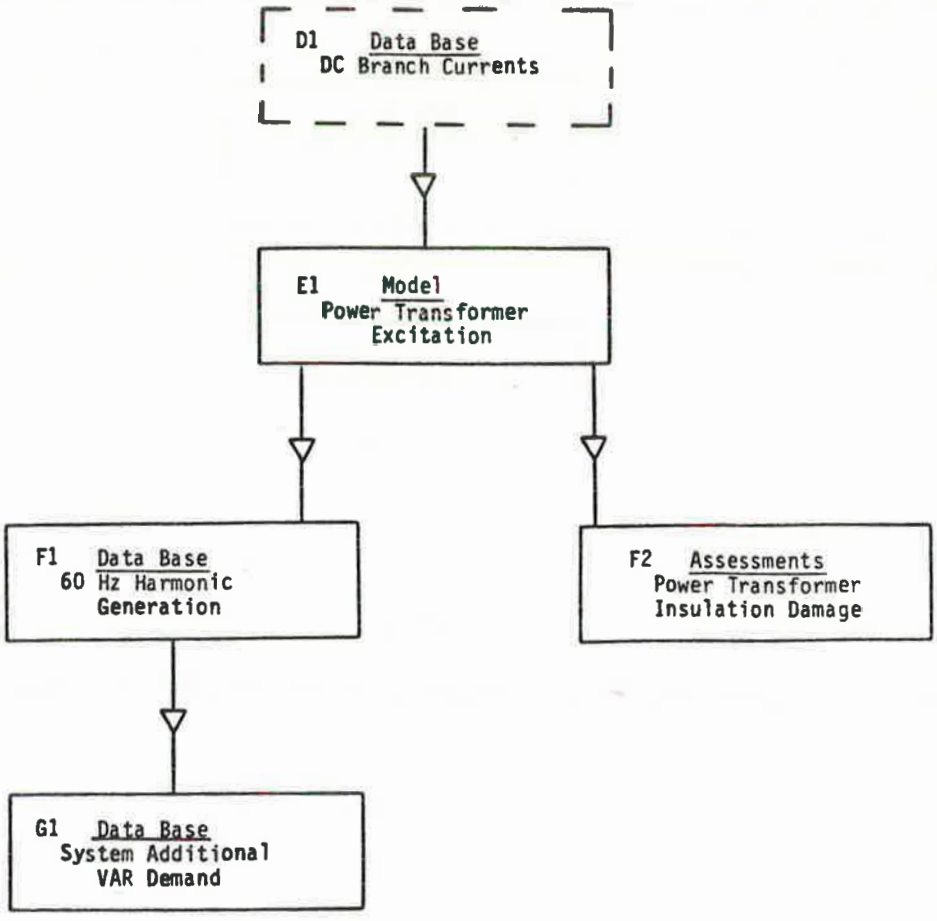

Fig. 21(b). Flowchart for power transformer analysis.

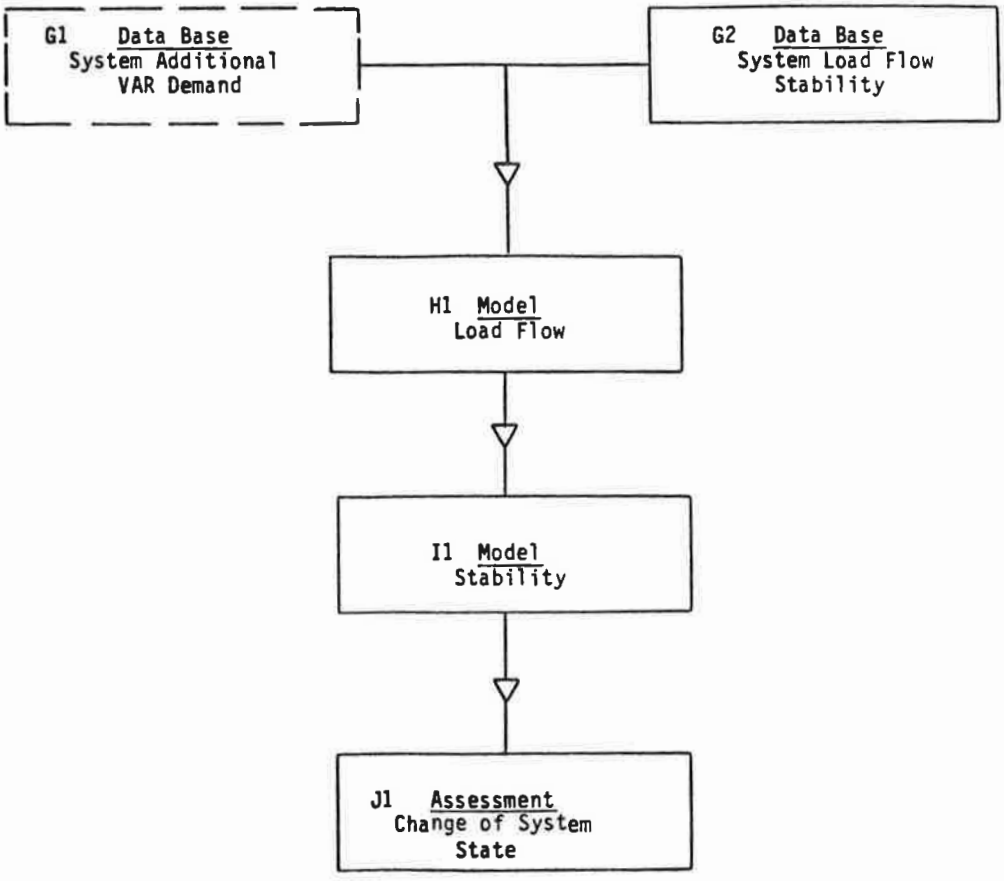

Fig. 21(c). Flowchart for system state analysis.

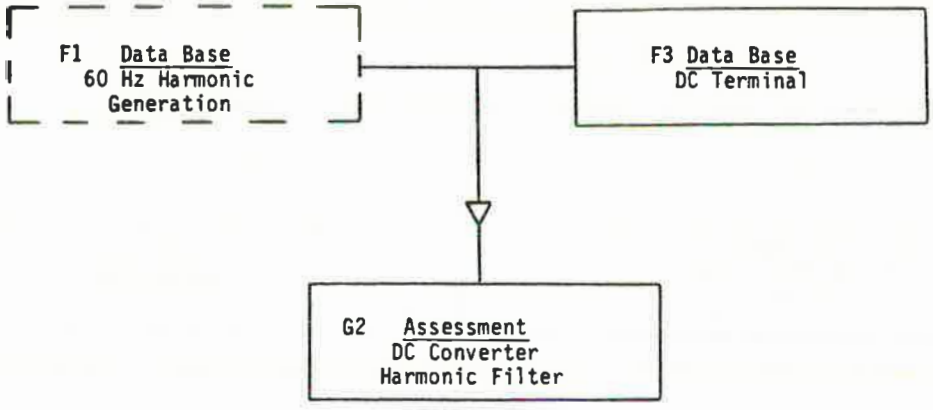

Fig. 21(d). Flowchart for DC transmission analysis.

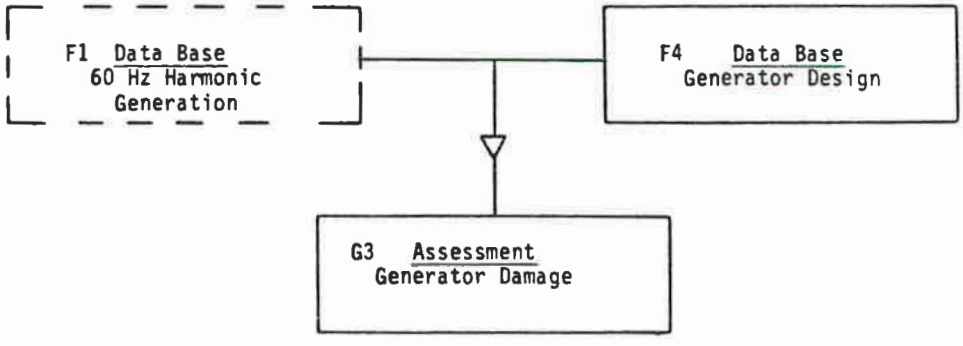

Fig. 21(e). Flowchart for generator analysis.

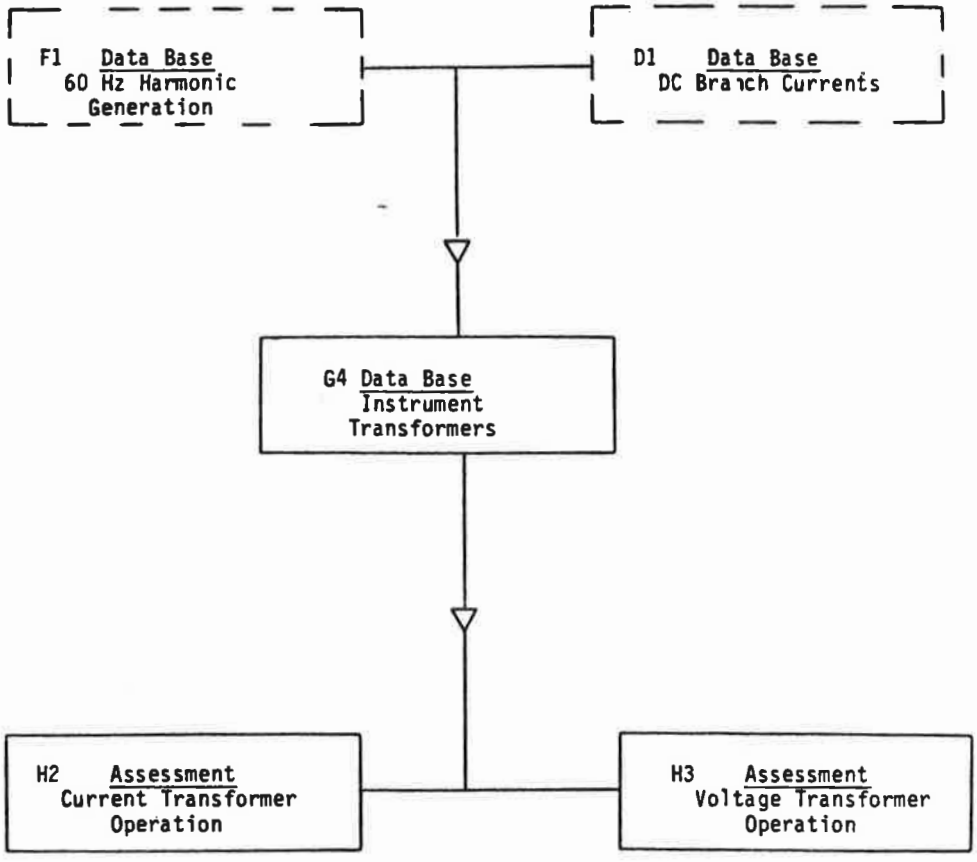

Fig. 21(f). Flowchart for instrument transformer analysis.

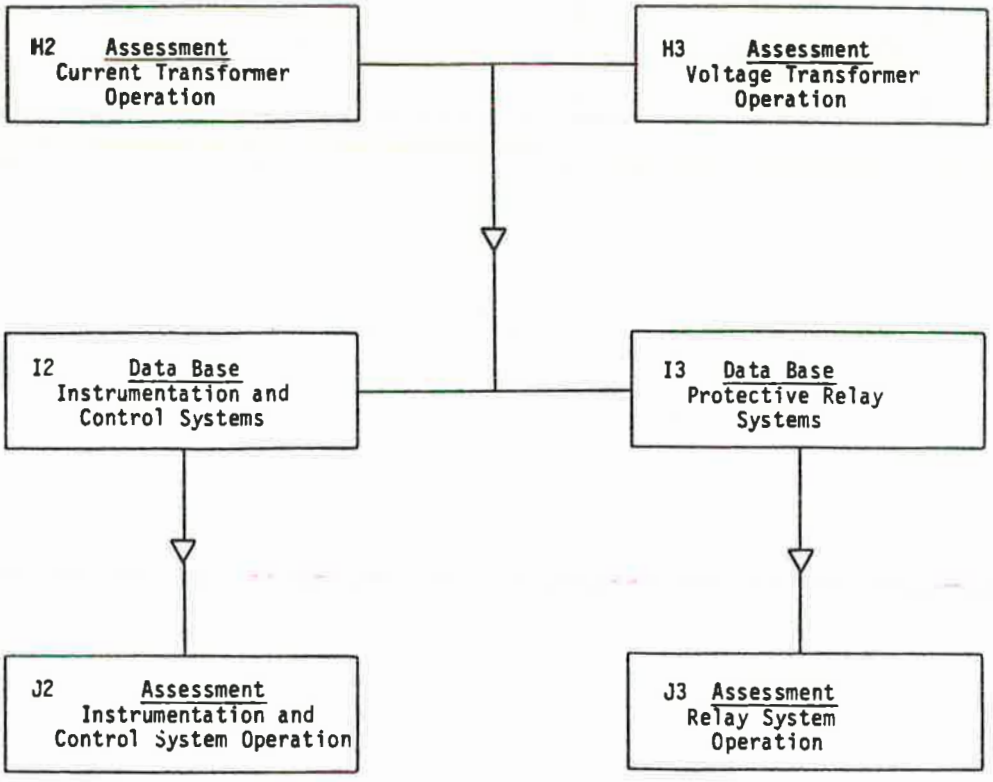

Fig. 21(g). Flowchart for instrumentation control system and protective relay system analysis.

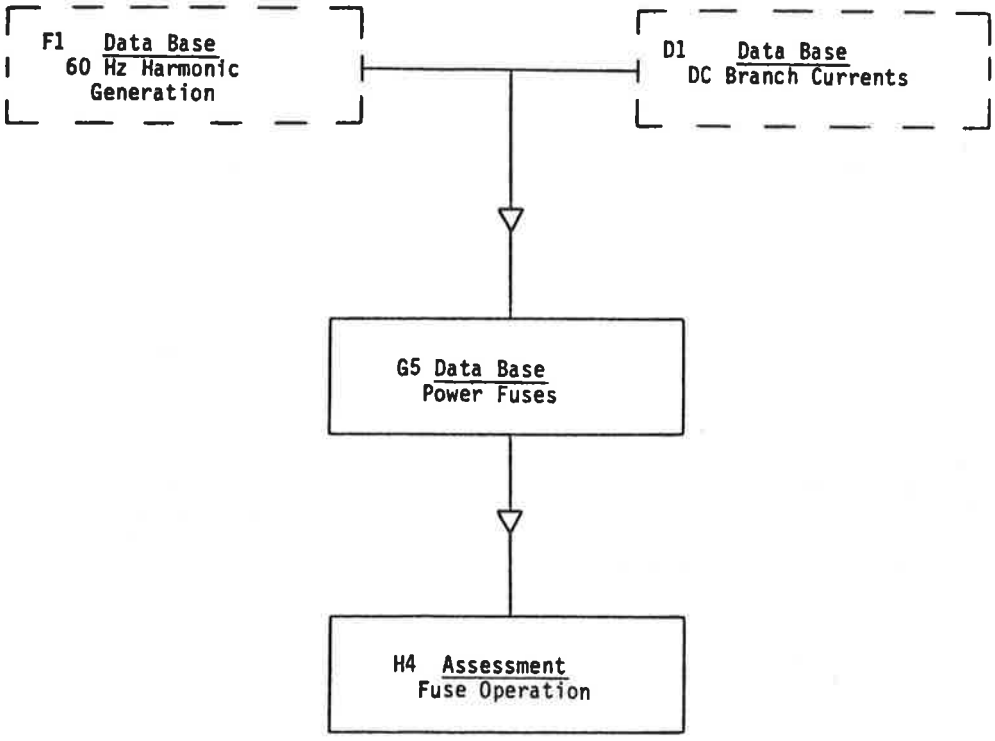

Fig. 21(h). Flowchart for power fuse analysis.

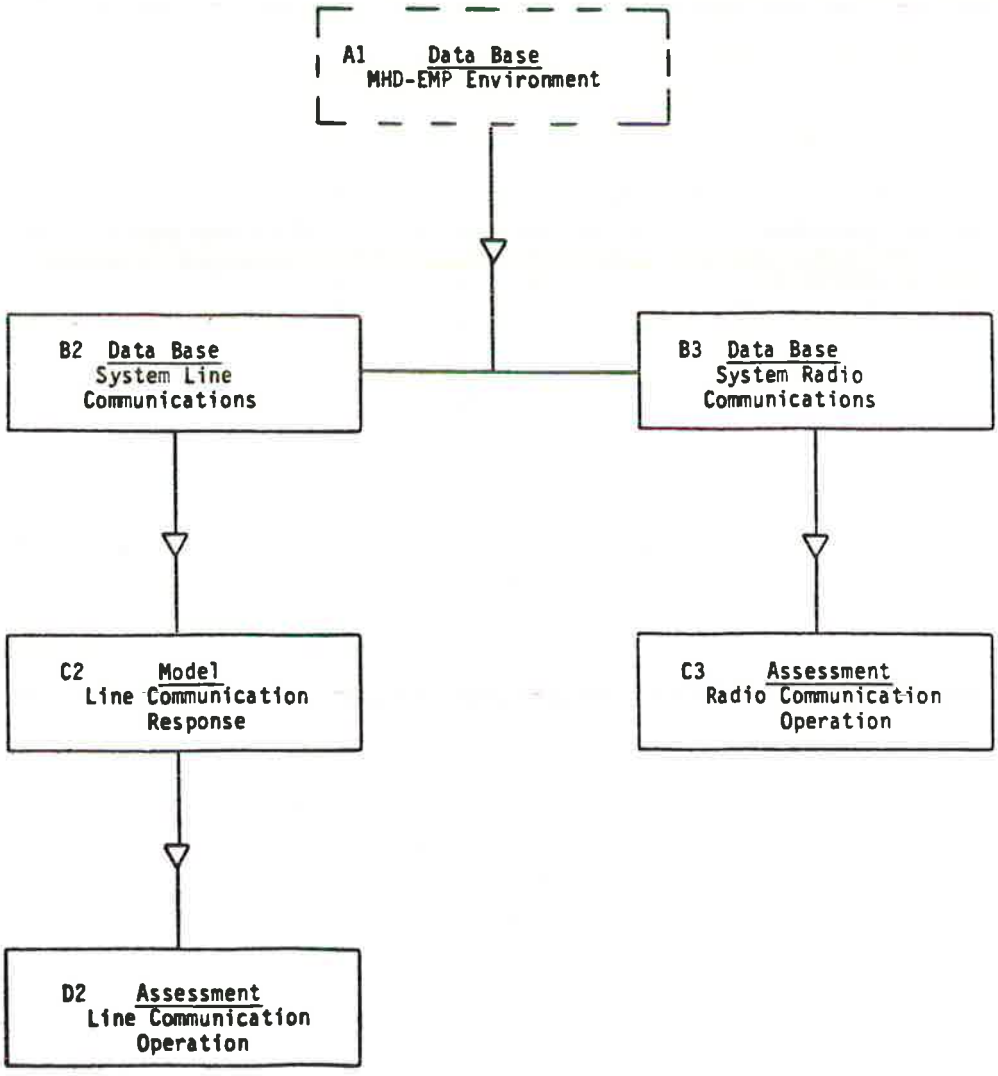

Fig. 21(i). Flowchart for utility communications system analysis.

The group of data bases will be used in Phase II of the Research Program to perform preliminary risk assessments. Based on the results of this analysis, a smaller set may be selected to reflect a "reasonable" worst-case environment(s). These environmental data bases will be used for more detailed assessments in Phase III of the program.

4.3.2 Data Base: Power System Grid (B1)

In this task, a data base will be established for the power system grid exposed to the tangential electric field. The data base must include the following information:

- "State" of the electric power system in terms of 60 Hz electric connection.
- Spatial orientation and circuit length for applicable transmission, subtransmission and distribution networks.
- DC resistance per unit length for the conductors contained within the above networks.
- Location, winding resistance and winding connection for all power transformer and shunt reactor banks contained within the grid.
- Location and terminating dc resistance for all power ground points contained within the grid.
- Location of all power system components, such as series capacitors which serve to block the flow of dc current.

4.3.3 Model: Power System Response Networks (C1)

In this task, the previously compiled data bases will be processed into a set of equivalent dc power system response networks. The number and complexity of these networks will be determined by the dc open-circuit nodes in the power system grid.

Each network will consist of lumped resistive branch elements and distributed dc voltage sources. The network will then be solved to compute the time varying dc branch currents. Additional discussion

concerning the topology, equipment models and dc source quantification within these networks is contained in Section 5 of this report.

4.3.4 Data Base: DC Branch Currents (D1)

This portion of the methodology concludes with the establishment of a data base which contains a listing of the time varying magnitude of all dc branch currents. The currents will be assumed to flow simultaneously with the 60 Hz current in applicable conductors and windings.

4.4 Power Transformer Analysis

It is known that the simultaneous ac and dc excitation of a power transformer can result in the following phenomena:

- Possible insulation deterioration or damage due to internal localized heating conditions.
- Harmonic generation due to transformer core half-cycle saturation.
- Increased transformer VAR requirements.

Each of the above conditions must be addressed by the methodology for those network branches where this type of excitation will occur. The data base containing the dc branch currents was established as task D1. The incorporation of this information with applicable transformer excitation models will allow for the assessment of potential insulation damage, and create both an harmonic data base and an additional VAR demand data base.

4.4.1 Model: Power Transformer Excitation (E1)

In this task, the dc excitation current is evaluated by transformer excitation models into an equivalent value for combined excitation. Tests on full-scale single-phase core-form transformers, as well as analytical studies [15] have shown that the equivalent ac exciting

current can be approximated by

$$I_{eq} = I_{ac} + K\, I_{dc} \qquad (11)$$

where

I_{dc} = dc current per phase
K = proportionality constant
I_{ac} = ac magnetizing current

A value of 2.8 for K has been found to fit data for GIC current magnitudes. Additional research should be performed to validate the approximation and the value of K for MHD current levels. It is instructive to note that for any appreciable dc level, the total equivalent exciting current I_{eq} can be roughly estimated by neglecting the I_{ac} term in equation (11). To illustrate this point, Table 4.2 depicts a range of approximate values of transformer ac excitation current for units of different voltage levels. In any assessment, actual transformer data should be employed.

Table 2

APPROXIMATE RMS EXCITING CURRENTS FOR POWER TRANSFORMERS

Nominal Winding Voltage (kV)	Percent of Full Load Current 0.5% (Amps)	1.0% (Amps)	4.0% (Amps)
69	.5	1	4
115	.82	1.66	6.63
230	1.66	3.31	13.25
345	3.5	7.0	28
500	6.15	12.3	49
800	8.2	16.4	65.7
1200	12.6	25.2	100.8

An example of a typical power transformer ac magnetization curve is shown as Figure 22. The data represents a medium size generator step-up unit. Normal operating conditions are at point A on the graph. By the relationship shown in equation (11), an additional dc excitation of 6.786 per-unit exciting current results in transformer operation at a 1.3 per-unit excitation level (point B). For a high-voltage wye-grounded winding whose 1.0 per-unit exciting current equals 7.0 amperes, (I_{ac}), a corresponding value of I_{dc} equal to 47.5 amperes (rms) is required.

Equation (11) has been derived for two-winding transformers. However, it can also be applied to autotransformers if an equivalent value for I_{dc} is first calculated to account for the unequal value of current in the series and common windings. For this case, I_{dc} is obtained by the expression:

$$I_{dc} = \frac{NI_s + I_c}{N + 1} \qquad (12)$$

where:

I_s = dc current in series winding
I_c = dc current in common winding
N = the turns ratio of the series winding with respect to the common winding (N_s/N_c)

4.4.2 Assessment: Transformer Insulation Damage (F2)

To access the possibility of insulation damage due to overexcitation, for any transformer, the value of I_{eq} obtained in task E1 is located on the transformer magnetization curve and the corresponding value of per unit excitation is obtained. Transformer damage threshold curves are normally presented as an inverse time, per-unit, excitation relationship. The interpretation is that, for a given per-unit excitation, a time duration of more than the corresponding time may result in thermal degregation of the insulation. It is important to understand that this comparison does not indicate the amount of damage but merely the threshold of damage. More detailed investigation is required to obtain the quantitative risk. A typical curve for the permissible short-time overexcitation of power transformers is shown as Figure 23. As indicated in the graph, a per-unit overexcitation equal to 1.3 (point B) which exists for longer than 18 seconds (0.3 minutes) may place the transformer at risk.

4.4.3 Data Base: 60 Hz Harmonic Generation (F1)

Another aspect of simultaneous excitation of power transformers is the local generation of 60 Hz harmonics in the exciting current. Spectral content of the current waveform has been empirically measured for various lower levels of dc current combined with normal ac excitation. Given the fact that the harmonic response is a complex function of transformer design and construction, the existing limited amount of test data cannot be expanded to achieve accurate generalization for all types and designs.

Within the power systems community there is general appreciation that the effects of increasing excitation are more pronounced in single-phase core form transformers. The relative impact on three-phase three or five-legged core designs or three-phase shell designs has not enjoyed the same degree of analysis to provide conclusive opinions. For autotransformer banks, a series of experiments conducted by Minnesota Power and Light indicates the following:

- For the same neutral dc magnitude, a bank comprised of three single-phase units is a greater harmonic generator than a corresponding three-phase autotransformer installation.
- The magnitude of the second harmonic current varies directly with the dc excitation.
- For the same neutral dc magnitude a three-phase shell-form autotransformer is a more significant harmonic current generator than a corresponding three-phase three-legged-core autotransformer.

In the absence of an extensive, existing data base for all common types of transformer constructions, additional research using both emperical and analytical techniques is required before this task can be accomplished.

4.4.4 Data Base: System Additional VAR Demand (G1)

As a pre-requisite to system analysis such as load flow and stability, the increased VAR requirements caused by transformer over-excitation must be developed.

This data base can be established in two ways [7]. The more precise approach for a given transformer design is founded on the harmonic content of the exciting current as follows:

$$Q = V \sqrt{\sum_{i=1}^{n} I_i^2} \qquad (13)$$

where:

Q = reactive power
V = RMS value of the applied 60 Hz voltage
I_i = RMS value of the ith harmonic component of the exciting current
n = highest order harmonic value

As an alternate approach, the reactive power could be approximated from the following:

$$Q = V\ (I_{exc} + K\ I_{dc}) \qquad (14)$$

where

- Q = reactive power
- V = RMS value of the applied 60 Hz voltage
- I_{exc} = normal RMS exciting current at normal operating voltage with no dc current per phase
- K = proportionality constant
- I_{dc} = DC current per phase

Previous research [7] has indicated that K=2.8 appears to be a reasonable approximation. It will be necessary to validate this approach for MHD-EMP level dc currents.

4.5 System State Analysis

It is expected that system reactive power requirements will increase due to power transformer increased excitation. The location and magnitude of these increased VAR demand loads have previously been established via the data base compiled in task G1. The impact of the system change in "state" must be assessed from the following aspects:

- System Load Flow
- System Short-Term Stability
- System Switching Surge

For each assessment several base-case steady state conditions for the power system must be specified. The additional reactive power demand would then be integrated into the system model to quantify response.

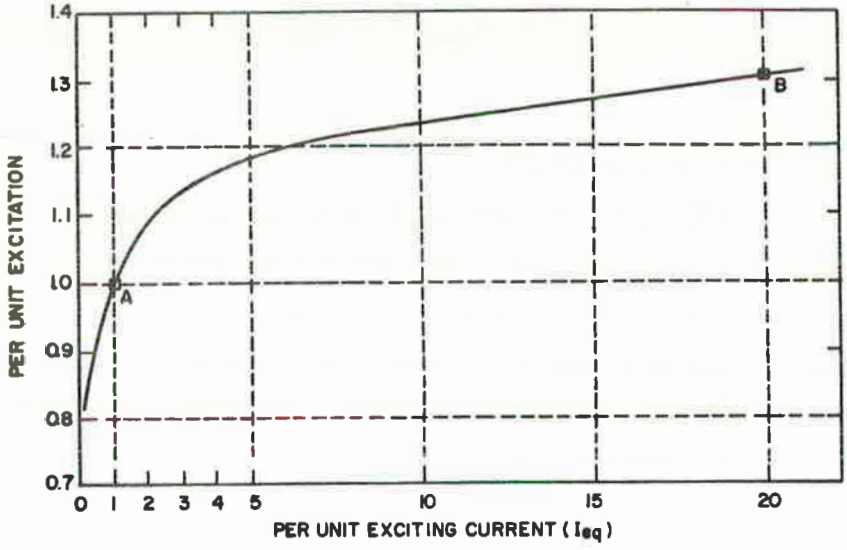

Fig. 22. Typical magnetization curve for power transformer.

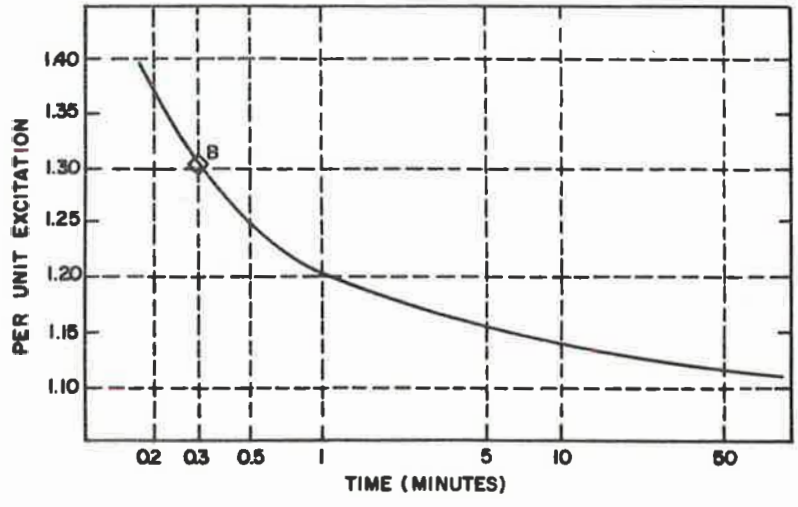

Fig. 23. Typical threshold of damage curve for power transformers.

4.5.1 Data Base: System Load Flow and Stability

This data base establishes the base case steady state condition of the system prior to the introduction of MHD-EMP effects. The type of data required is consistent with that usually given for conventional system studies. It must be emphasized again, that the state of the system, defined in this task, is "as modified" by any HEMP effects prior to the start of the MHD-EMP analysis.

4.5.2 Model: Load Flow (H1)

The required load flow models are identical to those contained in typical existing load flow digital programs. The additional reactive power demand at each bus of interest can be modeled as shunt reactive loads. The output of the simulation will reveal the following system summaries:

- New real and reactive power bus values and corresponding power flows in each line.
- Load area net generation and load, losses, tie line flows and net power export.
- Line losses.
- Buses with high and low voltages.
- Overloaded lines.
- Regulated bus data.

In those cases where system reactive power requirements exceed the capability of generation and other reactive power sources, the existing systems loads represented as constant MVA in typical load flow studies will be modified to become voltage dependent. At each affected bus, a percentage of the load would be changed from constant MVA to constant impedance, varying as the square of the bus voltage. This percentage would be set dependent on the level of the dc circulating current.

An understanding of the change in system load flow due to MHD-EMP effects can be gained from similar analysis for systems in a geomagnetic storm environment. Previous research [7] for a 500-kV line simulation and a maximum electric field of 6.2 volts/kilometer yielded the following load flow changes as tabulated in Table 3.

Table 3

GM STORM LOAD FLOW
500-KV LINE SIMULATION

System Aspect	System Change
System MVAR	Increase ≃ 90%
Bus Voltage	*Decrease ≃ 21%
System Load	Decrease ≃ 7%
Generation	Decrease ≃ 8%
System Losses	Increase ≃ 7%

*Worst Case Load Bus

The above change in system parameters is a direct result of the increase in system MVAR requirements due to power transformer overexcitation only and do not reflect any generation load reject on load shedding actions.

4.5.3 Model: System Stability (I1)

In addition to the quantification of the new steady-state load flow caused by the MHD-EMP environment, the effects on system stability as it moves from state to state must also be considered. The load flow defines the initial steady-state conditions. The stability program represents dynamic models of generation, load, reactive power compensation and HVDC transmission. The system would then be disturbed by the addition of the MHD-EMP caused reactive loads. The program

output would quantify the dynamic response of the system, such as generator swing angles as a function of time. In addition, the effects of load shedding schemes and line tripping must be considered.

In addition to the above, the effects of long-line energization, single and three-pole reclosing and other switching phenomena must be investigated using existing analysis techniques.

4.5.4 Assessment: Change of System State (J1)

The combination of load flow, stability and switching surge studies caused by and in the presence of an MHD-EMP environment will lead to an understanding of complete system operational response and final system state after the nuclear event. In the case of MHD-EMP assessment, several system base cases should be studied. These cases should range from systems essentially unaffected by the HEMP environment to cases where the power system is critically disturbed by HEMP prior to the MHD-EMP assessments.

4.6 DC Transmission Analysis

Based on previous analyses [7] of direct current transmission and terminal station operation during geomagnetic storm environments, dc system operation must be assessed for the following aspects.

- Terminal harmonic filter performance
- Probability of terminal commutation failure

In each of the above assessments, the spectral content of the power frequency harmonics (Data base F1) must be compared to the dc terminal data base to ascertain possible impact.

4.6.1 Data Base: DC Terminal (F3)

In task F3 the equipment present in the dc converter terminals is quantified in terms of harmonic filter rating and commutation performance. In terms of the odd harmonic filters (5, 7, 11, 13) and

the high-pass filters the parameters of fundamental current rating and harmonic current rating are quantified. The probability of commutation failure is based upon the comparison of voltage harmonic distortion level and commutator performance.

4.6.2 Assessment: DC Converters and Filters (G2)

The dc terminal assessment would quantify the probability of damage to harmonic filters due to sustained overload. In the case of protective systems which remove filters from operation during overload states, the impact of filter absence must be addressed. Failure of converter commutation must be viewed from the perspective of direct equipment damage and/or loss of dc transmission capability.

4.7 Generator Analysis

The over excitation of generator step-up transformers will result in harmonic current as seen by the generator windings. The second harmonic (negative sequence) current in particular could produce severe heating problems in the machines. The heating occurs due to rotor coupling and consequential flow in solid rotor forgings, non-magnetic rotor wedges and retaining rings with heat concentrated at shrink fit interfaces. The resulting I^2R loss causes melting and other damage to the rotor structure. Negative sequence currents may also result due to phase current imbalance caused by unequal excitation of the transformer bank.

4.7.1 Data Base: Generator Design (F4)

This data base will be formed from generator design information and applicable ANSI standards, which define the permissible magnitude/time duration of the square of the negative sequence current, in per unit.

4.7.2 Assessment: Generator Damage (G3)

The preliminary assessment consists of the comparison of the negative sequence current to the threshold levels for generator designs.

More detailed analysis, based on manufacturers specific data may be required to determine the probable extent of the damage.

4.8 Instrument Transformer Analysis

Knowledge of the steady state and transient performance of instrument transformers exposed to an MHD-EMP environment is of critical importance for instrumentation and protective relay system assessment. The simultaneous ac and dc excitation will result in transformer operation closer to or in the saturation state. The partial or full saturation will cause the secondary voltage or current waveform to deviate from the primary waveform. For transient fault conditions, a dc offset in the fault current of the same polarity as the dc branch current can substantially reduce the time to saturation.

4.8.1 Data Base: Instrument Transformers (G4)

The data base should contain the following information (1) bus location of the instrument transformer, (2) operating characteristics including saturation curves and time to saturation characteristics, (3) configuration of secondary connection, (4) connected ratio, and (5) burden. This information is used in conjunction with the harmonic data base (F1) and the dc branch current data base (D1) to quantify operational performance in terms of the modified nature of the secondary waveforms.

4.8.2 Assessment: Current Transformer Operation (H2)

Based on the magnitude and time history of the dc branch current exciting the current transformer, in conjunction with ac excitation, the percent error of CT response will be calculated. For a given magnitude of dc current, it is expected that higher CT ratios combined with lower secondary burdens will reflect better performance. The error will also be investigated to ascertain the change in ratio error and phase angle error for a given transformer. Secondary waveform harmonic content must be investigated. It is expected that the total harmonic content will be

a function of self-generated harmonics and harmonics caused by nearby power transformers. An analysis must be made of the possible magnitude of CT remanent flux and reduced time to saturation under fault conditions.

4.8.3 Assessment: Voltage Transformer Operation (H3)

In a manner consistent with the assessment described for current transformers, a similar analysis will be made for voltage transformers. It is expected that the voltage transformer will be less impacted in performance for a given level of dc current. Assessment of capacitive coupled voltage transformers (CCVT) must also be accomplished.

4.9 Instrumentation, Control and Relay System Analysis

Subsequent to the assessment of current and voltage transformer operation in an MHD-EMP environment, this information must be integrated into the analysis of instrumentation, control and protective relay schemes. For instrumentation, the assessment should consist of the quantification of measurement error introduced by the modified secondary waveforms of the instrument transformer. Control system operation must be investigated to ascertain the impact of misleading input information. Protective relay schemes must be investigated in the context of relay security and operational dependability.

4.9.1 Data Base: Instrumentation and Control Systems (I2)

This data base will contain the operating characteristics of measurement instrumentation including transducers and metering systems. Measured system parameters for assessment are voltage, current, frequency, real and reactive power. The control system data bases should include the operating characteristics for systems such as automatic generation control, load frequency and voltage control schemes. The ability of control systems to filter "bad" data must be included in this documentation.

4.9.2 Assessment: Instrumentation and Control System Operation (J2)

The assessment will quantify the amount of measurement error contained in the output of instrumentation systems. The total error will be the combination of the ratio and phase angle errors of the instrument transformers in conjunction with the modified uncertainty of transducers and metering systems. A sensitivity analysis should be performed based on instrument transformer secondary burden. Control system operational assessment is based upon the ability of these systems to perform their intended functions given distorted power system parameter input data.

4.9.3 Data Base: Protective Relay System (I3)

In this task, a data base is established for the protective relays installed on the system. Information contained in the base will include (1) type of relay, (2) relay settings, (3) relay operating characteristics and, (4) corresponding instrument transformer(s).

4.9.4 Assessment: Protective Relay System Operation (J3)

The assessment will consist of the quantification of relay system security and relay system dependability. A loss of security is defined as an undesired relay operation in the absence of these system conditions for which the relay must perform its intended function. The loss of relay system dependability is defined as the failure to operate or, operation with excessive delay for system abnormal conditions. For example, dependent on relay design, the primary effect of current transformer secondary distortion may be zero-crossing shift, peak reduction, rms value reduction or harmonic content. Relay systems of particular interest include current differential protection, overcurrent protection, undervoltage schemes and distance relaying applications based on line impedance parameters.

4.10 Power Fuse Analysis

The combination of normal power frequency current and the dc contribution from the MHD-EMP event may result in power fuse misoperation. This potential risk assumes increasing importance since the fuse is a single operation device. A blown power fuse requires manual replacement which can increase the time required for electrical service restoration. The dc current may also impact system device coordination.

4.10.1 Data Base: Power Fuses (G5)

This data base consists of fuse operating curves which depict the relationship between time and rms total current. A typical set of curves is shown as Figure 24.

4.10.2 Assessment: Fuse Operation (H4)

The power fuse data bases will be compared to the expected values of 60 Hz and power frequency harmonic rms current combined with the MHD-EMP dc value to ascertain the probability of fuse operation.

4.11 Utility Communication Systems Analysis

Utility communication systems can include a wide variety of methods. The information transfer may be voice, analog or digital in form corresponding to the telemetry, control and/or protective system functions required. For MHD-EMP assessment, communications can be considered as two general categories.

- Radio communication systems including point-to-point microwave and base station/mobile radio equipment.
- Wire based communication systems which can take the form of (1) power line carrier, (2) shield wire, (3) utility owned twisted pair and coaxial circuits, and (4) leased telephone line.

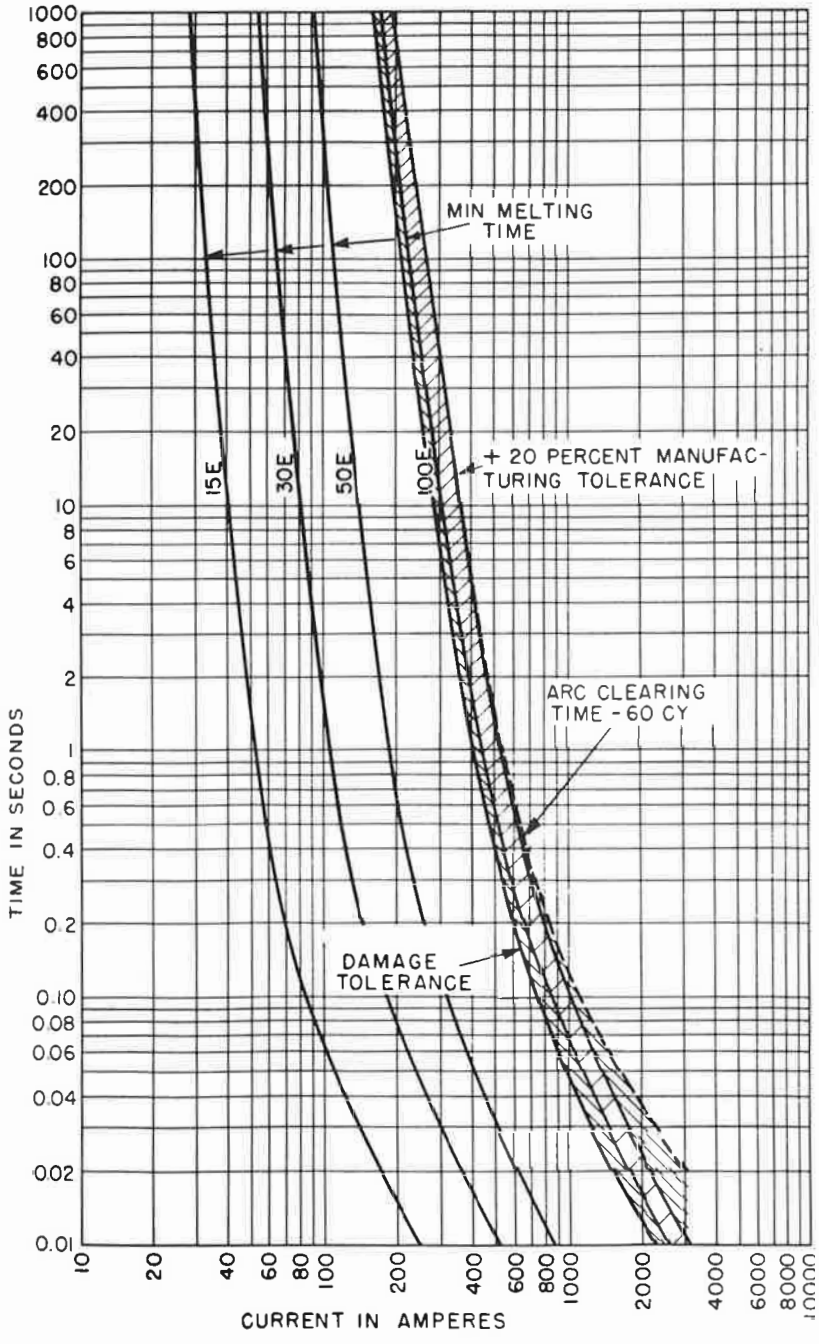

Fig. 24. Typical power fuse characteristic curves.

In the case of wire communications, the MHD-EMP environment is identical to that previously discussed for the power system grid. For assessment of radio communication links only, additional environmental definition concerning signal propagation in and through the atmosphere and ionosphere will be required. As a practical expedient, a single "reasonable worst case" environment could be defined for use with several surface electric field environments.

4.11.1 Data Base: System Line Communications (B2)

In this task the spatial orientation, circuit impedance in terms of dc resistance and ground connections for the line communication systems is detailed. In the case of power line carrier systems, this data base will have previously been defined in task B1.

4.11.2 Model: Line Communication System Response (C2)

Based on the information gathered in the previous task and the specified electric field environment, an equivalent dc network is simulated and resolved for the individual dc branch currents. This approach is qualitatively identical to that used in the power system response network.

4.11.3 Assessment: Line Communication Operation (D2)

Given the time dependent magnitude of the dc branch currents, the increase in channel noise and/or threshold of circuit upset is assessed. As an example, previously measured upset threshold for a type L-4 power feed loop circuit occurred between 420 and 600 milliamperes of dc current. In addition, an increase of 10 dB in intermodulation noise was experienced at a dc line current of 435 milliamperes.

4.11.4 Data Base: System Radio Communications (B3)

In preparation for assessment of utility radio communications in an MHD-EMP environment, the systems are categorized by (1) the frequency of the carrier, (2) the normal signal to noise ratio and, (3) type of function and/or information content.

4.11.5 Assessment: Radio Communication Operation (C3)

The propagation of the above types of radio communication system through the atmospheric environment is analyzed to determine the probability of and the duration of loss of communication channel. It is expected that higher frequency communications links will be more affected than lower carrier frequencies. For example, during a severe geomagnetic storm, a 1500 kHz signal was attenuated by 33 dB, while at 820 kHz, the attenuation was 19.8 dB. Mobile radio communications frequency bands between 1600 and 2850 kHz or 3.1 to 512 MHz may be severely affected.

4.12 Summary

The MHD-EMP assessment methodology is consistent with the techniques employed for power system analysis under geomagnetic storm environments. The spatial variability of the electric field excitation as a function of burst location introduces additional complexity for the MHD-EMP event. The higher intensity of the MHD-EMP electric field, in local areas, requires the analysis to be extended to subtransmission and distribution networks located in these areas.

The methodology is predicated upon the ability to quantify the magnitude and direction of quasi-dc circulating currents. This transient phenomena, in conjunction with normal power frequency current interacts with power and instrument transformers to place the system at some risk. Preliminary risk assessments, planned for subsequent phases of the research effort will serve to validate the approach documented herein.

5. NETWORK MODELS AND ANALYSIS CODES

5.1 Introduction

The geographic extent of the power system grid, subject to evaluation by the MHD-EMP assessment methodology, is explicitly dependent on the corresponding geographic profile of the surface tangential, transient electric field $\bar{E}(x,y;t)$. By convention, the surface coordinate origin (0,0) is located at the equivalent ground zero location for the high altitude nuclear burst. Previous MRC simulations [3] indicate that the affected area may be several million square kilometers. Within the continental United States, such an expanse will certainly contain an extremely complex power system grid operated by more than one electric utility.

In this section, it will be shown that the interconnected power system grid can be modelled as a series of isolated dc response networks for the quantification of the induced circulating currents. Each network is constructed from dc models of power system components, purely resistive in nature, and voltage sources corresponding to the electric field.

The section concludes with a discussion of the various digital analysis/simulation codes embedded in the methodology. The discussion includes identification of several existing candidate codes and requirements for additional code development.

5.2 DC Response Network Topology

The fundamental concept which allows the interconnected power system grid to be modelled as a series of dc networks is based on the fact that a continuous dc path must exist between ground points for the flow of the induced circulating currents. DC network discontinuity will occur due to:

- Prior fragmentation of the power system grid caused by HEMP environments.

- Existence of isolated-winding power transformers whose simulation models incorporate a dc open circuit.
- Series capacitors and other electrical equipments whose models are dc open circuits.

In order to illustrate the above concept, an example of a dc response network developed from a scenario of power system grid is presented in Figure 25(a) and 25(b). The grid of Figure 25(a) contains a typical mixture of isolated-winding power transformers, an autotransformer (bus 7) and shunt reactors (bus 5 and bus 6). The presence of the delta transformer winding connection at a bus will result in a dc open circuit condition in the response network model. The corresponding dc response network (Figure 25(b)) consists of appropriate dc resistance branches and dc voltage sources inserted at each ground location.

In this simple example, the magnitude of the electric field, $\varepsilon(x,y)$ is assumed to be constant and the direction $\bar{e}(x,y)$ is assumed fixed. Given these assumptions, it can be predicted that the induced dc circulating current will flow from the ground termination at bus 8 to the ground terminations at bus 1 and bus 3. The magnitude of each voltage source is a function of the length of conductor between each grounded bus and the spatial orientation of the conductor and the field direction. If required, each voltage source can be modelled as the respective equivalent Norton current source.

Any MHD-EMP power system assessment will entail the solution of many dc coupling response networks. Each network may represent transmission, subtransmission or distribution segments of the power system grid. Previous geomagnetic storm assessments [7] have concentrated on circuits of operating voltages at or above 69 kV. Maximum electric fields were simulated at 6.2 volts/kilometer. This maximum field value combined with typical line lengths at specific operating voltages and code size limitations were contributing factors in simulation limitation.

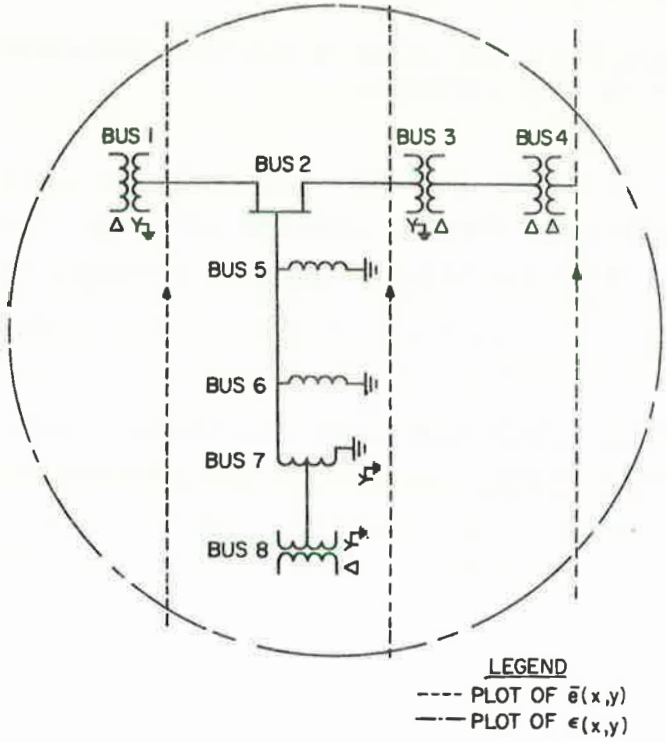

Fig. 25(a). Segment of power system grid.

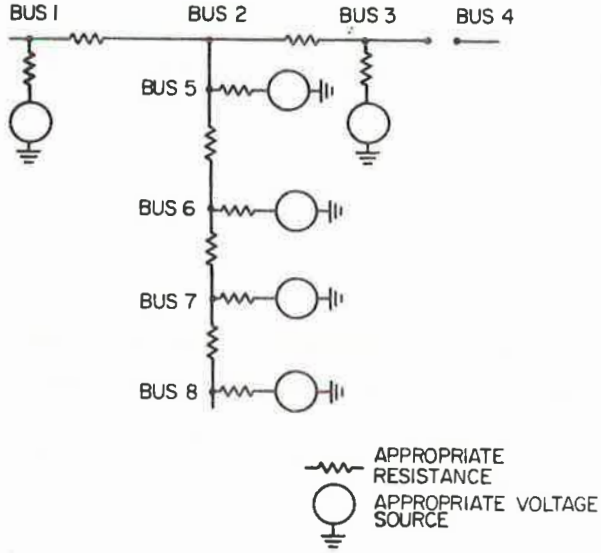

Fig. 25(b). DC response network.

For MHD-EMP environments it is expected that certain areas of the power system grid can experience electric field gradients several times greater than 10 V/km. Hence, lines of shorter lengths at lower operating voltage levels must be considered.

5.3 Models for Power System Components

The component models which constitute the MHD-EMP response network are strict dc equivalents for each type of equipment. This fact has both advantages and drawbacks. The advantages consist of a simple dc network which contains frequency independent models. A practical drawback to this approach is that the dc equivalents of power system components are not normally contained in the system data bases of most utilities since there are very few applications where such models are needed in frequent utility studies. Typical dc component models are presented as Figure 26. These models are discussed below.

5.3.1 Transmission and Distribution Conductors

Transmission lines, distribution feeders and cables are represented by the lumped dc resistance of the conductors. The most accurate data is established by the direct measured values of dc resistance. A practical approximation can be derived by the application of a correction factor (0.95 to 1.0 depending on the size and construction of the conductor) to the relevant positive sequence resistance [8]. The correction is required due to the fact that skin and proximity effects for a dc current are negligible when compared to 60 Hz current. Table 4 depicts typical conductor 60 Hz resistance for select voltage levels.

Once the dc resistance of each conductor is known, the dc resistance of the line or feeder can be simulated by paralleling the phase conductors. For example, for a typical three phase line, the total lumped resistance incorporated into the response network is one-third of the value for a phase conductor.

Table 4

TYPICAL CONDUCTOR 60 HZ RESISTANCES FOR DIFFERENT VOLTAGE LEVELS

Voltage(kV)	Construction	60 Hz Resistance(ohms/kilometer)
69	(Typical)	0.1875
138	"H" Design	0.0786
138	Vertical Design	0.0867
345	Horizontal Design	0.0419
500	Delta Design	0.0344
500	Vertical Design	0.0314
765	Horizontal Design	0.0153
765	Horizontal Design	0.0133
1200	Delta Design	0.0222
1200	Horizontal Design	0.0071

5.3.2 Power Transformers

Power transformer models, incorporated into the system response networks, can be developed according to the following criteria:

- Existence of dc circuit connections within the transformer.
- DC resistance of transformer windings.

Select models developed per the above criteria are contained in Figure 26. The existence of a delta winding configuration will always result in an equivalent dc open circuit. With the exception of autotransformers, any ungrounded winding will result in an equivalent dc open circuit. In the case of the ungrounded autotransformer, the series winding only will be represented. All transformer configurations which

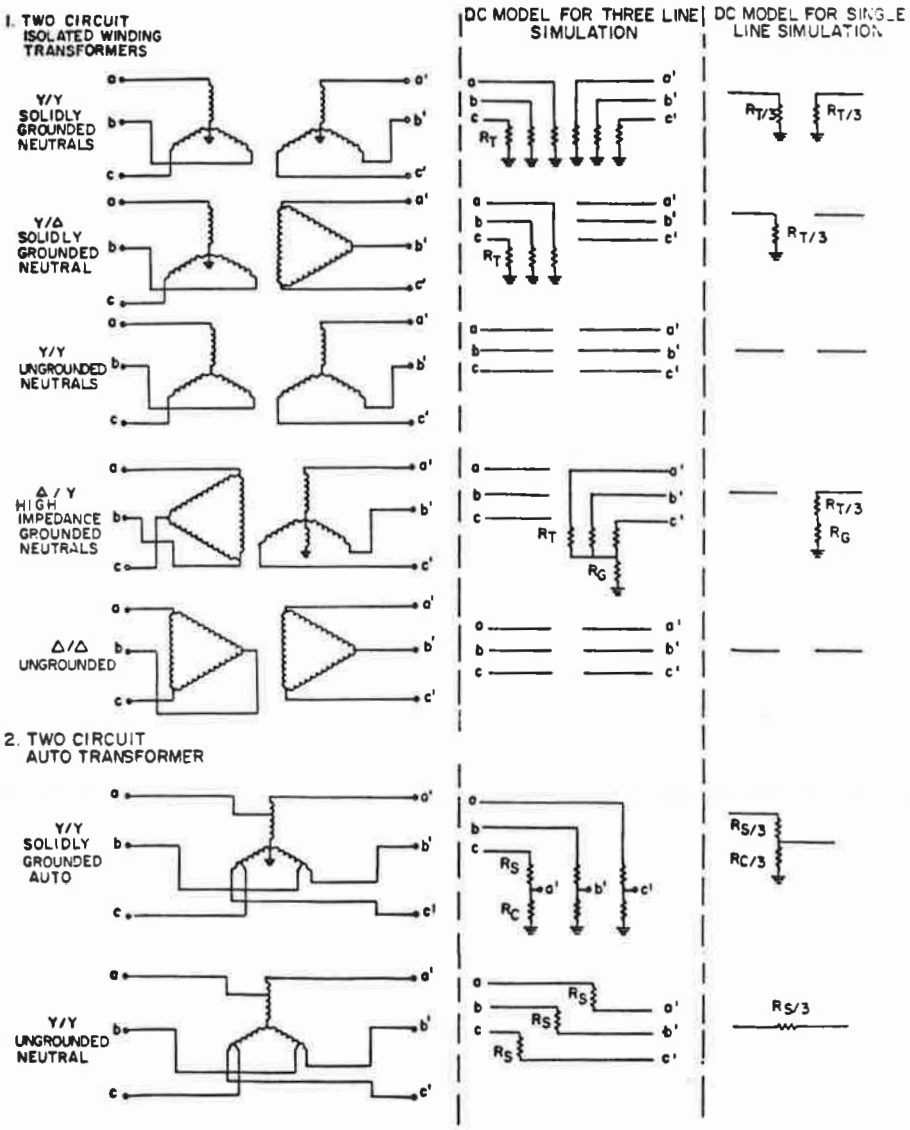

Fig. 26. DC models of power system components.

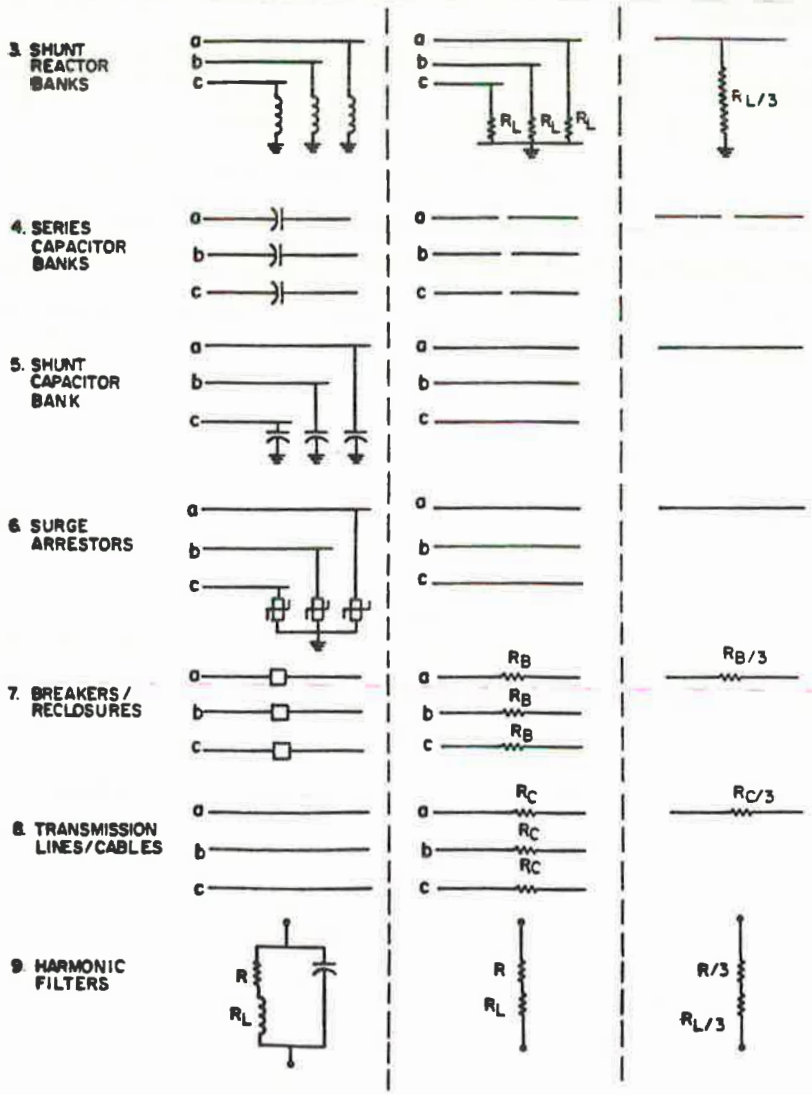

Fig. 26. DC models of power system components.(continued)

contain grounded windings can be represented by a lumped resistive element, per phase. Grounded autotransformer applications are represented by both the series winding resistance and the common winding resistance. Any additional resistance between the transformer ground connection terminal and the ground plane is modelled separately.

The value for any particular dc winding resistance can be obtained from manufacturer's data where the resistance is directly measured. In the absence of such data, approximate values can be derived from short-circuit impedance values. The assumption is made that the primary winding resistance and the referred value of the secondary winding resistance are equal. A similar approach is used for autotransformers. The resistance observed at the high voltage terminal (low voltage shorted) is the sum of the series winding resistance and the referred value of the common winding resistance. The referred value is based upon the ratio of series to common terms. The individual winding resistances are approximated by assigning half the short circuit resistance to the series winding and the referred remaining half to the common winding.

5.3.3 Shunt Reactors

Shunt reactors are required in the analysis of the circulating MHD induced currents since they provide a path to ground. The model consists of the dc resistance of the shunt reactor and can be calculated or approximated given the manufacturer's data. Reactance, as in the case of transformers, is not presented in the model. The three phase model consists of a resistance equal to one-third of the phase resistance.

5.3.4 Capacitors

Series or shunt capacitors are open circuits for the dc and quasi dc currents and hence they are left out of the system model. In fact, series capacitors act to sectionalize the power system and block the passage of the circulating induced currents.

5.3.5 Surge Arresters

Surge arresters of all designs result in an open circuit in the response network since they provide an extremely high resistance to ground at quasi-dc frequencies. A possible area of concern exists for arrester operation in the MHD-EMP environment. It has been reported [9] that dc current due to geomagnetic storms can result in a neutral shift which prevents the re-sealing of the arrester. This aspect of arrester performance will be investigated as part of joint HEMP/MHD-EMP assessments.

5.4 Grounding Resistance

The power system response network must also incorporate the dc grounding resistance which will exist between the system component model and the network ground plane. In the absence of measured values, a reasonable approximation must be made for this resistive element. In many cases, this terminating resistance is a significant percentage of total circuit resistance.

Previous studies for geomagnetic storm environments [7] have specified a value of 1 ohm for the resistance at each ground connection in lieu of measured data. Sensitivity analysis of magnitude of circulating current as a function of grounding resistance and comparison to measured neutral currents validate the above assumption. In the absence of measured data, any "reasonable" worst-case assessment must include practical estimates of soil conditions on a site-specific basis. For example, an analysis which includes an arid topology may require an estimate of several ohms per termination. In this case, the assumption of a terminating impedance based on some uniform value (0.5 ohms as used in previous analysis), will result in a significant overestimation for the magnitude of the circulating current.

In the case of high impedance grounds, where the 60 Hz impedance is established by a reactor, the effective dc resistance associated with that reactance would be incorporated in the response network.

5.5 Analysis Codes

As indicated by the assessment methodology, complete power system analysis will require the use of several network/system simulations. These simulations are best accomplished via digital codes and digital data processors. A conceptual flowchart indicating the type and relationship between elements of this body of code is shown as Figure 27. Code subsets and tasks are discussed as follows:

5.5.1 System Response Network Analysis

The calculation of circulating induced currents due to the MHD-EMP environment requires only a distributed source, dc system representation. The mathematical solution is straightforward, but the code must be able to represent a large network in a single analysis.

One good candidate for this analysis is the Electromagnetic Transients Program (EMTP) [10,11]. This program has become an industry standard and does not require any modification to existing code to perform the simulation. For large systems, the EMTP is installed in a CRAY and/or CDC 7600 environment. If appropriate, a dedicated version of EMTP could be developed for this analysis.

Data base input/output requirements for EMTP would be enhanced by the development of pre-processor and post-processor modules. The pre-processor should contain graphic digitizing capability, since many parameters of the MHD-EMP environment and power system grid data bases are graphic in format. The EMTP post-processor would create data format compatibility and automatic calculation of system harmonics and reactive power data bases required by subsequent analysis codes.

5.5.2 System Load Flow/Dynamic Simulation

There exists a number of load flow/dynamic simulation programs in common use within the power system analysis community. One such set of these programs is the Westinghouse WESTCAT™ System Planning and Analysis package. This library of power system analysis programs incorporates detailed load flow and dynamic system models implemented from a common

data base. Maximum system size for load flow is 4,000 buses, and 8,000 branches. The WESTCAT™ package also contains a short-circuit program, eigenvalue analysis, and network equivalent capability.

5.5.3 Switching Surge Analysis

The effects of long line energization, single and three pole reclosing and other switching operations in the MHD-EMP environment can be investigated by the use of the EMTP program. This program has been used by Mohan [12] and others to perform similar studies for geomagnetic storm environments.

5.5.4 Power Fuse Analysis

For lower-voltage distribution systems, the simultaneous presence of ac and dc current may affect the proper operation and coordination of power fuses. To evaluate this situation, an analysis code could be developed to assess this concern. It is expected that preliminary risk assessment on distribution systems will clarify the need for such a tool.

5.6 Summary

For MHD-EMP assessment, the ac power system grid topology can be simulated as a set of dc equivalent networks. Thus, the initial system response, transient induced branch currents, is approximated as a slowly time-varying dc phenomena. The reasonability of this approach is supported by:

- The very-low frequency content of the electric field excitation.
- Strong similarity between MHD-EMP and geomagnetic storm environments.
- Validation of this technique, for geomagnetic storm simulations, based on measured values of the magnitude and spectral content of the induced current and the associated impact on system parameters.

From a perspective of balanced uncertainty, preliminary investigation indicates that any errors introduced by a dc simulation in lieu of a very low frequency ac approach may be swamped by the uncertainty inherent in the environmental definition.

Digital code development required by the MHD-EMP assessment methodology can incorporate, with some modification, existing codes now used in storm assessment. The spatial extent of the MHD-EMP environment indicates the use of significant capacity load flow codes. At this time, the authors anticipate the use of an 8,000 branch program. Preliminary assessments will reveal any requirements for a larger capacity code.

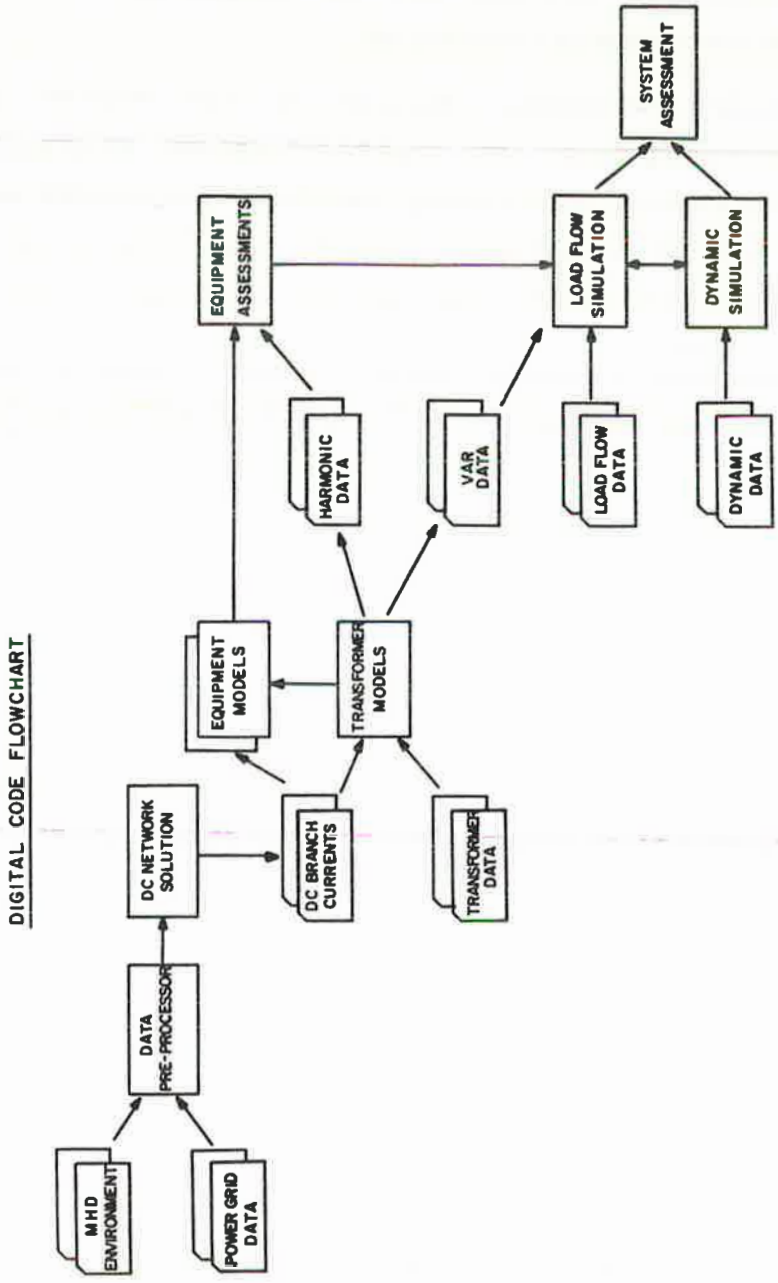

Fig. 27. Conceptual flowchart for MHD-EMP Assessment Codes

6. CONCLUSIONS AND RECOMMENDATIONS

Initial research to investigate the effects of an high altitude nuclear burst on the electric power system indicates that the MHD-EMP environment may place the system at some risk. The nature of the threat can be qualitatively defined in terms of quasi-dc induced currents caused to flow between system ground connections due to the existence of a transient, surface tangential, electric field. In preparation for quantitative risk assessment, an extensive methodology has been developed. This methodology incorporates the necessary environmental and power system data bases, coupling response mechanisms and power system analysis techniques necessary to perform quantitative assessment.

In the areas of MHD-EMP environmental definition, power system coupling response, methodology development and system analysis, the following conclusions are reached:

1. A high altitude nuclear weapon burst will produce both HEMP and MHD-EMP transient electromagnetic environments. The radically different natures of these transients, as seen by an electric power system requires separate system response models and assessment methodologies.

2. For power systems analysis, the MHD-EMP environment can be defined as a spatial and time dependent, surface tangential, transient electric field. Additional definition for radio frequency propagation will be required for those assessments which include utility radio communication systems.

3. Spectral analysis of typical MHD-EMP magnetic and electric fields indicates that the electric field can be approximated as a quasi-dc stimulus to the power system.

4. Previous MHD-EMP environmental formats are not of a form that can be directly used in power systems analysis. To facilitate this type of assessment a suitable approximate environment may be expressed in terms of three independent parameters: (1) spatially dependent magnitude of the electric field $\varepsilon(x,y)$; (2) spatially dependent direction of the electric field $\bar{e}(x,y)$; and (3) a time-dependent, spatially invariant function $f(t)$.

This definition of $\bar{E}(x,y;t)$ could be expanded, by a sum of products structure, to incorporate greater accuracy for a single burst or unified environmental definition in the case of multiple weapons' bursts.

5. The nature of the MHD-EMP environment exhibits sufficient similarity to the geomagnetic storm environment such that a parallel system response mechanisms and assessment methodology can be defined.

6. The system response network contains dc resistive models and time varying dc distributed voltage sources. The initial response of interest is quantified as the time varying dc induced currents flowing simultaneously with normal 60 Hz currents.

7. The existence of these dc branch currents is the basis for subsequent power system analysis. Over-excitation of electro-magnetic equipment such as transformers may result in direct damage to this equipment as well as power system operational upset.

8. Existing power system analysis digital codes, such as EMTP and WESTCAT™, can be modified and/or directly incorporated into the MHD-EMP assessment methodology. These, and similar programs, are currently used in geomagnetic storm/power system assessment.

This investigation of the MHD-EMP phenomena has revealed several areas of additional research required to perform detailed and accurate risk assessment. These investigations should be accomplished as part of the Phase II research effort prior to actual preliminary assessments.

The recommendations for additional research are:

1. Detailed development of an MHD-EMP environmental definition directly suitable for power systems analysis. Suggested basis for such research is the $\bar{E}(x,y;t)$ expression contained in this report. The research should be a coordinated effort of the Defense Nuclear Agency and Oak Ridge National Laboratory with assistance from the Phase I research team. Final definition would be incorporated into the overall scenario definitions supplied by ORNL to the research team.

2. Additional emperical and analytical investigation of power and instrument transformer response to simultaneous ac and dc excitation. This research should include

actual equipment testing and response simulation. Critical parameters include quantification of direct damage, harmonic generation, waveshape distortion, and increased reactive power requirements.

3. Investigation of simultaneous ac and dc current versus power system fuse performance. Fuse mis-operation, especially within distribution networks, may result in significant electric service interruption.

4. Operation of surge arresters under the MHD-EMP environment. The investigation should concentrate on the probability of re-seal failure.

7. BIBLOGRAPHY

1. Longmire, C., Technical Presentation, DOE/ORNL Project Review Meeting, October 20, 1983.

2. DNA EMP COURSE, BDM/W-82-305-TR, Prepared By the BDM Corporation, January, 1983.

3. Chavin, S., Crevier, W. F., Kilb, R. W., and Longmire, C. L., "MHD-EMP Code Simulation of Starfish," MRC-R-516, Mission Research Corporation, August, 1979.

4. Fajen, F. E., "Mice: An Implicit Difference Scheme For MHD Calculations," DNA-2877Z, Mission Research Corporation, March, 1973.

5. C. Longmire, Mission Research Corporation, Private Correspondence to F. M. Tesche, LuTech, Inc., April, 1982.

6. Albertson, V. D., and Van Baelen, J. A., "Electric and Magnetic Fields at the Earth's Surface Due to Auroral Currents," IEEE Transactions on Power Apparatus and Systems, Vol. PAS-89, No. 2, April, 1970, pp. 578-584.

7. "Investigation of Geomagnetically Induced Currents In the Proposed Winnipeg-Duluth-Twin Cities 500-kV Transmission Line," EPRI EL-1949, Electric Power Research Institute, July, 1981.

8. Albertson, V. D., Kappenman, J. G., Mohan, N., and Skarbakka, G. A., "Load-Flow Studies in the Presence of Geomagnetically-Induced-Currents," IEEE Paper F79-702-2, presented at the 1979 Summer Power Meeting, Vancouver, B.C.

9. Albertson, V. D., and Slothower, J. C., "The effects of Solar Magnetic Activity on Electric Power Systems," University of Min., Aca. of Science, Vol. 34, November 2, 1967, pp. 94-100.

10. Dommel, H., and Meyer, W. S., "Computation of Electromagnetic Transients," Proceedings of the IEEE, Vol. 62, pp. 983-993, July, 1974.

11. User's Manual - Electromagnetic Transients Program (EMTP), Bonneville Power Administration, Portland, Oregon.

12. Mohan, N., Kappenman, J. G., and Albertson, V. D., "Harmonics and Switching Transients in the Presence of Geomagnetically-Induced Currents," IEEE Paper F79 694-1, presented at the 1979 Summer Power Meeting, Vancouver, B.C.

13. Albertson, V. D., Clayton, R. E., Thorson, J. M., Jr., and Tripathy, S. C., "Solar-Induced Currents in Power Systems: Cause and Effects:," IEEE Transactions on Power Apparatus and Systems," Vol. PAS-92, No. 2, March/April, 1973, pp. 471-477.

APPENDIX A

DETERMINATION OF THE MHD-EMP ELECTRIC FIELD AT THE EARTH'S SURFACE

In the determination of the MHD-EMP induced currents flowing in grounded conductors on the earth's surface, it is necessary to first compute the tangential electric field which excites these conductors. This electric field arises from the interaction with the late-time MHD-EMP magnetic field and the conducting earth.

The geometry for this discussion is shown as Figure A-1. On the surface of the earth there is an impressed magnetic flux density, denoted as B_x, oriented in the x direction. The earth is assumed to have an electrical conductivity of σ mhos/meter, and a permeability μ equal to that of free space. This impressed magnetic field density is that computed from the MICE/MHD-EMP codes at the earth's surface.

Within the earth, the electric field is described by the following equation:

$$\nabla^2 \bar{E} = \mu\sigma \frac{\partial \bar{E}}{\partial t} \qquad \text{(A1)}$$

in which the displacement current term has been neglected [A1]. Because the earth is imperfectly conducting, it can support a volume current density, and this is related to the electric field by:

$$\bar{J} = \sigma \bar{E} \qquad \text{(A2)}$$

For an electric field which is locally oriented in the y direction and assumed to be independent of the x and y coordinates, this equation reduces to the following form:

$$\frac{\partial^2 J_y}{\partial z^2} = \mu\sigma \frac{\partial J_y}{\partial t} \qquad \text{(A3)}$$

Considering time harmonic (Fourier transformed) signals, this relation can be expressed in the frequency domain as:

$$\frac{\partial^2 J_y}{\partial z^2} = j\omega\mu\sigma \; J_y \tag{A4}$$

which may be solved to yield the spatial distribution of induced current in the earth as:

$$J_y(z) = A_o \; e^{-z/\delta} \; e^{-jz/\delta} \tag{A5}$$

where δ is the skin depth defined as:

$$\delta = \sqrt{2/\omega\mu\sigma} \tag{A6}$$

and $A_o = J_y(o)$ is the value of the volume current on the earth's surface.

The integral of the volume current from $-\infty$ to 0 in the z direction provides the equivalent surface current K_y and is given as:

$$K_y = \int_{-\infty}^{o} J_y(z)\, dz = \frac{A_o \delta}{(1 + j)} \tag{A7}$$

At the earth's surface, the volume current density is related to the local electric field as:

$$J_y(o) = A_o = \sigma E_y(o) \tag{A8}$$

and thus the surface current can be expressed as:

$$K_y = \frac{\sigma\delta}{(1 + j)} \; E_y = \frac{E_y}{Z_s} \tag{A9}$$

where Z_s is the equivalent surface impedance of the earth.

Since the surface current is related to the total magnetic field on the surface as:

$$K_y = H_x \tag{A10}$$

and given the fact that this is related to the magnetic flux as:

$$B_x = \mu_o H_x \tag{A11}$$

the electric field on the earth surface may thus be expressed as:

$$E_y = \frac{1 + j}{\mu\sigma\delta} B_x \tag{A12}$$

This last expression may be written as:

$$E_y(\omega) = \frac{1}{\sqrt{\sigma\mu j\omega}} j\omega B_x(\omega) \tag{A13}$$

which is of the form:

$$F(\omega) = G(\omega)\, H(\omega) \tag{A14}$$

In the time domain, it is possible to express this through the convolution operator * as:

$$f(t) = g(t) * h(t) = \int_0^t g(t - \tau)\, h(\tau)\, d\tau \tag{A15}$$

where g(t) and h(t) are the Fourier transform pairs of $G(\omega)$ and $H(\omega)$ respectively. The following Fourier transform pairs [A2] are noted:

$$\frac{1}{\sqrt{\sigma\mu j\omega}} \Leftrightarrow \frac{1}{\sqrt{\sigma\mu}} \quad \frac{1}{\sqrt{\pi t}} \tag{A16}$$

and

$$j\omega B_x(\omega) \Leftrightarrow \frac{\partial B(t)}{\partial t} \tag{A17}$$

Inserting these into equation (A15) yields the following expression for the time dependent electric field in terms of the magnetic field

$$E_y(t) = \frac{1}{\sqrt{\sigma\mu\pi}} \int_0^t \frac{1}{\sqrt{t - t'}} \frac{\partial B_x}{\partial t'}(t')\, dt' \tag{A18}$$

This equation may be evaluated by direct integration, or if desired, equation (A13) may be evaluated in the frequency domain and the inverse transform taken numerically to compute the transient field.

BIBLIOGRAPHY

A1. Ramo, S., and J. R. Whinnery, FIELDS AND WAVES IN MODERN RADIO, John Wiley and Sons, New York, 1964.

A2. HANDBOOK OF MATHEMATICAL FUNCTIONS, M. Abramowitz and I. Stegun, Eds., NBS Publication #55, June, 1964.

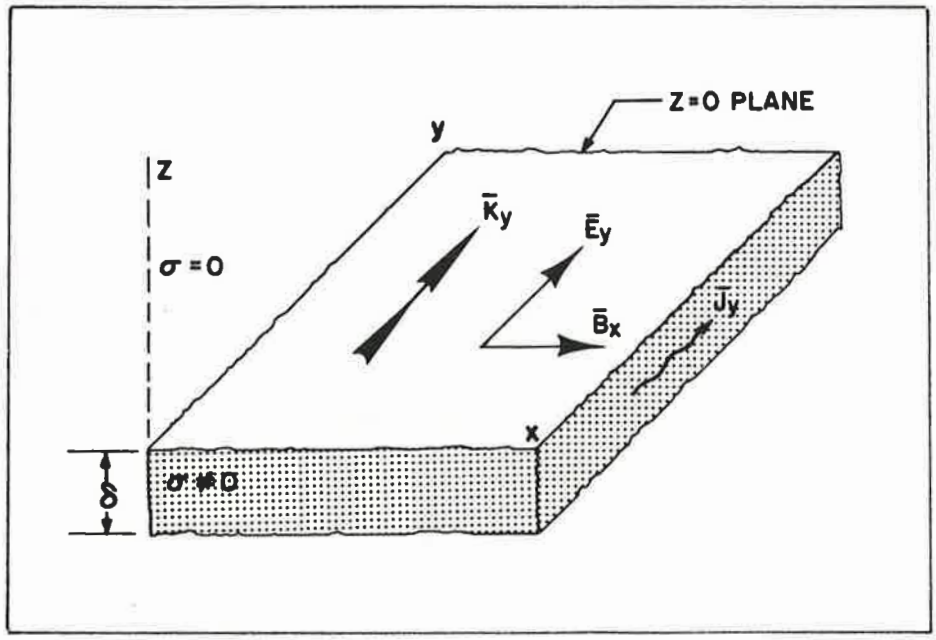

Fig. A1. Orientation of the electric ($\bar{E}_y$) magnetic ($\bar{B}_x$) and current vectors at the earth-air (Z=0) interface.

APPENDIX B

ELECTRIC FIELD EXCITATION OF ABOVE-GROUND CONDUCTORS

B.1 Introduction

This appendix serves to discuss the MHD-EMP excitation of above-ground conducting lines from an electromagnetic (EM) field point of view. In previous discussions of low frequency field coupling arising from geomagnetic storms [B1,B2] the excitation of such lines has been formulated in the context of a field-induced ground potential which tends to induce currents in conductors connected to the ground at two different points. An alternate and entirely consistent manner of representing the excitation of such grounded conductors is to consider the total tangential electric field incident on the conductor, and use this to determine the induced current. This alternate approach of viewing the coupling problem is discussed in detail. The appendix concludes with a discussion of the equivalence of the geomagnetic storm coupling approach to the excitation of conductors using an electromagnetic field perspective only. The equivalence is possible due to the quasi-static (very low frequency) nature of both MHD-EMP and geomagnetic storm phenomena.

B.2 General EM Field Interaction with Conducting Bodies

As a starting point, consider the general scattering problem illustrated in Figure B1. A perfectly conducting body having a surface denoted by S is located in free space and is illuminated by an incident plane-wave electric field, denoted as $\bar{E}^{inc}$. This incident electric field induces a surface current $\bar{J}$ to flow on the conductor and this in turn produces a scattered field in such a way that the total tangential electric field on the body surface (i.e., the incident plus the scattered field) is zero. The relation between the induced body current $J(\bar{r}')$ and the incident electric field $\bar{E}^{inc}(r)$ may be expressed [B3] via an integral equation of the form

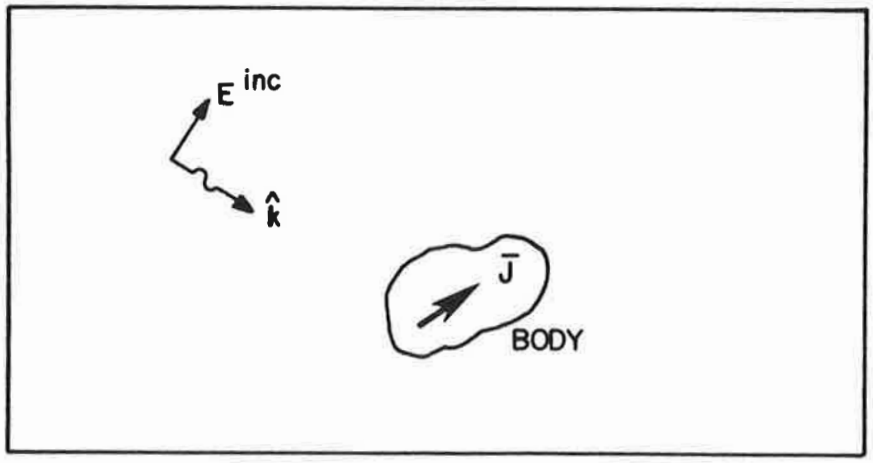

Fig. B1. Conducting body in free space, illuminated by a plane wave.

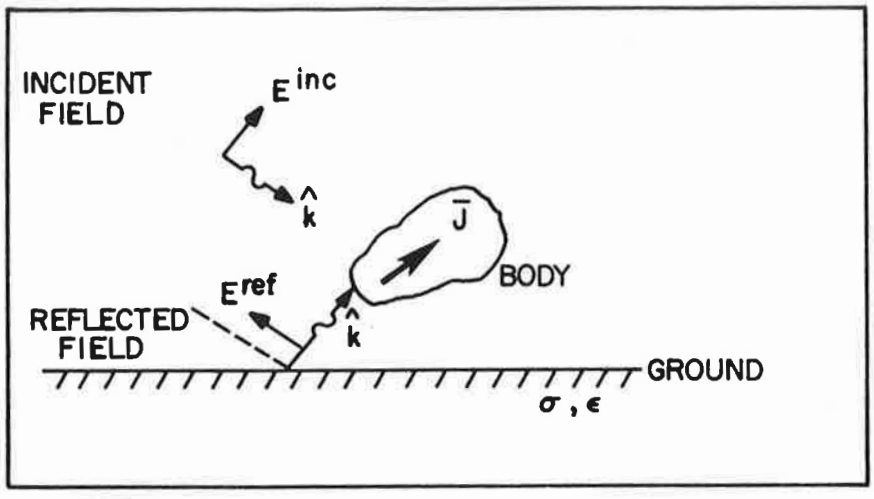

Fig. B2. Conducting body located over lossy half-space and excited by an incident plane wave.

$$\iint_S \bar{J}(\bar{r}') \cdot \bar{\bar{K}}(\bar{r}, \bar{r}')d\bar{r}' = \bar{E}_t^{inc}(\bar{r}) \qquad (B1)$$

where the function $\bar{\bar{K}}(\bar{r}',\bar{r})$ is the free space Green's tensor for the radiation problem, and represents the vector electric field at position $\bar{r}$ due to unit current elements at position $\bar{r}'$. As discussed [B3], this Green's function is defined as:

$$\bar{\bar{K}}(\bar{r}, \bar{r}') = \frac{j\omega\mu_o}{4\pi}\left[\bar{\bar{I}} + \frac{1}{k^2}\nabla\nabla\right]\frac{e^{-jk|\bar{r}-\bar{r}'|}}{|\bar{r}-\bar{r}'|} \cdot \qquad (B2)$$

In this and in the expressions to follow, ω is the angular frequency, $k = \omega/c$ and μ_o is the permeability of free space.

Note that in equation (B1) the term $\bar{E}_t^{inc}(\bar{r})$ denotes only the tangential component of the incident electric field on the body surface. The normal component is not needed for the determination of the scattering behavior of the body. Generally, the determination of the current distribution $\bar{J}(\bar{r}')$ in the above equation is impossible to do analytically, and numerical methods such as the method of moments [B4] are used.

B.3 Effect of Ground On EM Coupling

When the conducting body is located near another body, say over a conducting ground plane, it is necessary to modify the integral equation in equation (B1). As indicated in Figure B2, the tangential electric field on the body is now composed of not only the incident field, but also a component which has been reflected from the ground plane. As discussed [B5], since the incident field is a plane wave, it is possible to use plane wave reflection coefficients to represent the reflected field from the ground plane. This reflected field may be added to the incident field to provide the total incident field on the body.

For the vertically polarized incident electric field shown in Figure B3(b), the total electric field components at a height h above the earth are given by

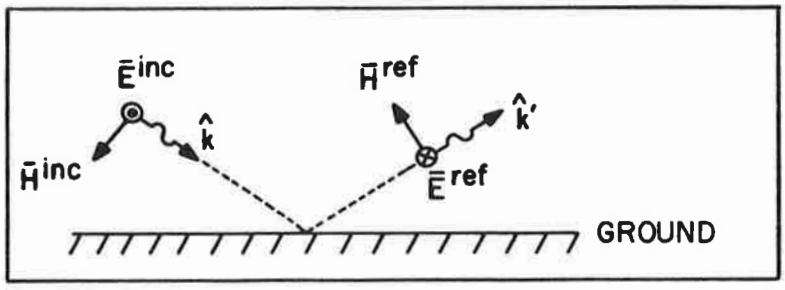

a. Horizontal Polarization

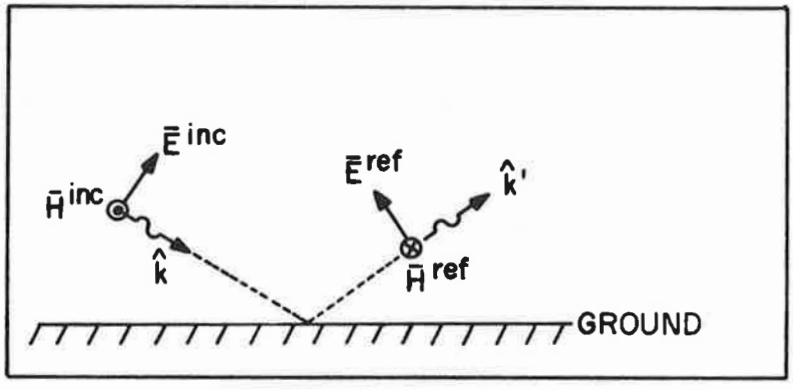

b. Vertical Polarization

Fig. B3. Vector directions for vertically polarized and horizontally polarized incident and reflected fields.

$$E_z(h,y) = E^{inc}\, e^{-jkycos\,\psi\,\cos\,\phi}\left[1 + R_v\, e^{-jk2hsin\,\psi}\right]\cos\,\psi \qquad (B3)$$

$$E_y(h,y) = E^{inc}\, e^{-jkycos\,\psi\,\cos\,\phi}\left[1 - R_v\, e^{-jk2hsin\,\psi}\right]\sin\,\psi\,\cos\,\phi \qquad (B4)$$

where R_v is the reflection coefficient for vertically polarized fields and is given by:

$$R_v = \frac{\varepsilon_r\left(1 + \frac{\sigma}{j\omega\varepsilon}\right)\sin\,\psi - \left[\varepsilon_r\left(1 + \frac{\sigma}{j\omega\varepsilon}\right) - \cos^2\psi\right]^{\frac{1}{2}}}{\varepsilon_r\left(1 + \frac{\sigma}{j\omega\varepsilon}\right)\sin\,\psi - \left[\varepsilon_r\left(1 + \frac{\sigma}{j\omega\varepsilon}\right) - \cos^2\psi\right]^{\frac{1}{2}}} \qquad (B5)$$

The angles ψ and ϕ describe the directions of incidence of the incident field, and are shown in Figure B4. The term ε_r represents the relative dielectric constant of the earth, such that $\varepsilon = \varepsilon_r\varepsilon_o$.

Similarly, the total field components for the horizontally polarized incident field shown in Figure B3(a) are given as

$$E_z(h,y) = 0 \qquad (B6)$$

$$E_y(h,y) = E^{inc}\, e^{-jky\,\cos\,\psi\,\cos\,\phi}\quad (1 + R_h\, e^{-jk2hsin\,\psi})\ \sin\,\phi \qquad (B7)$$

where the reflection coefficient R_h is given as:

$$R_h = \frac{\sin\,\psi - \left(\varepsilon_r\left(1 + \frac{\sigma}{j\omega\varepsilon}\right) - \cos^2\psi\right)^{\frac{1}{2}}}{\sin\,\psi - \left(\varepsilon_r\left(1 + \frac{\sigma}{j\omega\varepsilon}\right) - \cos^2\psi\right)^{\frac{1}{2}}} \qquad (B8)$$

In addition to the modification of the incident field for determining the induced body currents, it is necessary to modify the kernel of the integral equation. This is necessary because the radiation property of an elemental current moment is affected by the presence of the ground plane. As illustrated in Figure B5, a current

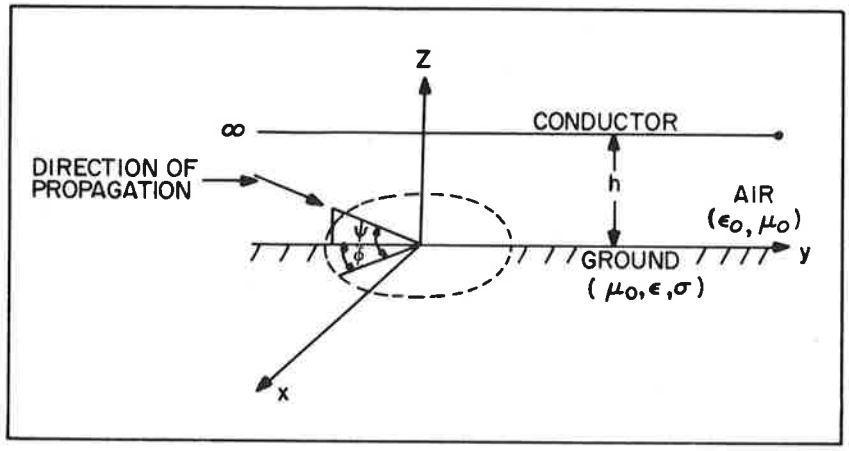

Fig. B4. Coordinates defining azimuth and elevation angles of incidence.

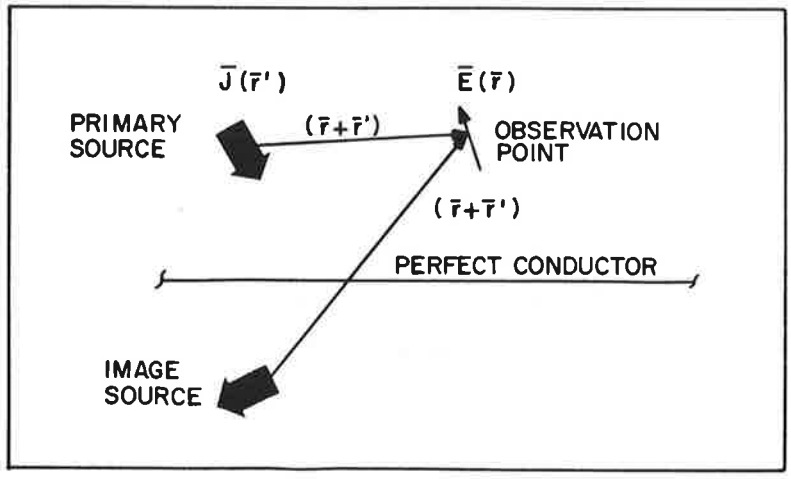

Fig. B5. Geometry of isolated current element over a perfect conductor.

element $\bar{J}(\bar{r}')$ is located above the ground and the electric field is observed at a point $\bar{r}$. If the ground were removed, the expression for the electric field is simply that given by the free space Green's function of equation (B2). For the case of the ground being a perfect conductor, a simple image theory [6] may be employed in order to calculate the field, as depicted in Figure B5.

For the case of a lossy ground (one having a finite conductivity) the general expressions for the electric fields become rather complicated, involving integrals over an infinite range which must be evaluated numerically. As discussed [B7], the electric field produced by a current element positioned above the ground plane may be expressed using a vector potential $\bar{\pi}$ and the following equation:

$$\bar{E} = \nabla\nabla \cdot \bar{\pi} + k^2 \bar{\pi} \tag{B9}$$

For a vertically oriented current element (one the z direction), located at the position z = h as shown in Figure B6, and having a moment $Id\ell$, the vector potential has been shown [B7], to also be only in the z direction and takes the form:

$$\bar{\pi}_v = \hat{z} \frac{j\omega\mu}{4\pi} Id\ell \left[\frac{e^{-jk|\bar{r}-\bar{r}'|}}{|\bar{r}-\bar{r}'|} + \frac{e^{-jk|\bar{r}+\bar{r}'|}}{|\bar{r}+\bar{r}'|} - \frac{2jk}{n} \int_0^\infty I_0(\lambda\rho) e^{-\beta(z+h)} \frac{\lambda d\lambda}{\beta^2} \right] \tag{B10}$$

For a horizontally oriented current element in the x direction, the potential has both x and z components, and is expressed:

$$\bar{\pi}_H = \frac{j\omega\mu}{4\pi} Id\ell \left\{ \hat{x} \left[\frac{e^{-jk|\bar{r}-\bar{r}'|}}{|\bar{r}-\bar{r}'|} - \frac{e^{|\bar{r}+\bar{r}'|}}{|\bar{r}+\bar{r}'|} + 2\int_0^\infty \frac{I_0 \lambda\rho\, e^{-\beta(z+h)}}{\beta+\beta_E} \lambda d\lambda \right] \right.$$

$$\left. - \hat{z} \left[\frac{2}{k^2} \cos\phi \int_0^\infty I_1(\lambda\rho) e^{-\beta(z+h)} \frac{\beta-\beta_E}{n^2\beta-\beta_E} \lambda^2 d\lambda \right] \right\} \qquad (B11)$$

In both of these expressions, the terms β and β_e are constants for the air and the earth regions respectively, and are solutions to a propagation equation which must be determined numerically. The term n is the complex index of refraction, defined as:

$$n^2 = \varepsilon_r + \frac{j\sigma}{\omega\varepsilon} \qquad (B12)$$

The parameters ϕ and ρ relate to the position of the field observation point, as shown in Figure B6.

The above expressions may now be used to construct the Green's tensor for the lossy ground. This simply consists of computing the x, y, and z components of the electric fields which are produced by x, y, and z directed current elements, in order to form the 3 by 3 tensor. As a result of these modifications, the integral equation for the body current then becomes

$$\iint_S J(\bar{r}') \cdot \left[\bar{\bar{K}}_{fs}(\bar{r}, \bar{r}') + \bar{\bar{K}}_g(\bar{r}, \bar{r}') \right] d\bar{r}' = E_t^{inc}(\bar{r}) + E_t^{ref}(\bar{r}) \qquad (B13)$$

where the kernel has been expressed as a free space part and another part representing the ground plane effects. In this expression, it is important to note that the domain of the integral equation remains over only the body. The ground plane effects are entirely accounted for by the modifications of the kernel and the tangential incident field.

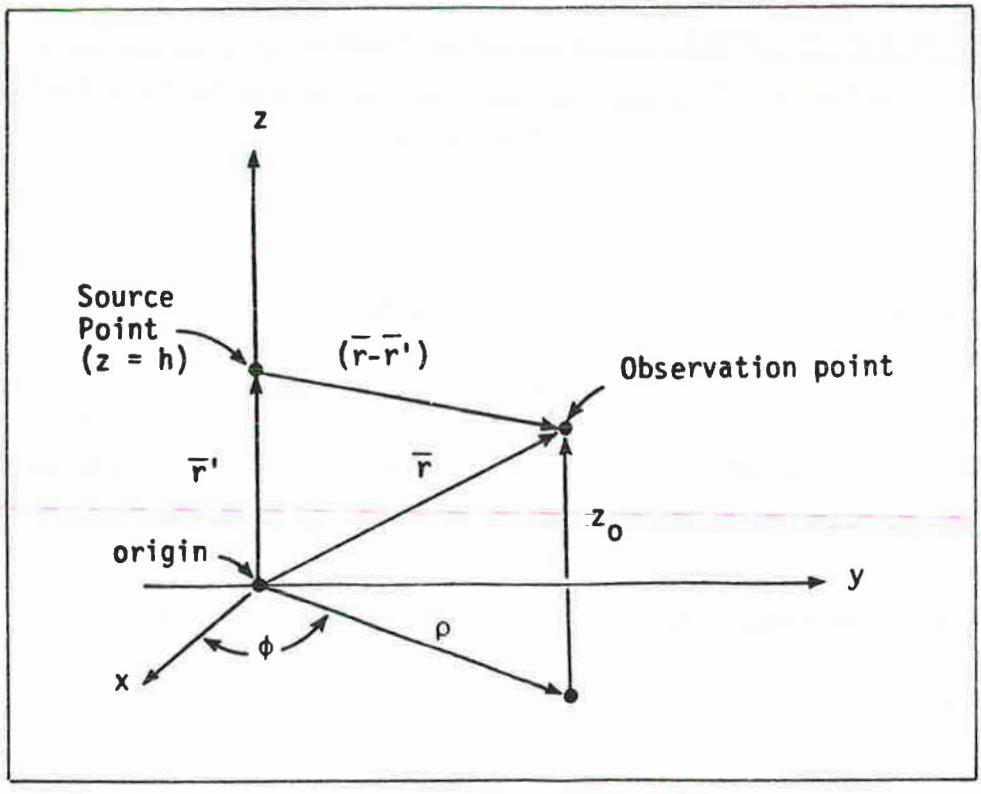

Fig. B6. Source and observation point locations for definition of lossy half-space Green's function.

B.4 Application to General Field Coupling to Long Conductors

The preceding concepts may now be applied to the case of a long conducting wire over a ground plane, as shown in Figure B7. In this case, it is desired to calculate the currents flowing in the wire, as a function of the incident field. Other investigators [B8,B9] have studied the behavior of such currents and it has been demonstrated that at low frequencies the integral equation (B13) may be solved in an approximate sense by using a simple transmission line model. As shown in Figure B8, the line above the ground is modelled as a lossy transmission line whose per-unit-length series impedance is approximated [B5] as:

$$Z = Z_i + Z_g + j\omega L \tag{B14}$$

where $j\omega L$ is the inductive impedance of the wire above the ground and is given by:

$$j\omega L = j\omega \frac{\mu_o}{2\pi} \cosh^{-1}\left(\frac{h}{a}\right) \tag{B15}$$

The term Z_i is the internal impedance of the wire, and is calculated to be:

$$Z_i = - \frac{j\gamma_w}{2\pi a \sigma_w} \frac{J_o(j\gamma_w a)}{J_1(j\gamma_w a)} \quad . \tag{B16}$$

where γ_w is the complex propagation constant in the wire material, and is expressed as:

$$\gamma_w = \sqrt{j\omega\mu(\sigma_w + j\omega\varepsilon_w)} \tag{B17}$$

The term Z_g is the ground impedance given by:

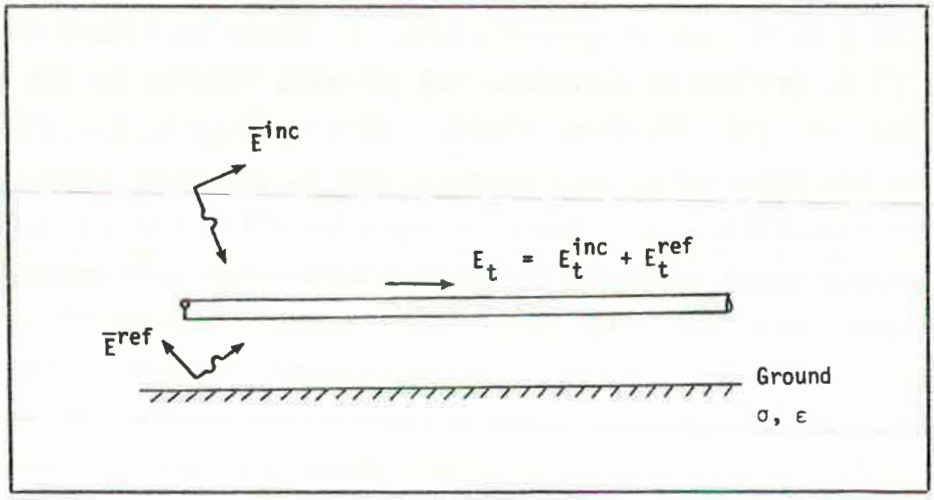

Fig. B7. Long electrical conductor over lossy ground, excited by an incident field.

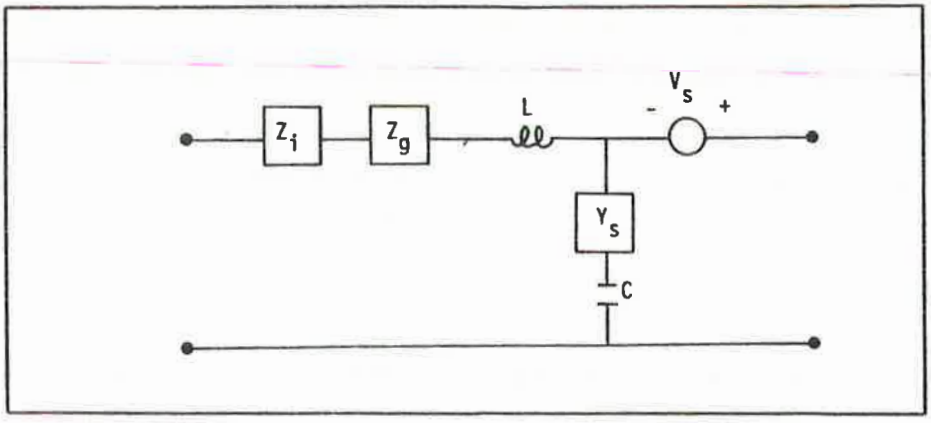

Fig. B8. Differential section of transmission line model for above-ground conductor.

$$Z_g \simeq - \frac{j\gamma_g}{4\pi h\sigma_g} \frac{H_o^{(1)}(j\gamma_g 2h)}{H_1^{(1)}(j\gamma_g 2h)} . \quad \text{(B18)}$$

where:

$$\gamma_g = \sqrt{j\omega\mu(\sigma_g + j\omega\varepsilon_g)} \quad \text{(B19)}$$

The shunt per-unit-length admittance of the transmission line model consists of a capacitive term in series with another element to account for the loss within the ground plane. The capacitive element of the line is given by the usual expression for a wire above a perfectly conducting ground:

$$j\omega C = j\omega \frac{2\pi\varepsilon_o}{\cosh^{-1}(h/a)} \quad \text{(B20)}$$

and the other series admittance element is approximated [B5] as:

$$\gamma_g = \frac{\gamma_g^2}{Z_g} \quad \text{(B21)}$$

The excitation of this line is in the form of a distributed per-unit-length voltage source, whose value is identical to the incident plus ground-reflected electric field tangential to the wire:

$$V_s(y) = E_t^{inc}(y) + E_t^{ref}(y) \quad \text{(B22)}$$

At the ends of the line, where the load impedances are located, there are additional lumped voltage sources representing the effects of the electric field tangential to the load conductors (i.e., the electric field normal to the earth surface). For lines which are typically very long, the contribution of these sources to the overall response is

typically neglected, so that only the horizontal electric field plays an important role in the excitation of the line. However, as has been demonstrated by Vance [B5], when the incident field is vertically polarized, this component of the electric field can, at times, have a significant impact on the overall response. In the present discussion, however, we are considering only horizontally polarized incident fields, and this excitation is zero.

Thus, as in the case of a general scattering body over the ground plane, the effects of the lossy ground on this transmission line manifest themselves through a modification of the current propagation relations (by the addition of a series resistance and the shunt conductance in the transmission line) and in a modification of the source excitation of the line.

B.5 Coupling of Quasi-Static Fields to Lines

In applying this formalism to the problem of MHD-EMP coupling to a power line, it is possible to make a number of simplifying assumptions. First, because of the very low frequency nature of the MHD-EMP environment, all inductors may be considered to be short circuited, and all capacitors can be treated as open circuits. When this is done, the per-unit-length equivalent circuit of the power line reduces to that in Figure B9. The resistive element in this circuit represents the loss in the conductor itself, plus any ground loss which may be present in the problem.

When a line of length L is attached to grounded loads at each end of the line, the low frequency equivalent circuit shown in Figure B10 results. The resistances R_1 and R_2 represent the effective dc resistances of any load equipment placed on the end of the line, plus a contribution of the footing (or grounding) resistances at the ends. The resistance R_t is the total line resistance and is given by:

$$R_t = R_L \times L \qquad \text{(B23)}$$

and the total voltage source is:

$$V_o = \int \left[E_t^{inc}(y) + E_t^{ref}(y) \right] \, dy \qquad \text{(B24)}$$

Because it is assumed that there is no vertical component of the electric field on the earth surface, only this tangential electric field contributes to the excitation voltage of the line.

Using this approach, the total quasi-dc current flowing in the line and in the terminating resistances can be expressed as:

$$I = \frac{V_o}{(R_1 + R_2 + R_T)} \qquad \text{(B25)}$$

In summarizing this calculative method for the quasi-dc problem, it is possible to say that the important excitation quantity for the line is the total tangential electric field along the wire, and the important line or load parameters are the resistance due to loss effects in both the conducting line and the ground, the footing resistances at each load end of the line and the resistances in the loads at the line ends.

B.6 Application to Multiconductor Lines

In many practical power system applications, the lines of interest are not simple, single wire lines, but consist of three-phase lines with a possible fourth conductor serving as a ground conductor for lightning protection. In such a case, it is important to develop a field coupling model useful for predicting the line currents.

The general field coupling to an open multiconductor line has been discussed [B10], where it is shown that each wire of the multiconductor bundle can have a different voltage source, depending on the variations of phase of the incident field as it passes over the transmission line. Generalizing the quasi-static per-unit-length model of the single wire line in Figure B9 to a multiconductor line, the equivalent section of

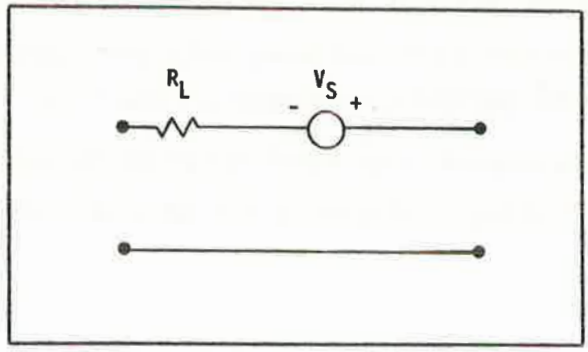

Fig. B9. Quasi-DC differential section of transmission line model for above-ground conductor.

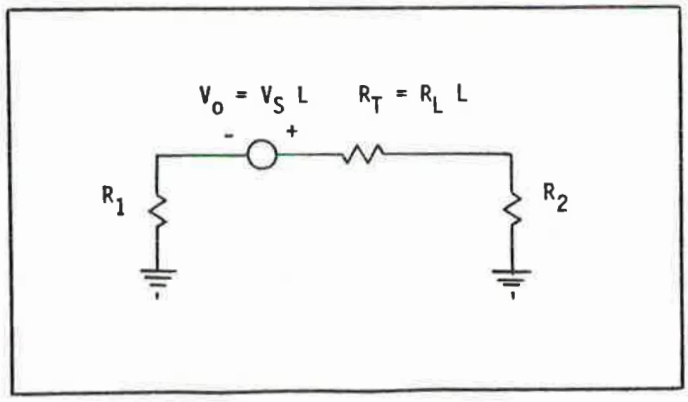

Fig. B10. Quasi-DC equivalent circuit for total line of length L, having load resistances of R_1 and R_2 at each end.

line shown in Figure B11 results. Each conductor can have a different per-unit-length resistance, depending on the size and composition of the conductors. In principle, each conductor has a slightly different per-unit-length excitation voltage, due to the phase variation of the incident field. In practice, however, for the quasi-static MHD-EMP fields, these phase variations are negligible, so that all sources on the conductors in Figure B11 are identical, and equal to the tangential electric field at the wire location. Because the electric field above the ground plane is a very slowly varying function of the height above the ground due to the low frequency (long wavelength) nature of the fields, this excitation is essentially equal to the tangential electric field on the ground surface.

Representing each load at the ends of the multiconductor line as a simple resistance, the overall circuit model for a length of multiconductor line is shown in Figure B12a. Note that in this model, the excitation voltage source in each line is the same as the others, and is given by equation (B24). Given a knowledge of the various load and line resistances, the individual conductor currents and the common mode (or bulk) current on the line may be computed using a simple dc analysis.

It is useful to compare this calculative approach to the electromagnetic coupling problem to that presented for the geomagnetic storms [B1,B2]. The electric and magnetic fields in and above the earth surface are calculated, based upon an assumed known distribution of auroral currents. Unlike the presentation here, the model for the earth [B1] consisted of several layers, which added somewhat to the complexity of the representation of the fields, but the basic concept of field calculation is very similar.

However, instead of computing the electric field on the conductors themselves and using these as the excitation sources, the electric field on the earth surface was computed. This induced "ground potential" was then used to compute the conductor currents. That this approach is identical to the field approach described in this appendix for quasi-dc excitations can be demonstrated in Figure B12b. From the voltage shift theorem [B11], it is seen that the identical voltage sources located in

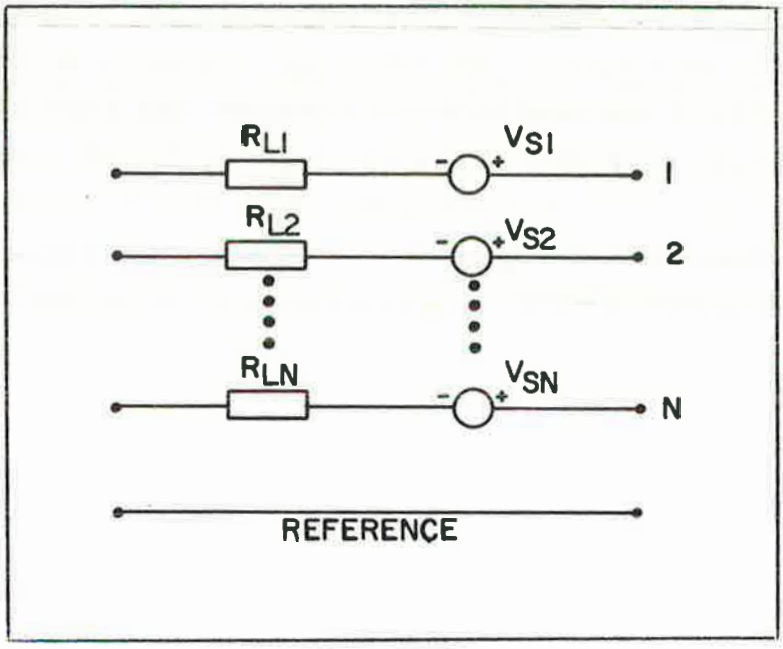

Fig. B11. Quasi-DC differential section for multi-conductor line.

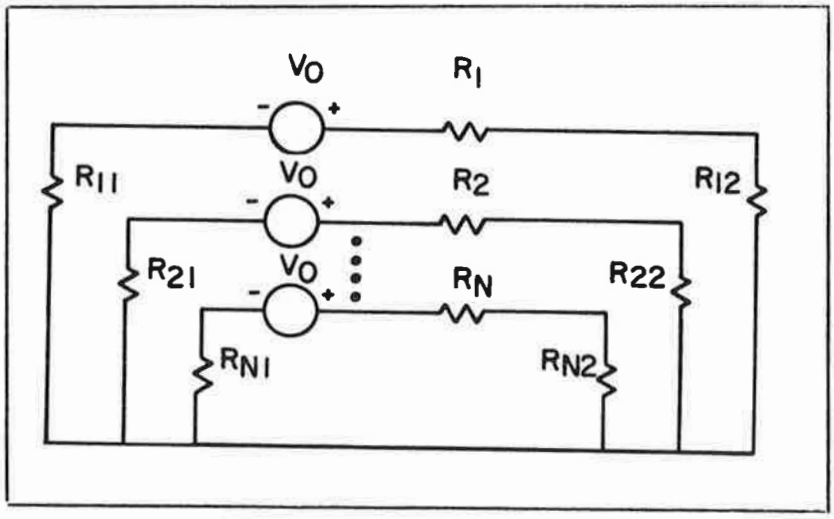

a. Phase Conductor Excitation

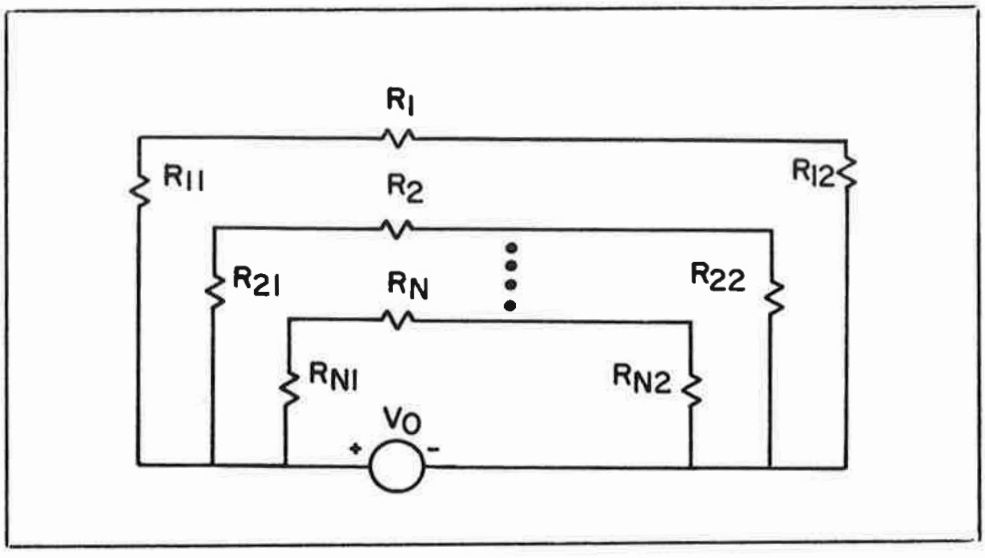

b. Reference Conductor Excitation

Fig. B12. Equivalent excitation models of a multi-conductor line.

the individual phase conductors in Figure B12a may all be shifted to an equivalent voltage source in the reference conductor, with no change in the net response of the circuit. This is equivalent to saying that the source of excitation of the line is a voltage source occurring in the ground, and hence is a "ground potential."

This approach is correct, as long as the voltage sources in each of the individual phase conductor are identical, as is true in the case of quasi-static MHD-EMP excitation. However, in the case of higher frequency excitation, such as that encountered in the high altitude EMP (HEMP) spectrum where the phase differences of the incident field from wire to wire become important, the ground potential concept breaks down. In this case the tangential components of the electric field on the wires must be used to determine the induced currents.

BIBLIOGRAPHY

B1. Albertson, V. D., and Van Baelen, J. A., "Electric and Magnetic Fields at the Earth's Surface Due to Auroral Currents," IEEE Transactions on Power Apparatus and Systems, Vol. PAS-89, No. 2, April, 1970, pp. 578-584.

B2. Albertson, V. D., et. al., "Load Flow Studies in the Presence of Geomagnetically-Induced Currents," IEEE Power Paper, F-79-702-2, Presented at the IEEE Summer Power Meeting, Vancouver, British Columbia, July 15-20, 1979.

B3. Van Bladel, J., ELECTROMAGNETIC FIELDS, McGraw-Hill, New York, 1964.

B4. Harrington, R. F., FIELD COMPUTATION BY MOMENT METHODS, reprinted by the author, 1968.

B5. Vance, E. F., COUPLING TO SHIELDED CABLES, Wiley Interscience, New York, 1978.

B6. Harrington, R. F., TIME HARMONIC ELECTROMAGNETIC FIELDS, McGraw-Hill, New York, 1961.

B7. Sommerfield, A., PARTIAL DIFFERENTIAL EQUATIONS IN PHYSICS, Academic Press, New York, 1964.

B8. Sunde, E. D., EARTH CONDUCTION EFFECTS IN TRANSMISSION SYSTEMS, D. Van Nostrand Co., New York, 1949.

B9. Fontaine, J. M., et. al., "Ground Effects in the Response of a Single-Wire Transmission Line Illuminated by an EMP," ELECTROMAGNETICS, Vol 2, No. 1, January-March, 1982.

B10. Tesche, F. M., and T. K. Liu, "Recent Developments in Electromagnetic Field Coupling to Transmission Lines," Transactions of the 4th Symposium and Technical Exhibition on EMC, Zurich, Switzerland, March 10-12, 1981.

B11 Balabanian, N. FUNDAMENTALS OF CIRCUIT THEORY, Allyn and Bacon, Inc., Boston, 1962.

ORNL/Sub-83/43374/1/V3
Dist. Category 97

INTERNAL DISTRIBUTION

1-24. P. R. Barnes
25. R. B. Braid
26. R. S. Carlsmith
27. F. C. Chen
28. L. G. Christophorou
29. R. I. Crutcher
30. S. J. Dale
31. W. Fulkerson
32. P. A. Gnadt
33. T. L. Hudson
34. J. M. MacDonald
35. F. W. Manning
36. B. W. McConnell
37. J. W. Michel
38-58. M. C. Miller
59. M. O. Pace
60. R. A. Stevens
61. J. P. Stovall
62-63. Central Research Library
64. Document Reference Section
65-66. Energy Information Library
67. Laboratory Records - RC
68-69. Laboratory Records Department
70. ORNL Patent Section

EXTERNAL DISTRIBUTION

71-80. N. C. Abi-Samra, Westinghouse Electric Corporation, Advanced Systems Technology, 777 Penn Center Boulevard, Pittsburgh, PA 15232

81. W. E. Adams, Director for Radiation, Defense Nuclear Agency, Washington, DC 20305

82. V. D. Albertson, Department of Electrical Engineering, 123 Church Street, S.W., University of Minnesota, Minneapolis, MN 55455

83. H. W. Askins, Jr., The Citadel, Charleston, SC 29409

84. C. E. Baum, NTYEE, Kirkland AFB, NM 87117

85. D. W. Bensen, Federal Emergency Management Agency, Research Division, 500 C Street, S.W., Washington, DC 20472

86. T. Bolt, ED-SD, U.S. Army Engineering, USAEDH, P.O. Box 1600, Huntsville, AL 35087

87. J. N. Bombardt, R&D Associates, 105 E. Vermijo Street, Suite 450, Colorado Springs, CO 80903

88. G. E. Brackett, Code H25, Navy Surface Weapons Center, 1091 New Hampshire Avenue, Silver Springs, MD 20903-5000

89. E. H. Brehm, Department GK/CN32, Brown, Boveri, and Cie, Aktiengesell Schaft, Postfach 351, D-6800 Mannheim 1, West Germany

90. F. C. Buchholz, Pacific Gas & Electric Co., 77 Beale Street, Room 2933, San Francisco, CA 94106

91. J. F. Buck, Wisconsin Electric Power Company, 231 W. Michigan, Milwaukee, WI 53201

92. L. M. Burrage, McGraw-Edison, P.O. Box 100, 11131 Adams Road, Franksville, WI 53126

93. H. S. Cabayan, Lawrence Livermore Laboratory, P.O. Box 5504, Livermore, CA 94550

94. F. L. Cain, Georgia Institute of Technology, Engineering Experiment Station, Atlanta, GA 30332

95. R. N. Carlile, Department of Electrical and Computer Engineering, University of Arizona, Tucson, Arizona 85721

96. I. J. Carney, Nuclear Survivability Organization, Boeing Aerospace Company, P.O. Box 3999, Seattle, WA 98124

97. V. L. Chartier, Bonneville Power Administration, P.O. Box 491-ER, Vancouver, WA 98666

98. K. K. Chen, Sandia National Laboratory, Drawer 1333, P.O. Box 5800, Kirkland AFB, NM 87185

99. H. E. Church, Aluminum Company of American, 1501 Alcoa Building, Pittsburgh, PA 15219

100. B. Cikotas, DNA/RAEE, 6801 Telegraph Road, Alexandria, VA 22310

101. C. F. Clark, Bonneville Power Administration, P.O. Box 3621, Portland, OR 97208

102. R. E. Clayton, Power Technologies, P.O. Box 1058, 1482 Erie Boulevard, Schenectady, NY 12301-1058

103. A. Clerici, Sanelmi, Via Pergolesi 25, 20124 Milano, Italy

104. H. W. Colborn, North American Electric Reliability Council, Research Park, Terhume Road, Princeton, NJ 08540-3573

105. D. E. Cooper, Southern California Edison Company, P.O. Box 800, 2244 Walnut Grove Avenue, Rosemead, CA 91770

106. R. Cortina, ENEL-Centro Ricerca, Automatica, VIA Volta 1, Cologno Monzese (MI), Italy

107. G. Dahlen, Royal Institute of Technology, S-100-44, Stockholm, Sweden

108. J. Darrah, Headquarters NORAD/G5, Peterson AFB, CO 80914

109. Defense Technical Information Center, Cameron Station, Alexandria, VA 22314

110. J. J. Dougherty, Electric Power Research Institute, P.O. Box 10412, Palo Alto, CA 94303

111. W. M. Druen, 8200 South Memorial Parkway, Suite D, Huntsville, AL 35802

112. J. C. Engimann, Commonwealth Edison, 1319 S. First Avenue, Maywood, IL 60153

113. D. M. Ericson, Jr., Sandia National Laboratory, Division 6414, Kirkland AFB, NM 87185

114. W. E. Ferro, Electric Research and Management, Inc., P.O. Box 235, Thomaston, ME 04861

115. W. G. Finney, Project Manager, Stanley Consultants, Inc., Stanley Building, Muscatine, IA 52761

116. M. Fitzgerald, MITRE Corp., P.O. Box 208, Bedford, MA 01730

117. F. Fisher, General Electric Corporation, Electric Utility Systems Engineering Department, Building 5, Room 306, Schenectady, NY 12345

118. P. B. Fleming, Science and Engineering Associates, Inc., Mariners Square, Suite 127, 1900 North Northlake Way, P.O. Box 31819, Seattle, WA 98103

119. R. Fullwood, Science Applications, Inc., 5 Palo Alto Square, Suite 200, Palo Alto, CA 94304

120. M. R. Gent, North American Electric Reliability Council, Research Park, Terhume Road, Princeton, NJ 08540-3573

121. S. M. Gillis, Economic and Public Policy, Department of Economics, Duke University, Durham, NC 27706

122. W. Graham, R&D Associates, P.O. Box 9695, Marina Del Rey, CA 90291

123. J. J. Grainger, 5004 Hermitage Drive, Raleigh, NC 27612

124. I. S. Grant, Power Technologies, Inc., 1482 Erie Blvd., Schenectady, NY 12305

125. A. R. Gritzke, U.S. Department of Navy, Theater Nuclear Warfare Project Office, Washington, DC 20360

126. J. Gut, Research Intitute for Protective Construction, Auf der Mauer 2, CH-8001 Zurich, Switzerland,

127. V. Guten, R-52, National Security Agency, Fort G. Mead, MD 20755

128. R. J. Harrington, George Washington University, Department of Electrical Engineering and Computing Science, Washington, DC 20052

129. M. F. Hebb, Florida Power Corp., P.O. Box 14042, Mail Code AB, St. Petersburg, FL 33733

130. M. H. Hesse, JEC 5008, Rennselear Polytechnic Institute, Troy, NY 12181

131. D. Higgins, JAYCOR, Santa Barbara Facility, P.O. Box 30281, 360 South Hope Avenue, Santa Barbara, CA 93105

132. D. W. Hilson, Tennessee Valley Authority, 1100 Chestnut Street, Tower 2, Chattanooga, TN 37402

133. F. C. Holdes, Pacific Gas & Electric Company, 3235-18th Street, San Francisco, CA 94110

134. W. S. Howington, Noranda Aluminum, Inc., P.O. Box 70, New Madrid, MO 63869

135. R. Hutchins, BDM Corporation, 1801 Randolph, S.W., Albuquerque, NM 87106

136. J. Hunt, Emergency Preparedness Administrator, San Diego Gas and Electric Company, P.O. Box 1831, San Diego, CA 92112

137. V. Inkis, Ontario Hydro, U7E1, 700 University Avenue, Toronto, Canada M5G1X6

138. Wasyl Janischewskyj, Electrical Engineering Dept., University of Toronto, Toronto, Canada M5S1A4

139. H. P. Johnson, Georgia Power Company, 270 Peachtree Street, 11th Floor, Atlanta, GA 30303

140. V. K. Jones, Science and Engineering Associates, Inc., Mariners Square, Suite 127, 1900 North Northlake Way, P.O. Box 31819, Seattle, WA 98103

141. F. R. Kalhammer, Director, Energy Management and Utilization Division, Electric Power Research Institute, 3412 Hillview Avenue, P.O. Box 10412, Palo Alto, CA 94303

142. W. Karzas, R&D Associates, P.O. Box 9695, Marina Del Rey, CA 90291

143. K. W. Klein, Chief of Power Delivery Branch, Department of Energy, CE-143, Division of Electric Energy Systems, Forrestal Building, Room 5E-052, 1000 Independence Avenue, S.W., Washington, DC 20585

144. N. Kolcio, American Electric Power, 1 Riverside Plaza, Columbus, OH 43216

145. J. Labadie, IRT, 6800 Poplar Place, McLean, VA 22131

146. H. T. Lam, South Carolina Public Service Authority, 1 Riverwood Dr., Monks Corner, SC 29461

147. T. R. LaPorte, Professor, Political Science, Institute of Government Studies, University of California, 109 Moses Hall, Berkeley, CA 94720

148. R. C. Latham, Duke Power Company, P.O. Box 33189, Charlotte, NC 28242

149. A. Latter, R&D Associates, P.O. Box 9695, Marina Del Rey, CA 90291

150. J. S. Lawler, Department of Electrical Engineering, University of Tennessee, Knoxville, TN 37916

151. K. S. H. Lee, Dikewood Division of Kaman Science Corp., 2800 28th Street, Suite 3780, Santa Monica, CA 90405

152-161. J. R. Legro, Westinghouse Electric Corporation, Advanced Systems Technology, 777 Penn Center Boulevard, Pittsburgh, PA 15235

162. M. Lessen, Consulting Engineer, 12 Country Club Drive, Rochester, NY 14618

163. Library, JAYCOR, 205 S Whiting Street, Alexandria, VA 22304

164. J. Locasso, Rockwell International, 3370 Meraloma Avenue, P.O. Box 4192, Mail Code 031-BB17, Anaheim, CA 92803

165. C. L. Longmire, Mission Research Corporation, P.O. Drawer 719, Santa Barbara, CA 93102

166. W. C. Maklin, IRT Corporation, 6800 Poplar Place, McLean, VA 22101

167. R. M. Maliszewski, American Electric Power Service Corp., 1 Riverside Plaza, P.O. Box 16631, Columbus, OH 43216-6631

168. J. N. Mallory, Southern California Edison Co., P.O. Box 800, Rosemead, CA 91770

169. J. D. Martin, Harris Corporation, PRD Electronics Division, 6801 Jericho Turnpike, Syossett, NY 11791

170. P. S. Maruvada, Hydro-Quebec Institute of Research, 1800 Montee Ste-Julie, Varennes, Quebec, CANADA J0L2P0

171. R. G. McCormack, CERL, Corps of Engineers, P.O. Box 4005, Champaign, IL 61820

172. G. F. Meenaghan, Vice President for Academic Affairs and Dean of the College, The Citadel, Charleston, SC 29409

173. C. Menemenlis, University of Patras, Patras, Greece

174. A. S. Mickley, Philadelphia Electric Corp., 2301 Market Street, Philadelphia, PA 19101

175. I. N. Mindel, IIT Research Institute, 10 West 35th Street, Chicago, IL 60616

176. D. L. Mohre, Cajun Electric Power Corp., P. O. Box 15440, Baton Rouge, LA 70895

177. B. B. Mrowca, Baltimore Gas & Electric Co., P.O. Box 1475, Baltimore, MD 21203

178. K. Muller, IABG, Einsteinstrasse 20, 8012 Ottobrunn, West Germany

179. Este-M Murtha, Booz Allen and Hamilton, General Services Administration, 18th & F Streets, N.W., Washington, DC 10405

180. H. P. Neff, Department of Electrical Engineering, University of Tennessee, Knoxville, TN 37916

181. B. O. Nettles (Code 203), Naval Electronic Systems Engineering Center, Charleston, 4600 Marriott Drive, North Charleston, SC 29418

182. D. R. Nevius, North American Electric Reliability Council, Research Park, Terhume Road, Princeton, NJ 08540-3573

183. G. B. Niles, Baltimore Gas & Electric Company, Principal Eng. Room 1020, P.O. Box 1475, Baltimore, MD 21203

184. B. Noel, Los Alamos National Laboratory, Mail Station 5000, P.O. Box 1663, Los Alamos, NM 87545

185. B. Nowlin, Arizona Public Service Company, P.O. Box 21666, Phoenix, AR 85036

186. R. Oats, Atomic Weapons Research Establishment, Building D57, Aldermaston, Reading, RG74PR, England

187. G. Orrell, Dep. Associate Director for National Preparedness, Federal Emergency Management Agency, 500 C Street, S.W., Washington, DC 20555

188. L. Paris, University of Pisa, Via Diotisalvi 2, 56100 PISA

189. R. Parker, RDA, P.O. Box 9335, Albuquerque, NM 87119

190. R. Parkinson, Science Applications, Inc., 5150 El Camino Real, Suite B-31, Los Altos, CA 94022

191. A. Pigini, CESI-Via Rubahimo 59-Milano, Italy

192. J. B. Posey, Ohio Brass Co., 380 N. Main Street, Mansfield, OH 44903

193. M. Rabinowitz, Electric Power Research Institute, 3412 Hillview Avenue, P.O. Box 10412, Palo Alto, CA 94303

194. W. A. Radaski, Metatech Corp., 358 South Fairview Avenue, Suite E, Goleta, CA 93117

195. J. J. Ray, Bonneville Power Administration, P.O. Box 3621, Portland, OR 97208

196. T. J. Reed, Westinghouse Electric Corporation, Advanced Systems Technology, 777 Penn Center Boulevard, Pittsburgh. PA 15235

197. R. L. Retallach, American Electric Power, 1 Riverside Plaza, Columbus, OH 43216

198. J. Richardson, National Academy of Science, 2101 Constitution Avenue, Washington, DC 20418

199. F. Rosa, Nuclear Regulatory Commission, Division of Systems Integration, MS P1030, Washington, DC 20555

200. D. H. Sandell, Harza Engineering Co., 150 South Wacker Drive, Chicago, IL 60606

201. J. A. Sawyer, MITRE Corp., MS-H070, P.O. Box 208, Bedford, MA 01703

202. R. A. Schaefer, Metatech Corp., 20 Sunnyside Avenue, Suite D, Mill Valley, CA 94941

203. M. Schechter, A.D.A., P.O. Box 2250(81), Haifa, 31021, Israel

204. H. Singaraju, Air Force Weapons Laboratory, Kirkland AFB, NM 87117

205. A. C. Smith, Jr., Beam Research Program, Lawrence Livermore National Laboratory, P.O. Box 808, Livermore, CA 94550

206. J. C. Smith, 1 Adams Avenue, P.O. Box 44, Canonsburg, PA 15317

207. R. Smith, DNA, RAEE, 6801 Telegraph Road, Alexandria, VA 22310

208. W. Sollfrey, RAND Corp., 1700 Main Street, Santa Monica, CA 90406

209. H. Songster, Electric Power Research Institute, Electrical Systems Division, 3412 Hillview Avenue, P.O. Box 10412, Palo Alto, CA 94303

210. G. K. Soper, Defense Nuclear Agency, Washington, DC 20305

211. S. Spohn, DB4C2, Defense Intelligence Agency, Washington, DC 20301

212. J. R. Stewart, Power Technologies, Inc., P.O. Box 1058, 1482 Erie Boulevard, Schenectady, NY 12301-1058

213. R. L. Sullivan, Department of Electrical Engineering, College of Engineering, University of Florida, Gainesville, FL 32611

214. I. O. Sunderman, Lincoln Electric System, P.O. Box 80869, Lincoln, NE 68501

215. R. W. Sutton, Science Applications, Inc., 1710 Goodridge Drive, P.O. Box 1303, McLean, VA 22102

216-225. F. M. Tesche, LuTech, Inc., 3742 Mt. Diablo Boulevard, Lafayette, CA 94549

226. L. Thione, CESI-Via Rubattino 54 20734, Milano, Italy

227. R. J. Thomas, 302 Phillips Hall, Cornell University, Ithaca, NY 14853

228. R. Torres, BDM Corporation, 1801 Randolph, S.W., Albuquerque, NM 87106

229. W. Tyler, NT, Kirkland AFB, NM 87117

230. M. A. Uman, Department of Electrical Engineering, University of Florida, Gainesville, FL 32611

231. E. F. Vance, Route 3, Box 268A, Fort Worth, TX 76140

232. D. R. Volzka, Wisconsin Electric Power Company, 231 West Michigan Street, Milwaukee, WI 53201

233. J. Vora, Nuclear Regulatory Commission, MS 5650 NL, Washington, DC 20555

234. C. D. Whitescarber, Martin Marietta Orlando Aerospace, Sandlake Road Complex (SLRC), Mail Point 399, P.O. Box 5837, Orlando, FL 32855

235. W. P. Wigner, 8 Ober Road, Princeton, NJ 08540

236. M. W. Wik, Forsvarets Materielverk, S-11588 Stockholm, Sweden

237. C. B. Williams, IRT Corp., 7650 Convoy Court, P.O. Box 80817, San Diego, CA 92138

238. W. H. Williams, Division Manager, AT&T Information Systems, Building 83, Room 1B23, 100 Southgate Parkway, Morristown, NJ 07960

239. D. D. Wilson, Power Technologies, Inc., P.O. Box 1058, Schenectady, NY 12301

240. U. P. Wissmann, AEG-Telefunken, General Electric Company, 1 River Road, Building 36-444, Schenectady, NY 12345

241. H. W. Zaininger, Zaininger Engineering Company, 3408 Vance Court, San Jose, CA 95132

242. Institute for Energy Analysis, ORAU - Library

243. Assistant Manager for Energy Research & Development, DOE/ORO Oak Ridge, TN 37830

244-897. Given for distribution as shown in DOE/TIC-4500 under Category UC-97a,b,c (Electric Energy Systems)

*U. S. GOVERNMENT PRINTING OFFICE: 1985-544-045/20008

13 FS- 1

AEROSPACE CORP
ATTN DR MASON WATSON
M3/386
PO BOX 92957
LOS ANGELES, CA 90009